June 2019

Functional Characterization of the Ovarian Tumor Domain Deubiquitinating Enzyme 6B

Jasmin M. D'Andrea
University of South Florida, jdandrea1@mail.usf.edu

Functional Characterization of the Ovarian Tumor Domain Deubiquitinating Enzyme 6B

by

Jasmin M D'Andrea

A thesis submitted in partial fulfillment
of the requirements for the degree of
Master of Science
with a concentration in Cell and Molecular Biology
Department of Cell Biology, Microbiology, and Molecular Biology
College of Arts and Sciences
University of South Florida

Major Professor: Younghoon Kee, Ph.D.
Meera Nanjundan, Ph.D.
Margaret Park, Ph.D.

Date of Approval:
June 6, 2019

Keywords: OTUD6B, p21, LYRIC, Cell cycle

Acknowledgments

I would like to thank my Major Professor Dr. Younghoon Kee for providing me with a challenging graduate school educational experience and the opportunity to significantly advance my skills, techniques, and knowledge of molecular and cell biology. I appreciate his guidance, patience, and advising in concerns to my scientific projects and educational development. I would also like to thank my committee member Dr. Meera Nanjundan for her assistance in the completion of several experimental investigations and her advice on experimental problem solving; specifically, her guidance concerning my protein lysis protocol and qPCR primer designs. I would also like to thank my committee member Dr. Margaret Park for her flexibility to meet with me to review data analysis programs and discuss experimental projects; her advice and comments were always greatly appreciated. I would also like to thank Robert Hill for helping me with troubleshooting various CMMB lab equipment and keeping our facilities running for my demanding experimental schedule. Lastly, I would like to thank my labmates and their undergraduate volunteer students for the always entertaining working environment and their help throughout these past months. Specifically, I would like to thank Angelo De Vivo, Anthony Sanchez, Dr. Jeonghyeon Kim, and Jose Yegres for being the best mentors I could have hoped for; I owe so much of my gained experience to them. I thank Angelo and Anthony for having the patience to show me their techniques multiple times and deal with my many questions and arguments. I am certain that they will make fantastic PIs in the coming future and I wish them all the best.

Dedication

This work is dedicated to my family and friends who have supported me in my goals over the past two and a half years. To my parents, who have sacrificed so much for my educational successes, words of gratitude will never compensate for all you have given me; thank you for all your guidance. To my grandparents, thank you for providing me my home away from home while I completed my studies in Florida, your doors have always been open for me and I truly appreciate being able to visit when work was too stressful; I have always enjoyed time spent with you. To my friends new and old, thank you for always providing me with fun and new experiences that make life in graduate school worth living. Thank you for all your patience and understanding when I have failed to reply to messages for months or have been unable to visit due to a busy work schedule. A special thanks to everyone who made the time to visited me while at school, I feel so blessed to have you all in my life. I would also like to thank Robert Madden for providing me with a life full of laughter while in graduate school, you have been my rock through the good times and the bad and have always been the most supportive. I am so excited to see what adventures lay ahead for us. Lastly, I would like to thank James Stowe for being a constant reminder that nothing in life worth doing is easy, that I should never give up no matter how difficult things may get, and that the ability to pick yourself up from failure is one of the most admirable qualities to possess. There is not a day since you left us that I have not thought of you, may you rest in peace. Again, I thank you all for your support and encouragement while I worked towards my degree.

Table of Contents

List of Figures iv

Abstract vii

Chapter One: Ubiquitin and the Ubiquitin System 1
The Ubiquitin System 1
The Ubiquitin System as a Regulatory Posttranslational Modification 2
The Deubiquitinating System 3
The Ovarian Tumor Domain Family as Unique Regulatory Enzymes 6
The Ovarian Tumor Domain Deubiquitinating enzyme OTUD6B 8

Chapter Two: Features of the Cell Cycle 14
Cell Cycle Progression 14
Cyclin Dependent Kinase Inhibitor p21 16
Cyclin Dependent Kinase Inhibitors 16
Structure and Function of p21 17
Structure 17
Role in Cell Cycle Progression 18
Inhibitor of Apoptosis 19
Regulators of p21 Induction 21
P21 Regulation 22
P21 Stability 22
P21 Inhibitors and Degradation 23
Checkpoint Signaling Cascades 25
DNA Damage Checkpoint Signaling Cascades 25
ATM and Downstream Proteins of the DNA Damage Checkpoint Signaling Cascade 25
ATR and Downstream Proteins of the DNA Damage Checkpoint Signaling Cascade 28
Mitotic Spindle Assembly Checkpoint Signaling Cascade 32
Deubiquitinating Enzymes Implicated in Cell Cycle Progression and Cellular Checkpoint Kinase Cascades 34
Deubiquitinating Enzymes Known to Participate in Cell Cycling Events 34
Deubiquitinating Enzymes Known to Participate in Checkpoint Signaling Cascades 35

Chapter Three: OTUD6B Protein Levels Impact p21 Expression 38
Rational 38
Experimental Design 39

Cell Lines and Chemical Reagents 39
Plasmids 40
Creation of p3xflag-CMV-9-OTUD6B Plasmid 40
Creation of pOZ-FH-N-OTUD6B Plasmid 43
Mutagenesis of OTUD6B Catalytic Cysteine 45
OTUD6B Knockout Cell Line 47
DNA Transfections 50
RNA Interference 51
Protein lysis and Western Blotting 51
Immunofluorescent Microscopy 52
Results 53
OTUD6B Protein Depletion Results in an Induction of the Cyclin Dependent Kinase Inhibitor p21 53
OTUD6B Depletion Does Not Stabilize p21 Protein Levels 56
p21 Levels are Increased in OTUD6B KO Cell Lines but Cannot be Fully Rescued 56
p21 Levels are Increased in a p53 Dependent Manner Under OTUD6B Knockdown Conditions 57
Conclusions and Future Directions 60

Chapter Four: OTUD6B Expression Regulates Cell Proliferation Rates 66
Rational 66
Experimental Design 67
Cell Lines and Chemical Reagents Agents 67
RNA Interference 68
Cell Cycle Analysis 68
Cell Doubling Rate/Trypan Blue Staining 69
Senescence β-galactosidase Cell Staining 69
Immunofluorescent Microscopy 70
Chromatin Enriched Fractionation 71
DNA Transfections 72
Plasmids 72
Mutagenesis of OTUD6B Predicted Nuclear localization Signal (NLS) 72
Creation of p3xFlag-CMV-9 Stable cell lines 75
Protein lysis and Western Blotting 77
Results 78
OTUD6B Protein Depletion Suppresses Cell Cycle Progression and Cellular Proliferation 78
OTUD6B Depletion Promotes Cellular Senescence 81
OTUD6B is a Primarily Cytosolic Protein Regardless of Cellular Exposure to DNA Damaging Agents 83
OTUD6B depletion results in a mild induction of DNA damage markers 87
Conclusions and Future Directions 91

Chapter Five: OTUD6B Potential Binding Partners and Role in Migration 99
Rational 99

Experimental Design 100
Cell Lines and Chemical Reagents 100
Plasmids 100
DNA Transfections using Turbofect 100
DNA Transfections using Polyethylenimine (PEI) 101
RNA Interference 101
Isobaric tags for relative and absolute quantitation (iTRAQ) 102
Large Scale Immunoprecipitation for Mass Spectrometry 102
Wildtype p3xflag-CMV-9-OTUD6B 102
p3xflag-CMV-9-OTUD6B-C188S 103
Small Scale Immunoprecipitation 104
Protein lysis and Western Blotting 104
Immunofluorescent Microscopy 105
Cell Migration Assay 104
Results 108
LYRIC is a potential binding partner of OTUD6B 108
OTUD6B is a potential regulator of LYRIC stability 112
OTUD6B Depletion Alters Migration Abilities in Cancerous Cells 113
Conclusions and Future Directions 117

References 125

List of Figures

Figure 1: Schematic representation of the E1-E2-E3 cascade 1

Figure 2: Ovarian Tumor Domain Family 7

Figure 3: Prediction of disordered regions and binding partners within OTUD6B transcript variant 1 amino acid sequence 9

Figure 4: Cancer study summary of OTUD6B gene expression alterations in various cancers 12

Figure 5: ATM and downstream proteins of DNA damage checkpoint signaling cascade 27

Figure 6: ATR and downstream proteins of the DNA damage checkpoint signaling cascade 29

Figure 7: Mitotic spindle assembly checkpoint signaling cascades 33

Figure 8: Creation of p3x-flag-CMV-9-OTUD6B plasmid 42

Figure 9: Creation of pOZ-FH-N-OTUD6B plasmid 44

Figure 10: Creation of p3x-flag-CMV-9-OTUD6B-C188S plasmid 46

Figure 11: Creation of OTUD6B Knockout cell line in HEK293T cells 49

Figure 12: Depletion of OTUD6B protein levels results in p21 induction in multiple human cancer cell lines 54

Figure 13: p21 levels decrease compared to control conditions when OTUD6B is overexpressed 54

Figure 14: p21 levels are induced in HeLa cells under OTUD6B knockdown 55

Figure 15: p21 protein levels are not stabilized by OTUD6B knockdown 56

Figure 16: p21 levels are increased in OTUD6B KO cell lines but cannot be fully rescued 57

Figure 17: p21 induction under OTUD6B knockdown does not occur through NF-Kβ signaling 58

Figure 18: MIA-PaCa-2 cell line suggests p21 induction under OTUD6B protein depletion occurs in a p53-dependent manner 59

Figure 19: p21 basal levels are partially rescued by OTUD6B wildtype and catalytically inactive mutant introduction 62

Figure 20: Schematic representing the novel relationship between OTUD6B and p21 65

Figure 21: Creation of OTUD6B NLS mutant 74

Figure 22: Verification of OTUD6B mutant and OTUD6B 42_46del p3xFlag-CMV-9 expressing stable cell lines 77

Figure 23: OTUD6B depletion in asynchronous cells results in minor G1 phase cell cycle arrest 79

Figure 24: OTUD6B depletion results in slowed cell cycle progression into G2..... 80

Figure 25: Decreased OTUD6B protein expression slows proliferation in HEK293T kidney cells 81

Figure 26: OTUD6B depletion induces p21 and β-galactosidase staining in WI-38 fibroblasts 82

Figure 27: Bleomycin and Etoposide treatment do not exhibit nuclear localization of exogenous OTUD6B 85

Figure 28: UV irradiation treatment does not exhibit nuclear localization of OTUD6B..... 86

Figure 29: OTUD6B protein decrease results in a mild increase of pATM foci 88

Figure 30: OTUD6B protein decrease does not induce ϒ-H2AX levels 89

Figure 31: OTUD6B depletion suggests no increased levels of apoptosis under Bleomycin treatment 91

Figure 32: Methods of wound healing assay..... 107

Figure 33: Verification of successful IPs for MS analysis and resulting potential binding partners of OTUD6B identified through MS analysis..... 109

Figure 34: Verification and analysis of OTUD6B knockdown with iTRAQ-MS analysis 111

Figure 35: iTRAQ and IP results of LYRIC in relationship to OTUD6B 112

Figure 36: Decreased OTUD6B protein expression suggests decreased LYRIC protein expression..... 113

Figure 37: The rate of cellular migration in HeLa cell lines under OTUD6B protein depletion..... 114

Figure 38: Overall Survival Kaplan-Meier Estimate of breast cancer patients with amplified OTUD6B 115

Figure 39: The percentage of wound closure in MDA-MB231 cell lines under OTUD6B protein depletion 116

Figure 40: Volcano plot data of RPF2 protein fold change under OTUD6B depletion..... 118

Figure 41: Volcano plot data of ASCC3 protein fold change under OTUD6B depletion..... 119

Figure 42: iTRAQ-MS and IP-MS results of LYRIC interacting partners 122

Abstract

The posttranslational modification ubiquitination is major regulatory mechanism used throughout cell signaling pathways such as cell cycle regulation and the DNA damage response. As such, the E3 ligases and their deubiquitinating enzyme counterparts, which conjugate and deconjugate ubiquitin to and from protein substrates respectively, must be tightly regulated to prevent aberrant cellular behaviors that could lead to diseases such as cancer.

Of the five families of deubiquitinating enzymes, the Ovarian Tumor Domain (OTU) family is fairly unique and under-studied; many of its family members hold a linkage specificity to certain ubiquitin chains and a number of them have been implicated in the DNA damage response and innate immune signaling. Among the understudied isopeptidases within this family, the Ovarian Tumor Domain Deubiquitinating enzyme 6B (OTUD6B), has remained functionally ambiguous and its binding partners are unconfirmed. Studies suggest OTUD6B may be involved in translational regulation, cell growth, or be vital for 26S proteasomal formation; it is currently undecided if OTUD6B function is vital development, cellular growth, and proliferation or if it is an inhibitor of such events.

In the following work, we bring clarity to this dispute by showing that decreased OTUD6B induces p21 protein level increase, cellular senescence, and decreased cell growth and migration rates, suggesting OTUD6B functions is a promoter of cell proliferation. We also provide evidence that OTUD6B is a binding partner of the Lysine-rich CEAMCAM-1-associated protein (LYRIC), an oncogene implicated in promoting metastasis in various cancers. Such findings highlight a potentially new, cancer promoting, pathway involving the regulation of p21 and LYRIC protein levels, as well as adds transparency into the contradicting results observed within OTUD6B published literature. Such new understanding of OTUD6B

functional properties may bring insight to the field of ubiquitin dependent regulation mechanisms and possibly position OTUD6B as a new therapeutic target against cancers.

Chapter One: Ubiquitin and the Ubiquitin System

The Ubiquitin System

Ubiquitin is a ~8.5kDa protein containing 76 amino acids [1]. Through the E1-E2-E3 cascade, the carboxyl group of its G76 residue usually becomes covalently attached to the ε-amino acid group of lysine residues within its conjugating partner, resulting in monoubiquitination, or attached to the ε-amino acid group of lysine residues on addition ubiquitin proteins, resulting in ubiquitin chains [2, 3]. As ubiquitin can form polyubiquitination chains, there are six lysine residues (K6, K11, K9, K33, K48, and K63) and an N-terminal methionine from which a chain can form [1, 4].

Conjugation of ubiquitin is carried out by three enzymes (Figure 1). First, through the use of ATP, E1 ubiquitin-activating enzyme adenylates one ubiquitin molecule which will act as an ubiquitin donor while it catalyzes a thiol ester bond between its catalytic cysteine and the carboxyl group of the G76 residue within another ubiquitin protein, preparing it for a nucleophilic attack [3, 5, 6]. Next the thiol-bonded activated ubiquitin molecule is transferred from the E1 enzyme to the catalytic cysteine of the E2 ubiquitin conjugating enzyme creating a thioester bond (Figure 1) [5, 6]. The final enzyme, E3 ubiquitin ligase attaches to both the target substrate and the E2 enzyme with the conjugated ubiquitin

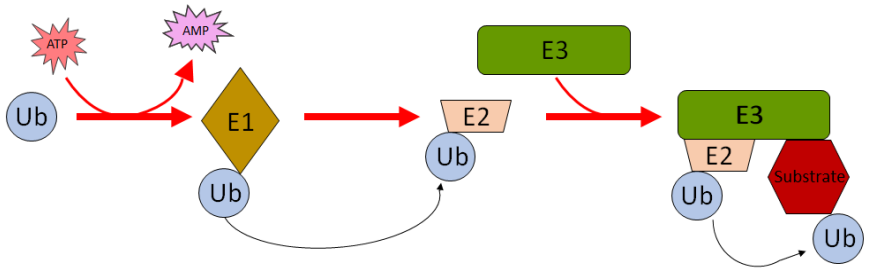

Figure 1. Schematic representation of the E1-E2-E3 cascade. Through the use of ATP, E1 ubiquitin-activating enzyme binds to ubiquitin. E1 transfers activated ubiquitin to E2 ubiquitin conjugating enzyme which then binds to E3 ubiquitin ligase enzyme. E3 ligase facilitates the activated ubiquitin to the targeted substrate. Adapted from Nguyen et al. (2014) [6].

(Figure 1) [3, 5, 6].This E3 ligase then facilities the transfer of activated ubiquitin to a lysine on the targeted substrate, creating an isopeptide bond between the two proteins (Figure 1) [3, 5, 6].

There are two different types of E3 ligases: really interesting new gene (RING) E3 ligases, which do not directly bind to ubiquitin but rather act as a scaffold protein to encourage E2-substrate binding and subsequent ubiquitin transfer, and homologous to the E6-AP carboxyl terminus (HECT) domain E3 ligases, which interacts with the E2 conjugating enzyme on their N-terminus to catalytically attach the ubiquitin to its target substrate [3, 7-9].

Interestingly, a single E1 enzymes can activate ubiquitin for a large array of downstream E2 enzymes and a single E2 enzymes can subsequently transfer the activated ubiquitin to several different E3 ligases [3]. The large varying number of E1-E2-E3 cascade enzymes allows for greater diversity of potential ubiquitin modifications [1, 4]. Additionally. the variability in chain formation provided by the eight potential amino acid residues also allows for several different types of ubiquitin modifications as discussed below, thus further increasing ubiquitin functional roles.

The Ubiquitin System as a Regulatory Posttranslational Modification

Posttranslational modifications provide additional functional diversity and regulation to cellular events such as assistance in protein folding, localization, activation or deactivation, and complex formation [10]. Phosphorylation, for example, is used extensively throughout processes such as receptor activation, signaling pathway propagation, cell cycle progression, and chromosomal integrity maintenance [11]. The advantage of this modification is that it is easily reversible allowing for quick protein alterations and thus making it a great asset for cellular regulation [10].

Ubiquitination is similar to phosphorylation in that it is also a reversible posttranslational modification and as such, it has become a useful regulatory mechanism [10]. Moreover, there are different forms in which ubiquitin can be attached to a target protein, increasing the regulatory

potential of this modification. The functional effects of some chain formations are well known. For example, polyubiquitination linkages for four ubiquitins or more on the 48 lysine of a target protein traditionally marks the protein for degradation by the 26S proteasome in which the ubiquitin chain is recognized by one of two 19S regulatory subunits, the targeted protein is unfolded, and the unfolded protein then enters the 20S proteasome for breakdown [1, 5, 6, 12]. Other ubiquitin conjugations, such as K63 linkages on methionine 1 and polyubiquitin chains on K63 of target proteins, can lead to more complicated functions like the NF-Kβ activation or DNA damage responses and kinase activation, respectively [6, 10]. In addition, some proteins experience monoubiquitination modifications in which a single ubiquitin is added to a substrate, such as K561 ubiquitination on Fanconi Anemia protein D2 (FANCD2) for DNA damage repair [13]. Despite already well-known functions of ubiquitin modifications, a complete understanding of all possible arrangements and their resulting consequences has not been achieved.

The Deubiquitinating System

Deubiquitination is carried out by deubiquitinating enzymes (DUBs) which are isopeptidases that can hydrolyze the bonds between ubiquitin molecules and their attached proteins [4]. About 95 different DUBs are currently known to exist and they can be categorized into five different families: ubiquitin-specific proteases (USP), ubiquitin C-terminal hydrolases (UCHs), Machado-Joseph domain-containing proteins (MJDs), Jab1/Mpn/Mov34 (JAMM) proteases, and Ovarian Tumor domain-containing proteases (OTUs) [14]. Apart from JAMM DUBs, all enzymes within these families are cysteine dependent; they contain a catalytically active cysteine which induces a nucleophilic attack on the isopeptide bond between the ubiquitin and its bound partner [2]. Additionally, most of these groups contain a “catalytic triad” within their peptide chains, which includes not only the catalytic cysteine, but also a histidine, and an asparagine or aspartate [4]. These catalytic triads vary in structure and help facilitate the cleavage of ubiquitin from its targeted protein [4].In some cases, these triads also

encourage deubiquitination regulation [4]. JAMM DUBs depend on metal groups, such as zinc, to carry out their cleavage abilities [2, 4].

The regulatory roles these enzymes play within cellular systems is equally as vast as their ubiquitinating counterparts; deubiquitination can regulate cellular pathways by inhibiting events of protein degradation or by activating/deactivating specific cascades [1]. Many DUBs are known to associate with large protein complexes, removing ubiquitin from them to help maintain appropriate complex activation [2]. An investigation of 75 different DUBs and their subsequent binding partners via mass spectrophotometry identified that one third of these isopeptidases bound to protein groups involved in proteomic degradation, transcription, RNA splicing, or responses to DNA damage [2]. Research has also reported a direct interaction between HECT or RING based E3 ubiquitin ligases and DUBs in some cases, suggesting a cyclic ubiquitin regulatory mechanism [2]. Though shown to associate with large complexes, most DUBs also have very few directly-interacting partners, making them ideal targets for drug development [2, 14].

The predicted regulatory functional roles of these DUBs yields their own strict regulation. Having few interacting partners is, in part, due to several DUB families retaining a linkage specificity to help regulate their protease activity. This involves identifying ubiquitin from ubiquitin like molecules, certain chain topologies, and even chain lengths [10]. For example, the OTU OTUDB1, can specifically deubiquitinate lysine 48 linkages while its family members OTULIN and OTUD7B target Met1 ubiquitin modifications and lysine 11 linkages, respectively [10].

Linkage specificity is achieved through a few suggested models: additional ubiquitin binding domains within the DUBs which encourage binding, specific recognition of ubiquitin sequences, specific DUB tertiary structures which position ubiquitin targets of longer chains at enzyme catalytic sites, or ubiquitin substrate interaction inducing structural changes of DUB tertiary structures towards altered

states of activity [4, 10, 15]. The later of these models is shown by OTUDLIN functional activity, in which a glutamine within the proximal ubiquitin of the Met1 chain positions the catalytic triad to its active form [4]. However some DUBs, such as the USP family, contain little to no ubiquitin linkage specificity [4].[15] In these cases, other regulatory mechanisms are used such as well-defined recruitment factors, other posttranslational modifications, inhibitory protein binding, and other external factors [4].

Recruitment supervision ensures that these enzymes are localizing to appropriate cellular compartments and interacting with the correct cascades or complexes, even in the absence of DUB linkage specificity [4]. Other domains within DUBs not only encourage linkage binding regulation but can also facilitate this recruitment [4]. In addition, external proteins can recruit DUBs towards their interacting partners such as USP10 localization to its NF-Kβ binding partners through the enzyme MCPIP-1 [4].

Additionally, posttranslational modifications such as phosphorylation and even ubiquitination, can have negative or positive effects on DUB active states and localization [4]. OTUD5 for example, only holds deubiquitinating activity when it is phosphorylated on serine 177 [4, 10]. Phosphorylation restructures the protein to encourage ubiquitin binding [4]. Phosphorylation however, negatively regulates OTULIN DUB activity by inhibiting binding to its target E3 ligase in the NF-Kβ pathway [4].

Although rare, DUBs can also be inhibited by direct protein binding as well [4]. An example of this event occurs on monoubiquitinated PCNA during events of replication. Here, the protein Spartan binds to PCNA to propagate the stress signal and through this interaction the USP/UAF1 complex, which deubiquitinates PCNA, becomes unable to interact with PCNA [4]. Another common regulatory mechanism also observed in DUBs is external factors such as multiunit protein complexes that, when bound to DUBs, increase their deubiquitinating capacity [4]. An example of this include USP15

interaction with the COP9 signalosome; through this interaction the complex's deubiquitinating activity is increased which regulates IκBα stability and TNF stimulation [4, 16].

DUB regulation is maximized by the fact that many of these mechanisms work together to mediate the same DUB function [4]. The tight regulation observed for these enzymes highlights their importance in the cellular pathways that they regulate. In the unfortunate event that one of these regulations is not maintained, organism integrity becomes compromised. This idea is strengthened through the knowledge that many DUBs have been implicated in neurological, immune, and cancer related human diseases [10].

The Ovarian Tumor Domain Family as Unique Regulatory Enzymes

Ovarian tumor domain deubiquitinating enzyme family (OTUs) is the second largest DUB group [10]. Moreover, they hold ubiquitin linkage specificity as opposed to the largest DUB family, USPs, and many of them contain additional ubiquitin binding domains to regulate their function (UBDs) [10]. Phylogenetic analysis of OTUs and their catalytic domains in one study reports four subfamilies within this group: OTUB subfamily, OTUD subfamily, A20 subfamily, and OTULIN subfamily (Figure 2) [10].

Although this analysis would suggest that DUBs within each subfamily would have similar, if not identical, linkage specificity to their family members, deubiquitinating activity analysis on 17 of these OTUs revealed that OTU linkage preferences vary even within the subfamilies [10]. Examination of OTU DUB structure by Mevissen et al. (2013) suggested that this variability depends largely on the structural differences within the catalytic triads as well as the certain UBDs present in each OTU [10].

Eight OTUs are known to contain UBDs such as ub-interacting motifs (UIM), UBX-like domains (UBL), c-terminal zinc fingers (ZnF), or c-terminal UB-associated domains (UBA) [10]. Studies have suggested that some of these domains help to position the targeted ubiquitin towards the DUB catalytic center (i.e. the catalytic triad). For example, deletion of the UIM in OTUD1 leads to a decrease in the

OTUDs activity level and abolishes its linkage preference towards K63 chains [10]. However, not all OTUs contain UBDs nor have all UBDs shown to be required for linkage specificity, such as OTUD3 deubiquitinating preference towards K6 and K11 in the absence of UBA [10].

Three structural loops make up the catalytic triad observed in DUBs: a conserved Cys loop containing the catalytic cysteine, a His loop containing a histidine which interacts with the distal ubiquitin within ubiquitin chains, and a variable loop which is positioned opposite the His loop and may interact with the targeted ubiquitin [10]. The variable loop, and to a lesser extent the His loop, hold varying amino acid sequences among the OTUs [10]. This variability in sequence is suggested to help dictate the linkage specify seen among each of the OTUD subfamily members [10].

Despite what is known about OTU protein structure in general, many of these OTUs' functional roles and binding partners remain elusive [10]. One currently understood aspect is their roles in immunity, specifically their regulatory roles in innate immune signaling pathway, and DNA damage

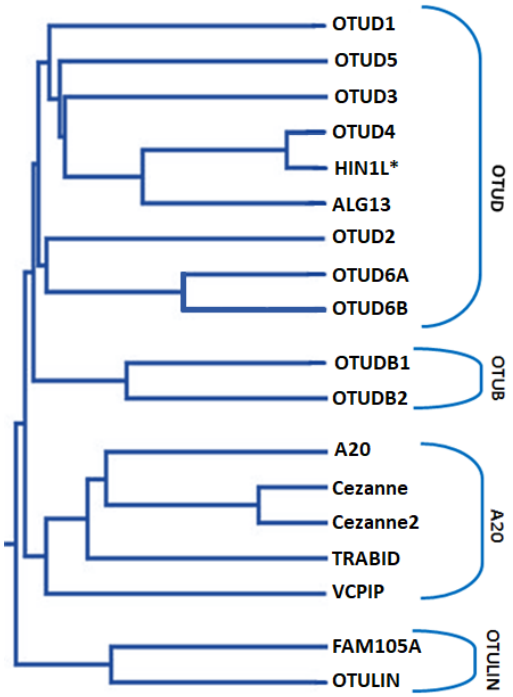

Figure 2. Ovarian Tumor Domain Family. Phylogenetic analysis of human OTU subfamilies based on their catalytic domain sequence similarities. * represents a pseudogene. Adapted from Mevissen et al. (2013) [10].

response pathways [10]. For example, A20, OTUD7B, OTUD5, OTULIN, and OTUB1 all regulate the innate immune pathways involving the NF-κB pathway and the Interferon Regulatory Factor (IRF) transcription factors by inhibiting essential proteins within these pathways from activation or marking others for proteasomal degradation [1]. In regards to the DNA damage response, it has been suggested that OTUD4 forms a complex with USP7 to regulate alkylated DNA reversal and that OTUDB1 inhibits histone H2A ubiquitination by RNF168 [14].

The ubiquitin chain specificity held by this family of DUBs is unique and because of this, it has been suggested that their functional activities may specifically emanate from the ubiquitinated status of the cell rather than from their specific binding partners [14]. Due to their linkage specific deubiquitinating abilities, rendering them as appealing inhibitory targets for drug development, the benefit of fully understanding the functional roles of these OTUs cannot be overlooked.

The Ovarian Tumor Domain Deubiquitinating enzyme OTUD6B

OTUD6B is a ~34kDa DUB found within the OTUD subfamily of OTUs and is located on chromosome 8q21.3 [17]. Its full-length protein structure is composed of cysteine dependent OTU catalytic domain, three coiled-coil domains, and a disorder region at the N-terminus (Figure 3) [17]. The variable loop of the enzyme's predicted ubiquitin-binding region is D185, the H-loop is H307, and the C-loop is C188 [17]. The full-length protein contains seven exons [17].

It has been determined that two main isoforms exist for this OTU; while the first isoform is the largest, containing all three coiled coil domains and the N-terminal disordered region, the other transcript variant is a truncated version [17, 19]. The shorter transcript includes an additional third exon between exons 3 and 4 that results in a premature stop codon and a protein length of only three residues [19]. This alternative, out-of-frame third exon also includes an additional start site at its 3' end however, resulting in a shorter transcript which lacks two N-terminal coiled-coil domains and is termed

splice variant 2 [19]. Missing both the N-terminus and two of the three coiled-coil domains results in this splice variant 2 also missing the predicted disordered region, two potential binding sites and the predicted nuclear localization signal (NLS) (described in Chapter 4, Experimental Design, Mutagenesis of OTUD6B Predicted Nuclear localization Signal). Thus, this shorter transcript proposes potential functional differences between the two isoforms as the disordered region could create binding sites for OTUD6B interacting partners and the NLS sequence suggests a role within the nucleus.

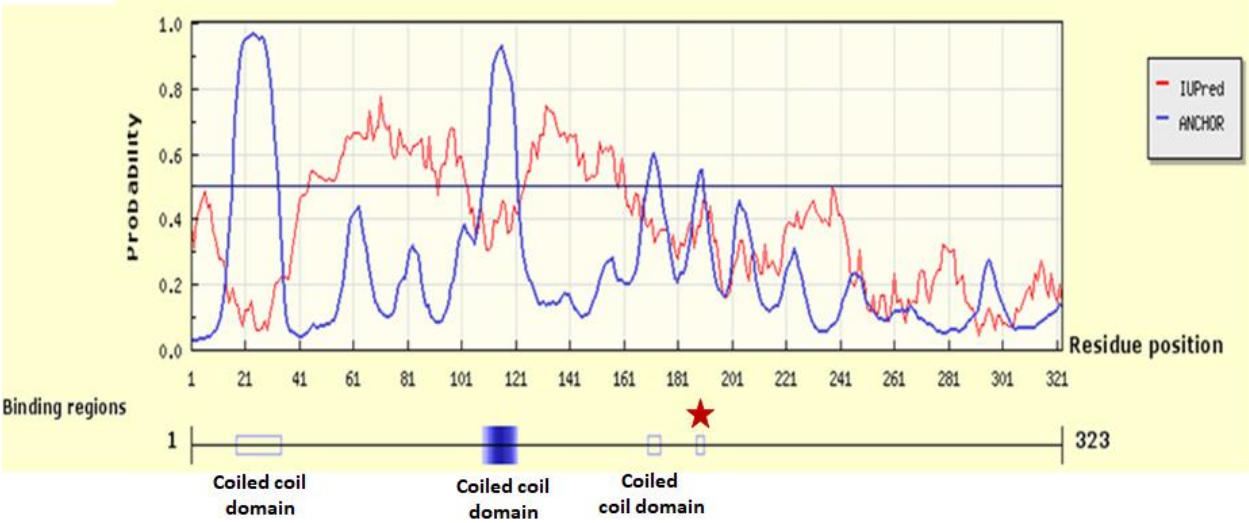

Figure 3. Prediction of disordered regions and binding partners within OTUD6B transcript variant 1 amino acid sequence. Red line indicates predicted regions of disorder. Blue line indicates predicted regions that may facilitate binding to substrates. Y axis indicates the probability of each region throughout the amino acid sequence participating in disorder or binding where above .5 probability indicates strongly likelihood of binding, indicated by the blue line, or disorder, indicated by the red line. Three coiled coil domains are labeled on the 323 amino acid long OTUD6B sequence by blue boxes and positively correlate with predicted binding regions. Red star represents the catalytic cysteine at amino acid 188. Prediction plot was adapted from IUPred2A [18].

In support to this, it has already been suggested that there are functional differences between these two transcript variants. Sobol et al. (2016) showed that OTUD6B isoform 1 seemed to inhibit protein synthesis while the shorter isoform 2 seemed to stimulate protein synthesis based on different rates of methionine surrogate azidohomoalanine (AHA) incorporation, a marker of protein synthesis [20]. Furthermore, Sobol et al. (2016) also showed that expression changes of OTUD6B isoform 2 protein levels was positively correlated with changes of c-Myc and cyclin D1 while OTUD6B isoform 1 showed no effect, ultimately supporting that these transcripts hold different, and to some extent, opposing

functions [20]. Thus, because all three coiled-coil domains, the predicted disordered region, and the predicted NLS sequence reside within the OTUD6B isoform 1, to understand the functional significance of these features, our work focuses on the full length OTUD6B transcript variant 1.

Despite this knowledge of OTUD6B structure and its predicted disordered N-terminus suggesting a binding site with in this peptide chain, OTUD6B interacting partners remain elusive. In one study by Sowa et al (2009), a large-scale immunoprecipitation (IP) followed by mass spectrometry screening was performed on DUBs to analyzes their binding partners. In this study it was found that OTUD6B had potential binding partners of Lysine-rich CEAMCAM-1-associated protein (LYRIC), also known as metastasis adhesion protein (MTDH), which is a poorly understood protein upregulated in various cancers and seems to promote tumorigenesis, Activating signal co-integrator 1 complex subunit 3 (ASCC3), a 3' to 5' DNA helicase involved in the repair of alkylated DNA, ribosome production factor 2 homologue (RPF2), also known as BXDC1, involved in ribosomal large subunit assembly, and OTUB1, another ovarian tumor domain DUB, which can remove K48 linked ubiquitin chains [2, 21, 22]. Analysis by Sowa et al. (2009) did not further investigate these binding partners, however they did conclude that OTUD6B was primarily observed within the ER and nucleus through Gene Ontology (GO) processes [2]. In a separate study using endogenous protein and m^7GTP 5'cap pulldown assays, OTUD6B was suggested to bind to the initiator tRNA complex during protein production [20]. Despite these reports, a fully investigated OTUD6B interacting partner has yet to be identified.

Moreover, OTUD6B linkage specificity also remain unclear. Deubiquitinating assays using ubiquitin-β-galactosidase fusion protein have confirmed OTUD6B enzyme as an active DUB, however it has not shown preference towards di-ubiquitin-propargylamide probe chains even with posttranslational modifications such as phosphorylation [10, 23, 24].

Though severely under-studied compared to some of its other OTU family members, OTUD6B has been repeatedly associated with cell progression and cellular development among a variety of different cell types. One study has reported that OTUD6B overexpression blocked cell proliferation in mice B lymphocytes, while decreasing OTUD6B protein levels had no effect on cell cycle progression [23]. The same study also reported quantitative PCR (qPCR) results showing the G1 to S phase cell cycle regulator cyclin D2 was down-regulated in OTUD6B overexpressed conditions, however no other cell cycle regulator was shown to be significantly altered [23].

In argument to these findings, clinical analysis of patients with biallelic variants of *OTUD6B* resulting in loss of function mutations showed symptoms associated with developmental delays such as microcephaly and brain structure abnormalities, loss of speech, delayed growth, and heart and musculoskeletal congenital malformities [17]. This study also reported that mice homozygous for *OTUD6B* gene knockout were sub-viable with most dying in the embryonic stage or shortly after birth; mice were also small and ventricular septal defects (resulting in hear chamber organizational abnormalities) were present in 80% of the offspring [17]. Such phenotypes were suggested to be related to impaired 26S proteasome assembly and reduced incorporation of the 19S subunit inferring that OTUD6B was implicated with 26S proteasome function [17]. Regardless of whether OTUD6B is in fact a requirement for accurate proteasomal assembly, such data strongly supports that OTUD6B protein expression is a requirement for cellular growth and development.

Large-scale cancer screening studies also support the idea that OTUD6B is required for cellular growth rather than an inhibitor of cellular growth. CBioPortal analysis of cancer patients' genetic expression summaries show that *OTUD6B* is amplified in several different cancers, with the most significant amplification found in prostate and breast cancer studies (Figure 4) [25, 26]. This amplification is found to be more significant than other OTU family members such as OTUD5 and the closely related OTUD6A [25, 26].

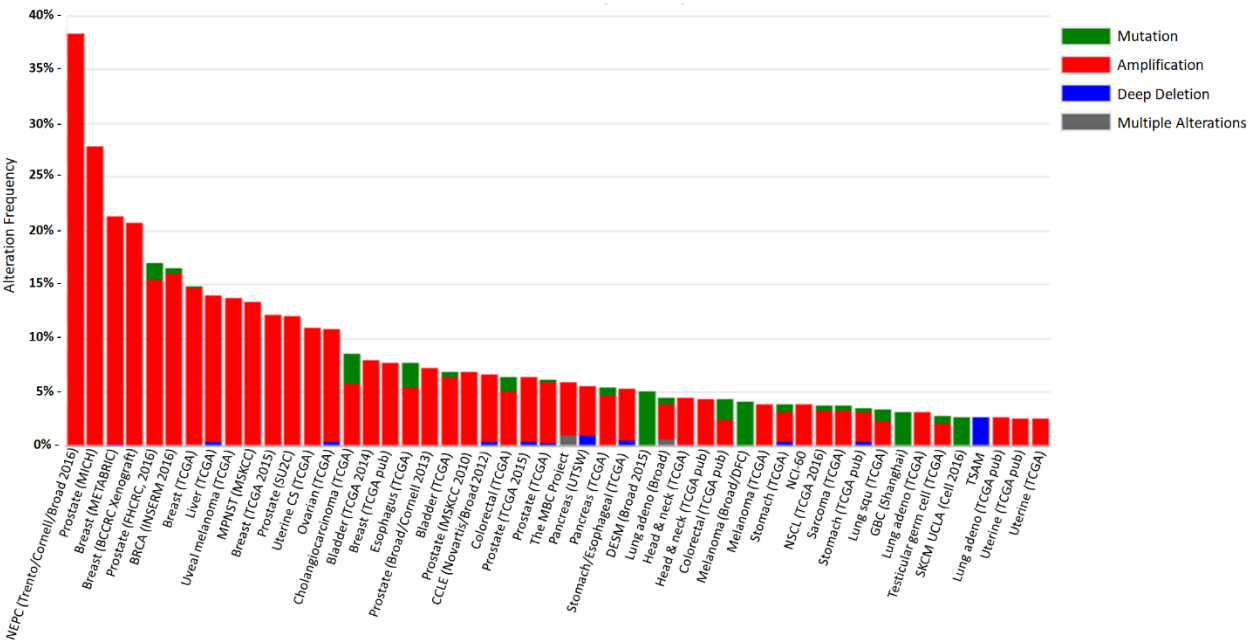

Figure 4. Cancer study summary of *OTUD6B* gene expression alterations in various cancers. Analysis of *OTUD6B* mutations, amplifications, deletions and other modifications among various cancer types adapted from cBioPortal [24, 25]. X-axis represents cancer studies included in the expression analysis. Y-axis represents the percent alteration frequency for each cancer study.

Interestingly, the most recently discovered data regarding OTUD6B function is actually centered around phenotypical impacts of a long non-coding RNA, OTUD6B AS1. In this study it was found that, in clear cell renal cell carcinoma (ccRCC), OTUD6B AS1 was significantly decreased compare to wildtype renal cell tissue counterparts [27]. Expression tests involving overexpression of this long non-coding RNA linked its function to reduced cell proliferation, migration, and overall survival [27]. Specifically, it was shown that OTUD6B AS1 directly impacted proteins related to the Wnt/β-catenin signaling pathway, which is often abnormal in colon cancers and is important to stimulate cell growth during development [27]. Although most long non-coding RNAs do not impact the protein levels of the genes they are associated with, it would be interesting to determine the direct mechanism and interacting partners of OTUD6B AS1 and whether this system correlates with phenotypes we have observed for OTUD6B protein function.

Ultimately, validation of binding partners and pathways associated with the presently understudied OTUD6B may provide insight into the contradicting results observed within the published literature of OTUD6B. Such research may also potentially elucidate OTUD6B ubiquitin chain preferences, which is currently unknown. As many DUBs have been implicated in important regulatory pathways such as DNA damage response and immune signaling, understanding OTUD6B functional properties will bring insight to the field of ubiquitin dependent regulation mechanisms and possibly position OTUD6B as a new therapeutic target against cancers.

Chapter Two: Features of the Cell Cycle

Cell Cycle Progression

Cells cycle through four different stages before dividing into two, identical copied, daughter cells. G1 phase of the cell cycle, also known as growth phase, allows the restart of synthesis processes which produce the necessary proteins and organelles needed for DNA replication in S phase. S phase, or synthesis phase, consists of DNA replication and the creation of sister chromatids. G2 phase of the cell cycle allows time for the cell to produce necessary proteins needed for M phase, or mitosis. In mitosis, cells undergo processes needed for accurate cell division including, chromatin compaction in prophase, kinetochore attachment to microtubules and centrosome movement to opposite ends of the cell in prometaphase, alignment of condensed chromosomes along the metaphase plate in metaphase, separation of sister chromatids to opposite ends of the cell in anaphase, and finally the reformation of nuclear membrane into two distinct cells and relaxation of chromosomes in telophase and cytokinesis [28, 29].

To control cell growth, cell cycle progression is tightly regulated. Key factors which stimulate particular phase entry are a family of serine/threonine kinases called cyclin dependent kinases (cdks) [30]. As their name suggests, the cdk functional ability to promote progression of the cell into its next phase of the cell cycle is dependent on cyclins, a family of about 30 non-catalytic proteins who's levels fluctuate through the cell cycle [31, 32]. Generally, upon binding to target cdks, cyclins induce a conformational change within the cdk, opening and subsequently activating the active site of these

kinases [32]. Once the heterodimeric cyclin-cdk complex is formed, it can proceed to phosphorylate various proteins to promote entry and progression through G1, S, G2, and M phases [32].

Generally, starting in G1 phase and upon mitogen stimulation, the first cyclin-cdk complexes to promote progression is cyclin D-cdk4 and cyclin D-cdk6 (further referred to as cyclin D-cdk4/6) [29]. Cyclin D-cdk4/6 complexes proceed to phosphorylate retinoblastoma tumor suppressor protein (pRB), inactivating pRB and allowing the release of E2F, a family of transcription factors which is held inactive by pRB [29]. Upon entering the nucleus, E2F promotes the expression of proteins needed for cell cycle progression [29].

Among the genes expressed by E2F are additional cyclins, cyclin E and cyclin A [29]. Cyclin E is needed for G1 to S phase transition and complexes with cdk2, at to a lesser extent cdk1, to promote phosphorylation of pRB [29]. Cyclin A however, is expressed throughout S phase and G2 depending on the heterodimer formed; cyclin A association with cdk1 promotes S phase entry while cyclin A association with cdk2 promotes progression through G2 and even into mitosis [29]. Both cyclin A and cyclin E when in complex with cdk1 promote the expression of transcription factors such as nuclear factor Y (NF-Y), FoxM1, and B-myb, which themselves are needed for the expression of G2 proteins [29]. Furthermore, expression of cyclin A by E2F creates a negative feedback loop in which cyclin A phosphorylates E2F, inactivating it and decreasing the expression of Cyclin E which is needed for DNA replication initiation; this negative feedback loop ensures that replication of DNA only occurs once [29, 33, 34]. In addition, WEE1 kinase, expressed in S phase, phosphorylates cdk2 to inhibit cyclin E and cyclin A-cdk2 activity [11]. In contrast to cyclin A-cdk2 heterodimers, cyclin A-cdk1 complexes are sequestered to the cytoplasm where they regulate mitosis progression and stabilize cyclin B [34].

Cyclin B expression rises throughout G2 phase and is an important component for initiation of mitosis [29, 33]. Mitotic entry is promoted by cyclin-B complexing with cdk1 and activation of this

complex is achieved via dephosphorylation by cdc25c; cdc25 stabilizes cyclin B-cdk1 complexes and allows for nuclear localization [11]. In early mitotic events, the cyclin B-cdk1 complex facilitates chromatic condensation through phosphorylation of condensin, nuclear envelope breakdown, and, through promotion of survivin expression, spindle pole assembly and organization [11, 35, 36]. Degradation of cyclin B by the activated APC/C complex is a major event in the initiation of cytokinesis such that G1 initiation in daughter cells do not express cyclin B levels [37].

Cyclin Dependent Kinase Inhibitor p21

Cyclin Dependent Kinase Inhibitors

To regulate cyclin-cdk complexes, cyclin dependent kinase inhibitors (CKIs) bind to cdks in response to specific stimuli during organism development or during events of genotoxic stress, effectively inhibiting cell cycle progression [30, 38]. CKIs are divided into two family groups based on structure: the INK family, which include p15, p16, p18, and p19 and only inhibit cdk4 or cdk6 cyclin-cdk complexes, and the cip/kip protein group which includes p21, p27, and p57 [30, 31, 38]. The cip/kip family group is known to bind to a broader range of cdks and also some cyclins and helicases [30].

P21, also known as WAF1, cip1, sdi1, mda6, and CAP20, was the first identified member of the CKIs and is generally considered to be a tumor suppressor gene, based on mice studies in which p21 knockouts were more likely to acquire spontaneous tumors among a variety of their tissues [30, 38]. Further studies on this inhibitor has tied its function to regulating cell cycle progression, apoptosis inhibition, differentiation control, cellular migration events, cytoskeletal behaviors, DNA repair pathways, and senescence, ultimately defining p21 as a key player in cellular stress response systems [30]. As it has been found to be a master regulator of these different pathways, p21 itself is tightly regulated and its protein expression is influenced by several different stimuli.

Structure and Function of p21

Structure

As they belong to the same family, p21, p27, and p57 contain conserved regions at their N-terminals that are necessary and sufficient to inhibit their target cyclin-cdk substrates [38]. The C-terminal region of these proteins however are not conserved among the group and contribute to the broad range of additional binding partners these proteins can participate with, such as p21 interacting with PCNA [30, 38]. Despite their ability to bind preferentially to cdk2, this family can bind to several different cyclin-cdk complexes such as p21's ability to bind to and inhibit cyclin D-cdk6 complexes during cell cycle arrest in G1 [11, 38].

P21 specifically, is composed of 164 amino acids which converts to about 19kDa in size [30]. When unbound to any protein and unmodified, p21 secondary structure is about 80% unstructured and it completely lacks tertiary structure [30]. Phosphorylation, however, is a major posttranslational modification for p21 regulation as this protein contains 13 serines, 8 threonines, and 2 tyrosines; upon phosphorylation, p21 structure can become more defined as well as alters its localization and protein interacting partners and capacities [30].

P21 has been shown to bind most favorably to cdks which share at least 50% sequence homology to its N-terminus and can bind to cyclins which share about 25-40% sequence similarity to its cyclin binding domains, one domain at the N-terminus and the other domain at the C-terminus [30]. Furthermore, p21 contains a residue, Y77, which can disrupt the ATP binding pocket of cdks, ultimately inhibiting cdk activation [30]. These features within the p21 structure are the driving forces of its cyclin-cdk complex inhibition and cell cycle regulation abilities. Additionally, it contains two nuclear export signals (NES) and one nuclear localization signal (NLS), highlighting its dynamic ability to migrate between the cytosol and nuclease [30].

Phosphorylation is an important posttranslational modification of p21 as it helps to regulate the proteins localization, stability, and activity depending on the situation [30]. Of the 23 phosphorylatable residues within p21, eleven have distinctly known functional impact: T57, S130, T145, S114 and S146 influence p21 ability to regulate cell cycle progression or the DNA damage response, often by altering cyclin-cdk complex binding partners [30]. In addition, T153, along with the previously listed residues, also promotes p21 cytoplasmic localization [30]. Other residues have been suggested to inhibit PCNA binding (S160) or influence p21 interaction with apoptotic signal-regulating kinase 1 (ASK1) (S98) [30].

Role in Cell Cycle Progression

P21 is able to regulate cell cycle through several mechanisms including inhibition of cyclin-cdk complexes, acting as a binding partner to PCNA, and as a co-repressor of some genes of mitotic proteins like WEE1, polo-like kinase 1 (PLK1), and Aurora B [30]. As an inhibitor of cyclin-cdk complexes, p21 can disrupt their functions by the direct binding of its cyclin binding domains (found at either termini) or by its cdk binding domain (found towards the N-terminus) to the cyclin or cdk subunit of the complex, ultimately inhibiting the complex from activating cdks [39]. In addition, it has been shown that p21 may also inhibit cdks 1 and 2 by interfering with the phosphorylation of their activation domains, although the mechanism remains under-defined [39].

As p21 can target a broad range of cyclins and cdks for inhibition, its activity can be observed throughout G1 and within G2 phases of the cell cycle under normal cellular conditions; generally targeting cyclin D-cdk4/6 complexes and cyclin E-cdk2 complexes during G1 to S transitions and cyclin A-cdk2 complexes during S to G2 transitions [31, 39]. P21 protein levels significantly drop during S phase but begin to increase again during G2 [30]. Increased p21 levels was found to be important for G2 cell cycle checkpoint arrest as it inhibits activation of cyclin B-cdk1 complexes; it has been shown that cells

deficient of p21 resulted in increased aberrant centrosomes and inappropriate cytokinesis [30]. Through these mechanisms, p21 expression deters cellular ability to initiate DNA replication and mitosis [40].

Competitive PCNA binding is facilitated by p21 through its PCNA binding domain which sequesters PCNA from DNA polymerase-delta and other proteins necessary for DNA synthesis as well as DNA repair mechanisms like mismatch repair [38, 39]. During initiation of S phase, p21 levels significantly decrease to encourage replication origin firing and the activation of proteins required for DNA synthesis such as PCNA [39, 40].

Interestingly, localization of p21 has been shown to have opposing results in its function. While its nuclear function tends to support antiproliferative outcomes and a pause in cell cycle progression, studies have shown that p21 cytosolic function may be oncogenic and anti-apoptotic [30]. Cytosolic localization of p21 is thought to be stimulated by phosphorylation at T57, S130, T145, S146, and S153 residues and may be supporting cell cycle progression and prevention of apoptosis through low level binding to cyclin D-cdk4/cdk6 complexes and the inhibition of several caspases [30]. These findings are supported by the observation that aggressive tumors with poorer prognosis often show increased levels cytoplasmic p21 [30].

Inhibitor of Apoptosis

While the major transcription factor of p21, p53, is an essential component for DNA damage induced apoptosis, studies have repeatedly shown that p21 is at least unessential in this process and in some cases, actually inhibits apoptotic events [38]. Experiments performed in a variety of cell lines such as MCF-7, osteosarcoma cells, and colon cancer cells have led to this conclusion; in p53 wildtype osteosarcoma cell lines, overexpression of p21 before and throughout etoposide treatment protected cells from death and only when MCF-7 breast cancer cells expressing p21 were exposed to both TNF-α and p21 antisense cDNA did such cells induce apoptosis [38]. Similar effects were observed in

radiosensitized human colon cancer cells [38]. These studies support that p21 inhibits apoptotic events regardless of apoptotic agent.

Despite these experiments, the actual mechanism behind p21 inhibiting apoptosis is lacking; several pathways have been proposed [38]. One theory is that p21 may directly interact with and inhibit proteins which support apoptosis, such as procaspase 3 and 8 and the ASK1 kinase, and under such events, stabilize the apoptotic inhibitor protein, C-IAP1 [38]. Another mechanism suggests that it is the binding of p21 to cyclin A-cdk2 complexes that promotes the anti-apoptotic phenotype because activated cdk2 has been shown to be necessary for chromatin condensation and cell shrinkage under cell death [38]. Under this mechanism, caspase-3 would be required to cleave and thus inhibit p21 function, allowing cyclin A-cdk2 complexes to form [38]. To some extent, overactivation of cdk2 via cyclin E complexes has been shown to play some role in this process as well, as shown in HCT116 colon carcinoma cells where p21 activity has been inhibited by E1A after DNA damage [38]. An additional, more general theory supports the idea that by simply promoting cell cycle arrest, especially G2 arrest as discussed below, p21 prohibits cells from undergoing stress induced apoptosis and under these conditions, cellular arrest allows for sufficient time to repair the cell from stress inducers or enters senescence [38]. Despite these reports, other studies have found evidence to support p21 acting as a proapoptotic factor under certain conditions such as p21 overexpression resulting in increased BAX expression levels in p53 deficient human hepatoma cell lines [38]. Evidence has also led to the suggestion that proapoptotic mechanisms may also be cell type specific as this BAX induced expression by p21 was not observed in other cells lines such as melanoma [38].

It is not fully understood how cells experiencing stress decide to induce apoptosis or undergo cell cycle arrest and evade cell death in a p21 manner, especially under conditions of p53 activation which can promote the expression of proteins needed for both pathways [38]. As discussed below, it has been suggested that p53 induced cell cycle arrest depends on the amount of p21 expressed and

stabilized upon initial checkpoint signaling events [11]. As p21 generally inhibits apoptosis yet encourages cell cycle arrest in events of cell stress, p21 has become a major marker for cellular senescence [41]. It is important to note that the generally agreed upon idea that p21 inhibits apoptosis results in p21 having oncogenic potential, making the targeting of this protein for anti-cancer therapies complex and difficult [38].

Regulators of p21 Induction

Evidence suggests that p21 regulation occurs mostly at the transcriptional level, especially when considering cases of increased protein expression [38]. The major positive regulator of p21 is the transcription factor p53; the p21 promoter contains two p53 responsive elements (p53RE) to which p53 and its homologues p63 and p73, can bind [31, 38]. P53 induced p21 transcription traditionally occurs during DNA damage and activation of the DNA damage checkpoint kinase signaling cascades, as well as oxidative stress conditions [31]. Additional proteins can encourage p21 induction in a p53 dependent manner such as GADD34, a member of Hsp40 protein family which phosphorylates p53, increasing p53 affinity to the p21 promoter, and liver kinase B1 (LKB1) which interacts with p53 to encourage p21 induction [31]. Some studies have also supported that, under IFN-ϒ stimulation, STAT1 is able to induce p21 expression in a p53 dependent manner, however most research supports STAT proteins as inhibitors of p21 transcription [31, 38].

Other proteins that promote p21 transcription by both p53 dependent and independent mechanisms include BRCA1a and BRCA1b, splice variants of BRCA1, which stimulate the p21 promoter region via their C termini and independently promote p21 expression via Sp1 binding sites within the p21 promoter [31, 42]. Ras GTPase is also able to induce p21 transcription by both p53 dependent and independent pathways through activation of the transcription factor E2F [39].

However, research has shown that when examined for p53 and p21 levels, most human tissues express p21 independently of p53 [38]. To support this, cancerous cells even showed p21 was found to be expressed by p53 independent mechanisms; in one study it was found that 60% of breast cancers overexpressed p21 which did not correlate with the expressed levels of p53 [12]. Examples of these p53 independent mechanisms include Sp1 family members (as p21 promoter contains 6 distinct Sp1 binding sites) with the assistance of the transcriptional coactivators p300 and CREB-binding protein (CBP), activator protein 2 (AP2), Kuppel-like transcription factors KLF6 and KLF4 via p300-CBP, CDX2 member of the caudal-related homeobox gene family, CCAAT/enhancer binding protein-α and -β, and family members of the helix-loop-helix (bHLH) family, BETA2 and MyoD, also through p300-CBP [38, 39, 42]. Often, these p53 independent factors of p21 induced expression occur by inducing the binding to *cis*-acting elements (within the same region of DNA as the gene of p21) within the p21 promoter and occur under a variety of stimuli specific to each p21-inducing protein such as TGF-β treated cells inducing NF-Κβ dependent and SMAD dependent p21 upregulation [31, 42].

P21 Regulation

P21 Stability

P21 is a short-lived protein and is degraded by the 26S proteasome via ubiquitination when it is bound to other proteins such as cyclin-cdk complexes [12, 40]. However, p21 is also unique in that when it is unbound and in free-form, it can be degraded by the 26S proteasome without ubiquitination processes [12, 40]. This is thought to be possible due to the lack of p21 structure in its unbound state, allowing it to freely enter the 20S subunit pore via diffusion [40]. In this process, p21 binds directly to the C8-α subunit of the 20S proteasome catalytic chamber of the 26S complex [12].

Interestingly, one study on p21 stability observed that upregulation of the RAF/MEK/ERK pathway and phosphtidylionositol 3 kinase (pl3k) resulted in cyclin D1 protein increase and stabilization

of p21 protein levels [12]. In this study, researchers showed that fibroblasts expressing overactive RAS protein increased p21 levels in a cyclin D1 dependent manner through p21 binding to cyclin D1 via its C-terminal cyclin binding site, which has previously been shown to overlap with the PCNA binding domain on the C-terminal end of p21; it has been shown that p21 binding to PCNA helps to reduce p21 turnover by blocking the C8-α subunit binding domain on the p21 C-terminus [12]. It was suggested that cyclin D1 binding to the second p21 cyclin binding domain also inhibited the C8-α subunit; researchers however were not able to determine if this inhibition of p21 degradation was due to cyclin D1-cdk complexes or cyclin D1 alone was binding to p21 [12]. Apart for cyclin D1, the binding of Waf1 Cip1 stabilizing protein 39 (wisp39) and heat shock protein 90 (HSP90) have also been suggested to protected p21 from proteasomal degradation [29]. Akt kinase has been shown to phosphorylate p21 at S146 to increase its stability as well as alter its localization [30]. Aside from protein stabilization, p21 mRNA levels have also been shown to be stabilized by p38 MAPK phosphorylation of RNA-binding protein, HuR, especially during activation of ATM-CHK2 DNA damage signaling cascades [11].

Phosphorylation has also been shown to regulate protein stability of p21; phosphorylation of T57, S130, T145, and S146 promote protein stability while phosphorylation of T57, S114, S130, and S146 can promote p21 degradation, depending on the kinase adding the posttranslational modification [30]. As discussed below, the role of p21 in multiple cellular events requires its stability and degradation to be dynamically controlled by a various pathway depending on the stimuli and situation [30].

P21 Inhibitors and Degradation

Major facilitators of p21 degradation are the E3 ligases SCF^{Skp2}, $CRL4^{cdt2}$, and APC/C^{cdc20} [30]. SCF^{Skp2}, or Skp1-Cullin-F-box/S phase kinases-associated protein 2, regulates p21 levels mostly during G1 and S phases of the cell cycle, however can also promote its degradation in G2 [30]. SCF^{Skp2} holds a higher affinity for p21 when it is phosphorylated on S130 and in complex with cyclin E-cdk2

heterodimers [30]. It is cyclin E- cdk2 complexes that phosphorylate p21 at serine 130 to promote its degradation [40].

$CRL4^{cdt2}$, or Cullin 4-RING ubiquitin ligase/Cdc10-dependent transcript 2, has been shown to regulate p21 levels under conditions of UV irradiation, when p21 is phosphorylated at S114 and bound to PCNA [30]. Under these specific circumstances, the $CRL4^{cdt2}$ ensures that p21 degradation is S phase specific, contributing to replication regulation processes [43].

During prometaphase, APC/C^{cdc20}, or Anaphase-promoting complex/cyclosome, cell division cycle 20, promotes degradation of p21 via a destruction D-box motif at the center of the p21 amino acid sequence [30, 40]. This degradation occurs when p21 is in complex with cyclin B/cdk1 heterodimers [30, 40]. APC/C complex is interesting in that it exhibits a duality of p21 regulation, in S phase, APC/C complexes with its cdh1 coactivator (APC/C^{cdh1}) to promote p21 stability by degrading SKP2 and its other coactivator cdc20 [40]. However, when APC/C is in complex with cdc20, it promotes p21 degradation during mitosis [40]. This decrease in p21 expression during mitosis is essential for increased levels of cdk1 and the prevention of errors during mitotic spindle assembly checkpoint events that could result in aneuploidy [40].

Aside from E3 ligases, other proteins negatively regulate p21 at the transcriptional level. Selenoprotein W (SWEP1) is involved in cell cycle progression by decreasing p21 transcription in a p53 inhibitory manner [31]. Delta EF1 also decreased p21 expression by blocking its transcription via binding to an E2box element at its promoter [31]. Additionally, in cancers, STAT family of proteins have been shown to repress p21 expression, resulting in tumorigenesis [31]. Similarly, overexpression of MYC has shown to repress transcription of p21, also promoting tumorigenesis [39]. Lastly, KAP1 has been shown to terminate p21 transcription by binding to its promoter and is important for G2 checkpoint kinase recovery [11].

Checkpoint Signaling Cascades

Checkpoint signaling cascades are important cellular events which connect cell cycle progression with the DNA damage response (DDR). Under instances of DNA damage, cells must be able to detect the damage and pause the progression of cell cycle to aliquot sufficient time for damage repair [11]. This pause in cell cycle progression is sometimes referred to as checkpoint activation cell cycle arrest and in most occurrences is a reversible process [11, 44]. Two pathways of checkpoint activation cell cycle arrest include the DNA damage checkpoints, which arrest cells in G1 or G2/M phases or slows replications in S phase, and mitotic spindle checkpoint, which arrest cells in M phase [11, 44].

DNA Damage Checkpoint Signaling Cascades

The DNA damage checkpoints involve DNA damage such as intra- or inter-strand crosslinking, DNA adducts, single stranded breaks, and double or single stranded breaks, leading to a network of signal transduction pathways [44, 45]. Depending on the break different repair mechanisms occur, however, in general, phosphatidylinositol-3 kinase-like protein kinases (PIKKs) family of protein kinases are the first to be activated and initiate repair. Included in this family are Ataxia-telangiectasia mutated kinase (ATM), ATM and Rad3 related kinase (ATR), and the DNA-dependent protein kinase catalytic subunit kinase (DNA-PKcs) [46]. ATM and ATR related DNA damage checkpoint and downstream proteins are discussed below.

ATM and Downstream Proteins of the DNA Damage Checkpoint Signaling Cascade

ATM is mostly considered to respond to DNA damage occurring in the form of double-stranded breaks through its DNA-scaffolding partner, the MRN complex, which consists of MRE11, RAD50, and NBS1 [11, 45, 46]. The MRN complex localizes to the site of DNA damage and recruits ATM, which then undergoes autophosphorylation at serine 1981 to transform from its homodimer inactive structure to a monomeric active structure (Figure 5) [46]. Upon this activation, ATM phosphorylates H2AX near the

site of damage at serine 139 which recruits Mediator of DNA damage checkpoint protein 1 (MDC1), which recruits additional ATM kinases (Figure 5) [11, 46]. Furthermore, ATM also recruits checkpoint kinase 2 (CHK2) to the site of damage and phosphorylates this kinase at threonine 68 (Figure 5) [46]. Activated CHK2 and ATM then promote the stabilization and phosphorylation of p53 at serine 15 (Figure 5) [11, 46]. This activation and stabilization of p53 induces the transcription of a variety of cell cycle regulators including p21 which inhibits cyclin D-cdk4/6 and cyclin E-cdk2 complexes (Figure 5) [11]. In addition, CHK2 also inhibits Cell Division Cycle 25A (Cdc25A), part of the family of dual-specificity phosphatases, to prevent the removal of phosphate groups from cyclin E-cdk2 complexes, keeping them inactive (Figure 5) [11]. Together, CHK2 and p21 thus both effectively pause cell cycle progression under DNA damage.

As ATM most commonly responds to double stranded breaks (DSBs), repair processes facilitated by its activation include non-homologous end joining (NHEJ) in G1 and homologous recombination (HR) in S and G2 phases [46]. Despite this, studies have shown that activated ATM and CHK2 are not entirely necessary for DNA damage checkpoint arrest in G2 due to the activation of the ATR-CHK1 checkpoint pathway [11]. Despite this, CHK2 will inhibit the activities of Cdc25A, and also Cdc25B and C, which prevents the removal of phosphates from cyclin A-cdk1/2 and cyclin B-cdk1 complexes, keeping them inactive, while p21 will bind to and thus inhibit both cyclin A-cdk1/2 and cyclin B-cdk1 to assist in G2 cell cycle arrest [11].

Unlike G2 DNA damage checkpoints, the ATM-CHK2 DNA damage checkpoint in G1 is reversable for several days after arrest has occurred and the steps to undergo re-entry into cell cycle progression are distinct from that of G2 [11]. During G1 cell cycle arrest, cells enter a state of quiescence in which levels of p53 and p21 are suspected to “oscillate” as the DSB is repaired [11]. This quiescent state appears to share some similarities with senescence, such as increased p21 levels, however agreement on the expression of other biomarkers between the two paused cell cycle states, such as increased β-

galactosidase expression, appears mixed and may be mostly contributed to cell type [47, 48]. Unlike senescent cell however, this quiescent state is reversible and exists only to provide enough time to DNA damage repair following a reintroduction into early G1 [11]. If the DNA damage intensity is too severe,

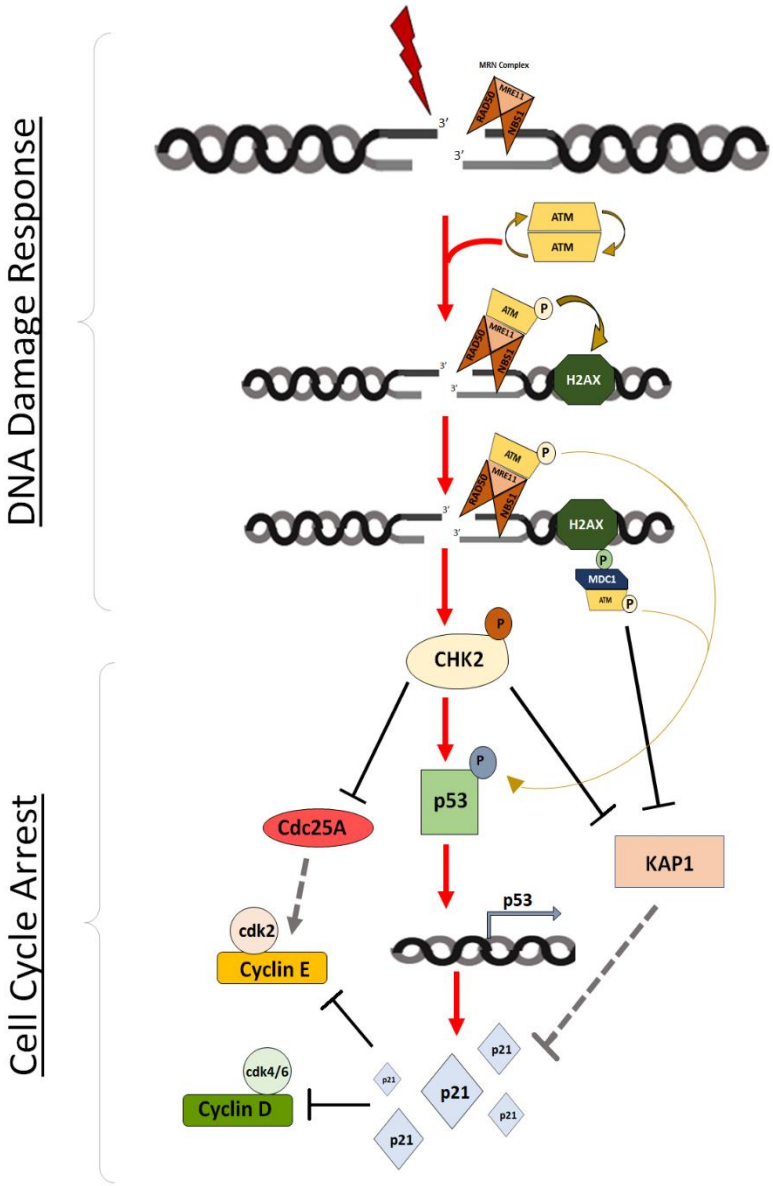

Figure 5. ATM and downstream proteins of DNA damage checkpoint signaling cascade. After a double stranded break the MRN complex localizes to the site of DNA damage and recruits ATM. ATM then undergoes autophosphorylation to transform into a monomeric active structure. This activation induces ATM phosphorylation of H2AX to recruit MDC1 and phosphorylation of CHK2. Activated CHK2 and ATM then inhibit the activity of KAP1 and promote the stabilization and phosphorylation of p53, which induces the transcription of a variety of cell cycle regulators including p21, which inhibits cyclin D-cdk4/6 and cyclin E-cdk2 complexes. In addition, CHK2 also inhibits Cell Division Cycle 25A (Cdc25) to prevent activation of cyclin E-cdk2complexes. Adapted from Woods et al. (2013) and Shaltiel et al. (2015) [11, 45].

and repair does not occur fast enough, potentially judged by the number of p53 oscillations, the quiescent cell will enter irreversible cell cycle arrest and G1 senescence [11].

Interestingly, the major player of this reversible arrest is not decreased ATM activity, as ATM inhibitors are not sufficient to allow cell cycle re-entry [11]. While ATM is necessary to initiate arrest, it is CHK2 and p38 MAPK that largely dictate arrest maintenance as they both stabilize p53, and p38 MAPK specifically stabilizes p21 mRNA (Figure 5) [11]. In addition, another factor regulating sustained arrest is downstream pathways which regulate p53 transcriptional targets, such as p21 [11]. KAP1, which terminates p21 transcription by binding to its promoter, is an example of such downstream pathways (Figure 5) [11]. KAP1 function is repressed by phosphorylation via ATM, CHK1, and CHK2; if KAP1 function is severely inhibited, prolonged p21 transcription and G1 arrest will occur [11]. Thus, while ATM initiates this DNA damage checkpoint signaling and p53 activation induces the cell cycle arrest through its transcriptional activity, other proteins, such as CHK2, p38 MAPK, and p21 levels are the significant regulators of prolonged G1 arrest or cell cycle re-entry [11].

ATR and Downstream Proteins of the DNA Damage Checkpoint Signaling Cascade

ATR is mainly considered to respond to DNA damage occurring in the form of single stranded breaks (SSB) that often arise through UV irradiation, replication stress, nuclease activity, and helicase activity following inter- or intra-stranded crosslinks [45]. After breaks are coated with replication protein A (RPA), ATR-interacting partner ATRIP is recruited to the single stranded region, bringing ATR; ATR is then activated by TOPBP1, which itself is recruited to site of damage by the 911 complex (comprised of RAD9, RAD1, and HUS1) (Figure 6) [46]. Activation of TOPBP1 via phosphorylation is strongly supported to be through activated ATM and the MRN complex, highlighting the interdependence between the two different pathways [46]. Upon its activation, ATR phosphorylates downstream Checkpoint kinase 1 (CHK1) at serine 317 and serine 345 (Figure 6) [45, 46]. With this activation, CHK1 is also stabilized by

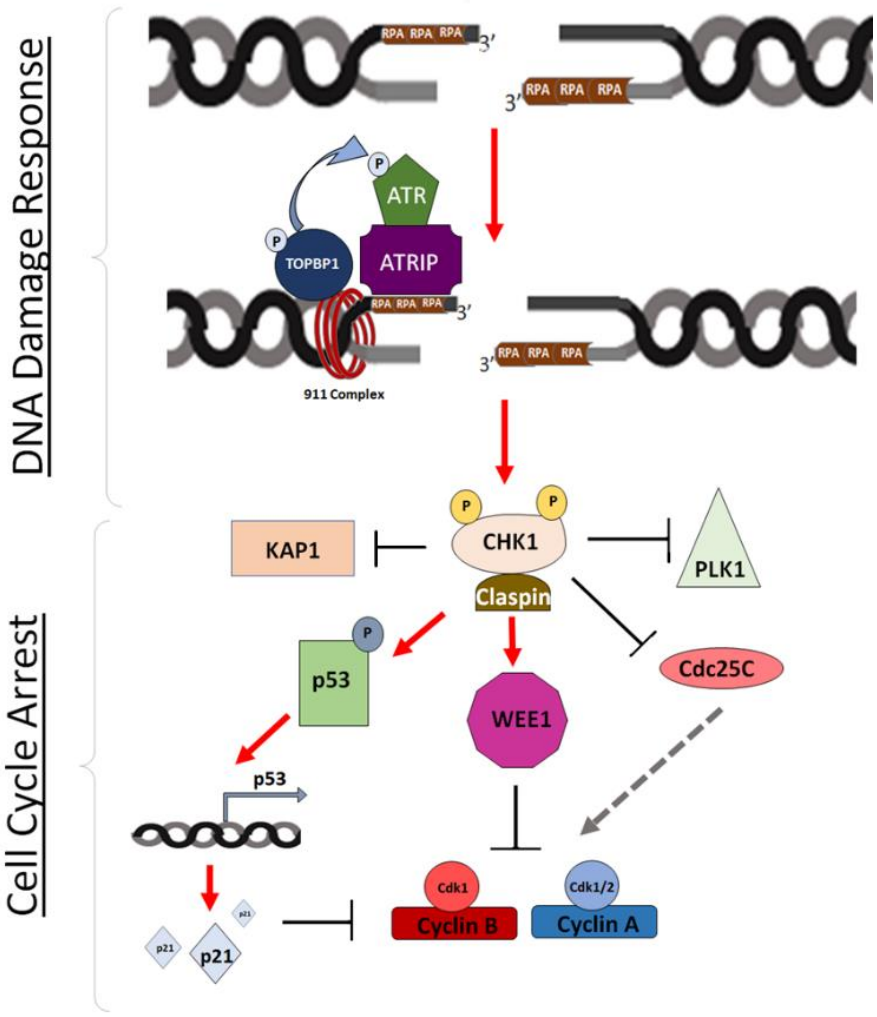

Figure 6. ATR and downstream proteins of the DNA damage checkpoint signaling cascade. ATR responses to DNA damage occurring in the form of single stranded breaks. After breaks are coated with RPA, ATRIP is recruited to the single stranded region with ATR. ATR is then activated by phosphorylated TOPBP1, which is recruited to the damaged site by the 911 complex. Upon its activation, ATR phosphorylates CHK1 which is stabilized by Claspin. CHK1 inhibits Cdc25C resulting in an inhibition of cyclin A-cdk1/2 and cyclin B-cdk1 complexes, stabilizes p53 to induce p21 expression, activates WEE1, and inhibits KAP1 and PLK1. Adapted from Woods et al. (2013) and Shaltiel et al. (2015) [11, 45].

Claspin, which is recruited to the site of damage via phosphorylated RAD17 by activated ATR (Figure 6) [45, 46].

As with ATM activation of CHK2, ATR-activated CHK1 results in the inhibition of the CdC25 family of phosphatases, specifically Cdc25C in G2 but also Cdc25A and B, resulting in inhibition of dephosphorylated cyclin A-cdk1/2 and cyclin B-cdk1 complexes, ultimately keeping them inactive (Figure 6) [11, 45, 46].

Additional downstream substrates of CHK1 include p53, which it stabilizes for increased p21 expression, WEE1 (known to inhibit CDK1 via phosphorylation) via phosphorylation, KAP1 via phosphoryation, and the miotic polo-like kinase 1 (PLK1), which holds a major involvement in mitotic entry as it assists with cdk1 activation, centrosome maturation, spindle formation, cytokinesis (Figure 6) [11, 45]. Through these interactions with downstream proteins, activated ATR and CHK1 successfully arrest cells [45]. Moreover, the ATR-CHK1 pathway specifically occurs only in S and G2 phases of the cell cycle and is essential for cellular arrest at G2 phase [11].

Contradictory to G1 cell cycle arrest through the ATM-CHK2 checkpoint signaling cascade, cell cycle arrest and subsequent re-entry is less common in the ATR-CHK1 G2 signaling pathway; in most cases, this G2 arrest is irreversible [11]. In one study, it was observed that within 8 hours of DNA damage, cells in G2 had achieved permanent senescence, compared to a time-frame of days for cells induced with DNA damage in G1 [11]. This drastic difference is due, in part, to cdk based protein interactions in G2 and whether there are sufficient levels of proteins essential for mitotic entry.

Cdk2 activity is important for re-entry into cell cycle progression for cells arrested in G2 [11]. Cdk2 activates transcription factors FoxM1, B-myb, and NF-y which are required for transcription of G2-specific genes [11]. Thus, decreased Cdk2 levels influence cellular ability to re-enter the cell cycle and progress into mitosis [11]. In addition to this dependence on cdk2, pre-activation of APC/C with its G1/S coactivator cdh1 can occur during DNA damage in G2 if cdk levels remain low enough to allow their interaction [11]. As APC/C targets many mitotic proteins for proteasomal destruction (such as PLK1 and cyclin B1), cells cannot effectively progress to mitosis so long as APC/C^{cdh1} remains active, thus promoting permanent cell cycle arrest and senescence [11]. These features of G2 arrest highlight the delicate balance of cdk levels required; in G2 there must be enough cdk for cell cycle re-entry, however low enough levels to allow for sufficient cell cycle pause and repair.

In addition to cdks, p53 levels also play an important role; it has been shown that p53 is sufficient to arrest cells at G2 independent of the occurrence of DNA damage [11]. As such, p53 levels are tightly regulated by inhibitors wip1, which dephosphorylates p53 to promote degradation, and mdm2, an E3 ligase that targets p53 for proteasomal degradation and inhibits its transcriptional abilities [11]. As p53 activity increases under G2 checkpoint cell cycle arrest, the importance of its regulators becomes imperative for cell cycle reentry. Luckily, p53 creates a negative feedback loop of its activity in which it is a transcription factor for both wip1 and mdm2 [11]. Of interest, it is this regulation that results in oscillating p53 levels observed during G2 arrest [11]. However, data has suggested that the strength of the first oscillation of p53 levels, the amount of p53 activated under initial G2 checkpoint signaling, is the deciding factor between irreversible G2 arrest and senescence versus re-entry into cell cycle and induction of mitosis [11]. This again, is in contrast to ATM-CHK2 G1 checkpoint arrest which seems more dependent on the number of p53 oscillations and the extent of the damage DNA [11]. Importantly, just as p53 is sufficient to induce permanent cell cycle arrest for cells in G2, cells absent of p53 are unable to participate in sufficient G2 checkpoint arrest even in the presence of DNA damage, progressing onto mitosis [11].

It has been shown that, possibly to avoid permanent senescence, G2 cells with activated checkpoint signaling may resume cell cycle progression and enter mitosis [11]. In most cases, cells that enter mitosis with damaged DNA will initiate cell death during the process of division, however with less severe damage, cells may bring damaged DNA into the G1 phases of daughter cells and reinitiate checkpoint arrest under conditions that allow a longer time for recovery [11]. Proteins suspected to be involved this this occurrence are PLK1, which must be completely degraded for G2 cell cycle arrest to occur, and cdk2 [11]. It is predicted that activated cdk2 present during mitotic exit influences the state of cell cycle upon entry into G1 under these events. PLK1, which activates cdk1/cyclin B1 complexes for

mitotic entry, has been shown to gradually increase in activity during DNA damage in G2 and that once a threshold is reached, cells will progress to mitosis, despite damage [11].

Mitotic Spindle Assembly Checkpoint Signaling Cascade

As stated previously, checkpoint signaling cascades are important cellular events which connect cell cycle progression with the DNA damage response (DDR). However, research has shown that that ATM and ATR DNA damage responses are inhibited during mitosis [11]. Specifically, PLK1 which mainly functions to encourage maturation of centrosomes in late G2, phosphorylates CHK2 to stop its recruitment to any DNA damage sites and inhibits CHK1 activity by encouraging SKP1-cullin-1-F-box-βTRCP-complex ($SCF^{\beta TRCP}$) to degrade claspin [11]. As a counter-event to this, the mitotic spindle assembly checkpoint is the signaling cascade used to regulate the exit of cells from mitosis.

Mitotic spindle assembly checkpoint occurs during mitosis when condensed chromosomes must achieve correct spindle microtubule attachment [37]. Without correct attachment, incomplete chromosome segregation may occur resulting in daughter cells with aberrant genomes and aneuploidy [37]. Under occurrences of miss-attachment, spindle assembly checkpoint proteins are recruited to form the mitotic checkpoint complex (MMC) which inhibits the anaphase promoting complex, APC/C, a multiprotein E3 ligase complex, until ideal pairing occurs [37].

APC/C is active from metaphase to the end of G1 and its activity is necessary for mitotic exit and G1 progression through degradation of cyclins, securin, and mitotic kinases [11]. This complex also requires two individual co-activators, Cdh1 and Cdc20, which are implicated in different phases of the cell cycle [37]. Cdc20 activates APC/C following chromosomal alignment [11].

Spindle assembly checkpoint proteins include the budding uninhibited by benzimidazoles 1 (Bub1), bub-related 1 (BubR1), monopolar spindle 1 (Msp1), AuroraB, mitotic arrest deficient-like 1 (Mad1), mitotic arrest deficient-like 2 (Mad2), bub-related 3 (Bub3), and bub3-interacting GLEBS-motif-

containing ZNF207 (BuGZ) (Figure 7) [37]. This complex of proteins is recruited to the kinetochore during prometaphase for assessment of chromosome attachment (Figure 7) [37]. Upon miss-attachment, Mad2, BubR1, and Cdc20 combine to form the mitotic checkpoint complex (MCC) which then binds to APC/C and adopts an open conformation, positioning APC/C away from UBE2C, the E2 ligase necessary for ubiquitin transfer to target substrates (Figure 7) [37].

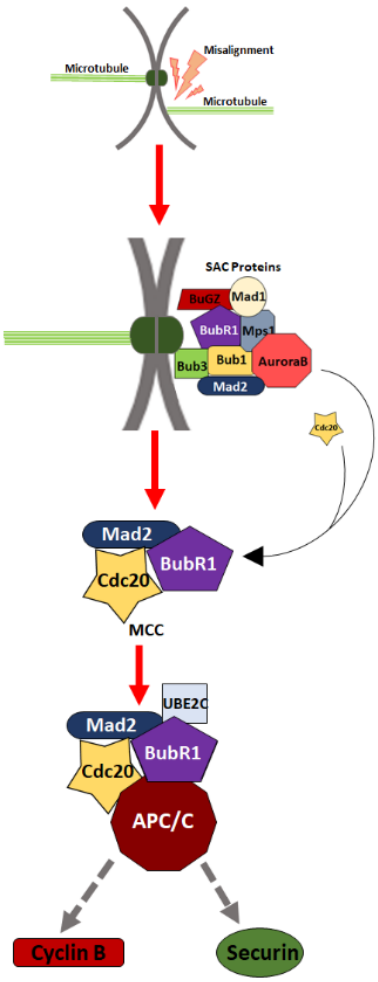

Figure 7. Mitotic spindle assembly checkpoint signaling cascades. During prometaphase, microtubules attach to kinetochores to align condensed chromosomes and the spindle assembly checkpoint proteins are recruited to the kinetochore to assess attachment. Spindle assembly checkpoint proteins include Bub1, BubR1, Msp1, AuroraB, Mad1, Mad2, Bub3, and BuGZ. Upon miss-attachment, Mad2, BubR1, and Cdc20 combine to form the MCC, which then binds to APC/C, positioning APC/C away from UBE2C and inhibiting APC/C from ubiquitinating cyclin B, securin, and other mitotic proteins for degradation. Adapted from Kapanidou et al. (2017) [36].

Upon alignment of sister chromosomes at the metaphase plate with properly attached kinetochores, the MCC is disassembled, releasing APC/C and its co-activator Cdc20, now phosphorylated by cdk1 for affective APC/C Cdc20 binding, to recruit substrates cyclin B and securin for ubiquitin

mediated proteasomal destruction (Figure 7) [37]. Degradation of securin allows for the separation of sister chromatid [40]. As cyclin B is degraded, the cyclin B-cdk1 complex becomes inactivated, initiating events of cytokinesis.

Interestingly, prior to the formation of the MMC complex, research has suggested that CHK1 also helps to regulate the mitotic spindle assembly checkpoint through activation of AuroraB kinase, despite the degradation of the CHK1 scaffolding protein claspin [45]. In support of this, studies have shown that depletion of CHK1 results in a failure to activate the spindle assembly checkpoint via improper localization of AuroraB and downstream MCC proteins [45].

Deubiquitinating Enzymes Implicated in Cell Cycle Progression and Cellular Checkpoint Kinase Cascades

Many proteins which are required for cell cycle progression are regulated by ubiquitination and the E1-E2-E3 ligase cascade. As such, deubiquitinating enzymes (DUBS) have also been discovered to play a part in supervising cell cycle progression and the occurrence of cellular checkpoints (Song and Rape, 2009).

DUBS which mainly act as housekeeping proteins of the cell must keep the level of intracellular ubiquitin relatively stable for future use [44]. Such enzymes achieve this by cleaving ubiquitin from proteins marked for degradation just prior to that protein making contact with the 26S proteasome [44]. If this cleavage does not occur prior to contact with the 26S proteasome, cellular division may be retarded due to a depletion of intracellular ubiquitin and experience 26S proteasome deficiencies [44].

Deubiquitinating Enzymes Known to Participate in Cell Cycling Events

As observed in a great many other pathways, DUBs can indirectly participate in cell cycle events by directly interacting with E3 ligases or transcription factors that function to mediate cell cycle and check points. BRCC36 of the JAMM/MPN-domain DUB family propagates the catalytic activity of the E3

ligase BRCA1/Bard1 which can, in turn, facilitate G2/M check point arrest in response to DNA damage [44].

USP1 of the USP family of DUBs was shown to inhibit proteasomal degradation of a family of transcriptional repressor proteins called inhibitors of DNA binding, promoting their stability and thus leading to the inhibition of p21 transcription [14].

The OTU family member A20 can inhibit the NF-κB pathway through deconjugation of K63 ubiquitin chains on several difference substrates such as the adaptor protein, TRAF6, the receptor-interacting kinase 1 (RIP1), and the inhibitors of NF-κB regulatory component (IκB) regulatory subunit, IKKϒ (NEMO) [44, 49]. Deubiquitinating of these proteins stabilizes NF-κB in the cytosol and prevents the initiation of proliferative and pro-cell survival events [44].

More directly, the DUB USP7 binds to the E3 ligase Mdm2 and prevents its autoubiquitination and self-degradation [44]. Depletion of Mdm2 in such a manner could lead to p53 accumulation and subsequent cell cycle arrest in G2 or G1 [14, 44]. USP7 also deubiquitinates the mono-ubiquitination of transcription factor Foxo4 to inhibit the transcription of p27 and resume cell cycle once the cell has overcome external or internal stressors [44].

In addition, the DUB USP28 has been shown to be required for transcription factor c-MYC induced apoptosis and proliferative functions; USP28 complexes with c-MYC and its E3 ligase $SCF^{Fbw7\alpha}$ to protect c-MYC ubiquitin mediated degradation [44].

Deubiquitinating Enzymes Known to Participate in Checkpoint Signaling Cascades

As a convenient regulatory mechanism, DUBs play functional roles in both DNA damage checkpoints and mitotic spindle assembly checkpoints. Previously mentioned, DNA damage checkpoints and checkpoint signaling cascades are imperative for relationship between DNA damage repair and cell

cycle regulation. As with cell cycle progression, multiple posttranslational modifications are found within DNA damage checkpoint signaling cascades such as deubiquitination processes. Specifically, one study found that 32 of the 95 known DUBs localized to sites of DNA damage [11, 14].

Several DUBs have been shown to facilitate the elimination or the modification of K63 ubiquitin chains formed at DSBs by RNF8 and such regulatory events impact downstream repair pathways activated during cell cycle checkpoint arrest [11]. To name a few, the previously mentioned BRCC36 DUB has been suggested to hold a nuclear function of recruiting BRCA1 at DSBs to facilitate HR and removing RNF8 induced K63 ubiquitins chains [14]. Another JAMM/MPN-domain DUB associated with K63 chain removal at DSB sites is POH1 which may function to promote HR repair over NHEJ in collaboration with USP5; USP5 is an additional DUB suggested to remove K63 ubiquitin chains at damaged sites based on siRNA studies which showed its localization to sites of DSB [14]. In another siRNA study, OTUB2 was also observed to remove RNF8 induced K63 ubiquitin chains, however its activity was shown to inhibit HR repair processes [14].

Furthermore, USPs 3 and 44 have also been shown to regulate double stranded break DDR by reducing the size and number of DNA damage foci when overexpressed [11]. In addition, according to one study, depletion of DUBs USP4, USP37, and the previously mentioned POH1 were found to specifically impact checkpoint kinase signaling as determined by comet assays [11].

DUBs involved in resuming cell cycle progression once DNA damage is repaired include USP1 which removes the monoubiquitination from FANCD2 and PCNA once they are no longer needed for repair of interstrand cross-links and translesion synthesis [44]. These monoubiquitination events are partially initiated by CHK1 under conditions of cell cycle arrest [45]. In one study, USP1 depletion or decreased deubiquitinating activity was associated with onset of senescence through increased levels of monoubiquitinated FANCD2, reducing replication fork progression, eventually initiating G2/M

checkpoint kinase activation [50]. Interestingly, the study did not observe accumulation of monoubiquitinated PCNA, suggesting this senescent phenotype is FANCD2 specific [50].

In the mitotic spindle assembly checkpoint, upon misorientation of chromosomes and microtubules, spindle assembly checkpoint proteins are recruited and form the mitotic checkpoint complex (MCC) which inhibits APC/C from initiating mitotic exit [37, 44]. Once chromosomes are correctly oriented and move to the metaphase plate, the MCC disassembles, allowing for cdc20 to be multi-ubiquitinated by APC/C as well as the ubiquitination of additional proteins such as cyclins [37, 44]. An additional regulatory mechanism exists however, through the DUB USP44 which deubiquitinates cdc20 [44]. This deubiquitination prevents premature spindle assembly checkpoint termination by stabilizing the MAD2-Cdc20 interacting within the MCC, until ideal attachment is achieved [44].

Despite these reports of DUBs regulating the DDR and checkpoint signaling cascades, a fuller understanding of DUBs in cell cycle arrest and initiation of cellular progression is desirable. Because ubiquitin is a dynamic regulatory mechanism not entirely unlike phosphorylation or other types of protein modifications, it is not surprising that E1-E2-E3 signaling cascades and correspondingly, deubiquitinating enzymes, are important players in the intricate pathways of cell cycle regulation, arrest, and progression. However, due to several deubiquitinating enzymes holding more than one function and often possessing more than one binding partner, it is likely that there are additional DUBs whose roles in such cellular regulation are not yet discovered. Focusing efforts to uncover additional DUBs that many also mediate the cell cycle will allow a clearer understanding of cellular proliferation dynamics and potentially introduce new therapeutic targets against cells which no longer adhere to healthy canonical behaviors.

Chapter Three: OTUD6B Protein Levels Impact p21 Expression

Rational

OTUD6B is a member of the OTUD family of DUBs [10]. Its functional capacities are currently underdeveloped however studies suggest it may be involved in translational regulation, cell growth rates, or be vital for 26S proteasomal formation [17, 20, 23]. Specifically, Sobol et al. (2016) has shown data to suggest that OTUD6B isoform 1 inhibits protein synthesis in non-small cell lung cancers and that the expression level of isoform 1 may be downregulated in support of cellular proliferation and transformation [20]. Additionally, in mice B lymphocytes it has been shown that OTUD6B overexpression reduces cell proliferation, alters cell cycle profiles to show increased G1 arrest, and increases the percentage of apoptotic cells via Annexin-V staining [23]. This study furthermore showed that in mice lymphocytes and HeLa cell lines, when OTUD6B was overexpressed, cyclin D2 levels were significantly decreased [23]. Cyclin D2, when in complex with cdk4, promotes the progression of cells from G1 phase to S phase within the cell cycle and is an important substrate for p21 cyclin dependent kinase inhibitor (cdki) [30].

More recently however, whole-exome sequencing analysis studies have reported that mice and humans with loss of function *OTUD6B* alleles experience developmental delays, congenital heart and musculoskeletal defects, and brain structure abnormalities [17]. The analysis of subjects' peripheral blood mononuclear cells also suggested a reduced incorporation of the 19S subunit of the proteasome and the accumulation of ubiquitin-protein conjugates, suggesting that OTUD6B was important for proteasome formation [17]. These findings contradict previous reports in that they support OTUD6B function being vital for development, cellular growth, and cellular proliferation, rather than inhibit such

events. Furthermore, genomic expression analysis of various cancers show that *OTUD6B* is amplified in several cancers; most notably cancers of the breast and prostate, further supporting OTUD6B in enhancing cell growth [25, 26].

Due to these contradicting results involving the role of OTUD6B in cellular proliferation, we explored if OTUD6B protein levels could impact major cell cycle regulators. Our findings have shown that OTUD6B levels negatively correlate with protein expression of p21 in various cancer cell lines and may regulate p21 expression in a p53 dependent manner. P21 is a major regulator of cell cycle progression in G1 and G2 phases of the cell cycle and its expression is tightly regulated by various transcription factors, E3 ligase complexes, and other enzymes [31]. It is also a downstream requirement for successful DNA damage checkpoint cell cycle arrest via p53 and CHK1/CHK2 activation [11]. Thus, this data not only supports OTUD6B as a propagator of cellular proliferation, and provides clarity into OTUD6B functional role in cancer and cell cycle regulation.

Experimental Design

Cell Lines and Chemical Reagents

HEK293T and HeLa cells were purchased from the American Type Culture Collection (ATCC). MDA-MB231, MCF7, U2OS, T80, and MIA-PaCa-2 cells were gifted from Dr. Meera Nanjundan at the University of South Florida's Cell and Molecular Biology Program. HEK293T, MDA-MB231, MCF7, U2OS, and HeLa cells were cultured in Dulbecco's Modified Eagle's Medium (DMEM) supplemented with 10% bovine serum and 10% Penicillin-Streptomycin with L-glutamine except for in cases of siRNA and DNA transfections. T80 ovarian cancer cells were cultured in RPMI supplemented with 10% bovine serum and Penicillin-Streptomycin with L-glutamine except for in cases of siRNA and DNA transfections. Cells were grown at 37^{O}C in 5% CO_2 atmosphere.

Cycloheximide (CHX) was purchased from Sigma-Aldrich and used at 10uM per sample at indicated timepoints 72 hours after siRNA transfection. Puromycin dichydrochloride (Puromycin) was purchased from Fisher Scientific and was used at 1ug/mL.

Plasmids

Plasmids used were OTUD6B Double Nickase Plasmid (h2): sc-407482-NIC from Santa Cruz technologies (described in Chapter 3, Experimental Design, OTUD6B Knockout Cell Line), Flag-HA-OTUD6B retroviral overexpression plasmid, with a pDEST_LTR_N_FLAG_HA_IRES_puro backbone, purchased from Addgene, a pOZ-FH-N-BMI1 retroviral endogenous expression plasmid previously developed in the Kee Laboratory, backbone acquired from Dr. Alan D'Andrea Laboratory at the Dana-Farber Cancer Institute, and p3XFlag-CMV-9 nonretroviral overexpression vector purchased from Addgene.

Creation of p3xflag-CMV-9-OTUD6B Plasmid

OTUD6B cDNA from T80 was cloned into p3XFlag-CMV-9 nonretroviral overexpression vector using procedures previously described in our laboratory [51]. Briefly, primers were designed to amplify OTUD6B isoform 1 flanked by restriction sites targeted by EcoR1 and Xbal for the forward and revers primers respectively:

Forward: 5' ATA **GAAT TCA** ATG GAG GCG GTA TTG AC 3'

Reverse: 5'ATA **TCT AGA** TT AGC TGC AAT TTT CAG TAA CTA TG 3'

where restriction sites are highlighted in bold and red letters indicate nucleotides inserted to ensure OTUD6B expression remained in-frame with the encoded Flag-tag sequence (Figure 8, A).

Conventional polymerase chain reaction (PCR) was used to amplify the targeted sequence from 736.4ng of cDNA following a PCR purification using AccuPrep PCR Purification Kit from Bioneer. PCR

reaction contained 1uL of T80 cDNA, .5uL of Phusion High Fidelity DNA polymerase (Thermo Scientific), 10uL of 5x HF buffer, 2uL of DNTPs, and 2uL of each the forward and reverse primer, brought up to a total reaction mixture of 50uL with H_2O. Annealing temperature was 55^oC with 35 cycles.

Digestion of 16uL of amplified OTUD6B cDNA and 500ng of empty p3xflag-CMV-9 plasmid occurred for 2 hours at 37^oC with 1uL of EcoR1 and Xbal restriction enzymes each and New England Biolabs (NEB) buffer 2.1. Insert was heat inactivated at 65^oC for 20 minutes. p3xflag-CMV-9 plasmid was run on a 1% agarose gel and gel extracted using AccuPrep Gel Extraction Kit from Bioneer. A 1 hour, room temperature ligation using 1uL of DNA T4 ligase and T4 ligase buffer (NEB) was performed at a 2:6 plasmid to insert volume ratio.

Potential p3xflag-CMV-9-OTUD6B plasmids were then transformed into Top10 competent E.coli cells via heat shocking method in which 50uL of E.coli are incubated with entire ligated reaction for 15 minutes on ice, followed by a 1 minute incubation in a 42^oC water bath, and then a 5 minute incubation on ice [52]. Transformed cells were grown up at 37^oC for 1 hour in 180uL of Lysogeny broth (LB) and then plated on LB Agar ampicillin resistant plates. Colonies that developed were inoculated with ampicillin and grown-up in 10mL volumes with LB for plasmid preparation (mini-prep) of potential p3xflag-CMV-9-OTUD6B plasmids using Qiagen QIAprep spin miniprep kit. 1-2ug of DNA from five mini-prepped clones were sent to Eurofins Lancaster Laboratories for DNA sequence verification (Figure 8, B). DNA sequencing and test digestions of potential p3xflag-CMV-9-OTUD6B plasmids show clone numbers 9 and 11 as successfully created p3xflag-CMV-9-OTUD6B plasmids (Figure 8, C-E). Plasmids were then further confirmed by western blot analysis plasmid expression test using DNA transient transfections (described in Chapter 3, Experimental Design, DNA transfections) (Figure 8, F). p3xflag-CMV-9-OTUD6B clone 9 reported a stronger identity similarity to OTUD6B isoform 1 nucleotide sequence and therefore was used for future experimental procedures when necessary.

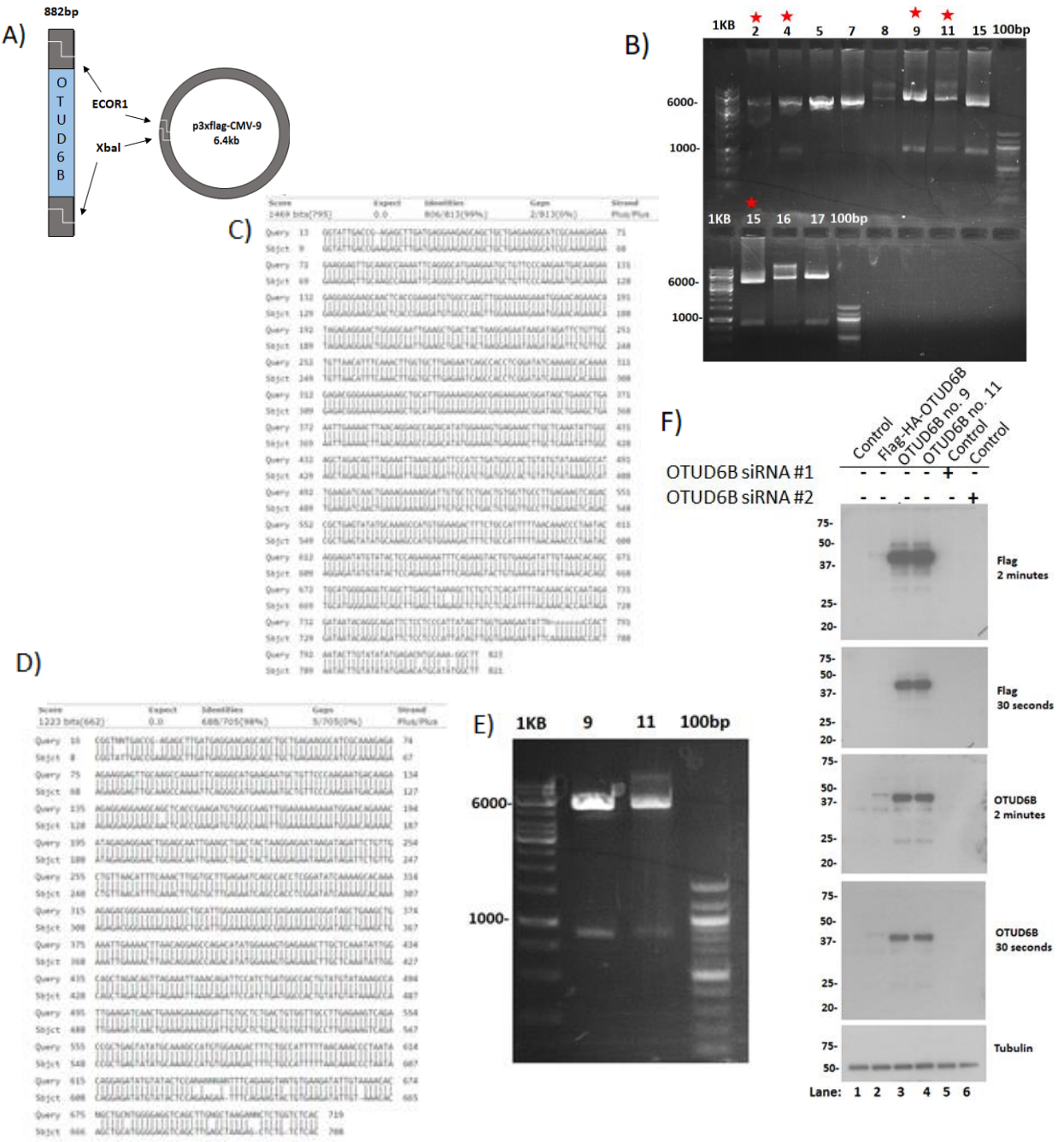

Figure 8. Creation of p3x-flag-CMV-9-OTUD6B plasmid. A) Schematic of OTUD6B cloned into p3XFlag-CMV-9 plasmid with EcoR1 and Xbal targeted restriction sites. B) Test digestions of 10 potential p3x-flag-CMV-9-OTUD6B clones. Test digestion was performed with restriction enzymes EcoR1 and Xbal for 1.5 hours. A 1% agarose gel was used and run for 30 minutes at 100 volts. Digested p3xflag-CMV-9 empty vector plasmid can be observed at ~6000 base pairs and OTUD6B insert can be observed at 881 base pairs. Samples 2, 4, 9, 11, 15 were sequenced (indicated with red stars). C) Nucleotide sequence alignment of p3xflag-CMV-9-OTUD6B clone number 9 and OTUD6B isoform 1 created through the Basic Local Alignment Search Tool (Blast) on NCBI. D) Nucleotide sequence alignment of p3xflag-CMV-9-OTUD6B clone number 11 and OTUD6B isoform 1 created through the Blast on NCBI. E) Test digestion of 3X-FLAG-OTUD6B plasmid clones number 9 and 11, confirmed through sequencing analysis. Test digestions were performed with restriction enzymes EcoR1 and Xbal1 for 2 hours. A 1% agarose gel and run for 30 minutes at 110 volts. Digested 3X-FLAG plasmid can be observed at ~6000 base pairs and OTUD6B insert can be observed at 881 base pairs. F) Expression test of p3Xflag-CMV-9-OTUD6B clones 9 and 11 transiently transfected into HEK293T cells. Control samples were treated with OTUD6B siRNA as indicated or control siRNA. siRNA numbers refer to sequences used (described in Chapter 3). Flag-HA-OTUD6B plasmid, with a pDEST_LTR_N_FLAG_HA_IRES_puro backbone, was used as a positive control. Tubulin was used as a loading control.

Creation of pOZ-FH-N-OTUD6B Plasmid

OTUD6B cDNA from T80 was cloned into pOZ-FH-N retroviral endogenous expression vector using procedures previously described in our laboratory [51]. Briefly, primers were designed to amplify OTUD6B isoform 1 flanked by restriction sites targeted by Xho1 and Not1 for the forward and revers primers respectively:

Forward: 5' ATA **CTC GAG** ATG GAG CCC CGG GTG AG 3'

Reverse: 5' ATA **GCG GCCGC** TTA G CTG CAA TTT TCA GTA AC 3'

where restriction sites are highlighted in bold (Figure 9, A).

Conventional polymerase chain reaction (PCR) was used to amplify the targeted sequence from 1uL of cDNA following a PCR purification using AccuPrep PCR Purification Kit from Bioneer (Figure 9, B). PCR reaction contained 1uL of T80 cDNA, .5uL of Phusion High Fidelity DNA polymerase (Thermo Scientific), 10uL of 5x HF buffer, 2uL of DNTPs, and 2uL of each the forward and reverse primer, brought up to a total reaction mixture of 25uL with H_2O. Annealing temperature was 55^{o}C with 35 cycles.

Digestion of 16uL of amplified OTUD6B cDNA and 500ng of pOZ-FH-N-BMI1 plasmid occurred for 2 hours at 37^{o}C with 1uL of Xho1 and Not1 restriction enzymes each and New England Biolabs (NEB) buffer 3.1. Insert was heat inactivated at 65^{o}C for 20 minutes. Excised BMI1 and digested pOZ-FH-N plasmid backbone were run on a .7% agarose gel and gel extracted using AccuPrep Gel Extraction Kit from Bioneer (Figure 9, C-D). A 1 hour, room temperature ligation using 1uL of DNA T4 ligase and T4 ligase buffer (NEB) was performed at a 1:7 plasmid to insert volume ratio.

Potential pOZ-FH-N-OTUD6B plasmids were then transformed into Top10 competent E.coli cells via heat shocking method in which 50uL of E.coli are incubated with entire ligated reaction for 15 minutes on ice, followed by a 1 minute incubation in a 42^{o}C water bath, and then a 5 minute incubation

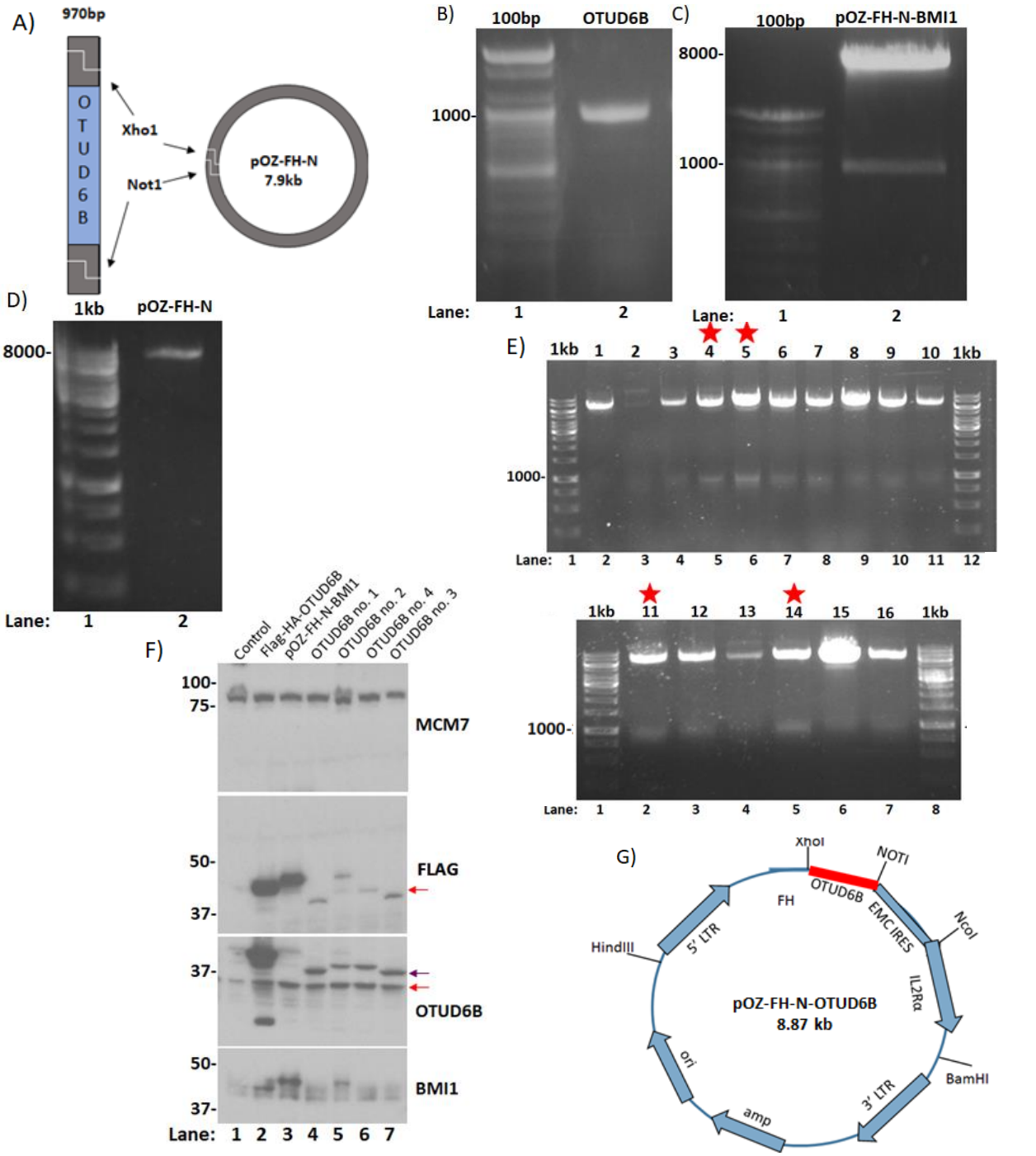

Figure 9. Creation of pOZ-FH-N-OTUD6B plasmid. A) Schematic of OTUD6B cloned into pOZ-FH-N plasmid with Xho1 and Not1 targeted restriction sites. B) Amplified OTUD6B from T80 cDNA after PCR at a 55^{o}C annealing temperature. C) Results of digested pOZ-FH-N-BMI1 after restriction digest. Digested BMI1 can be found at 1110bps and digested pOZ-FH-N can be found at ~8kb. Digested pOZ-FH-N was gel extracted for future ligation. D) Results of pOZ-FH-N gel extraction. 5uL of extracted plasmid was used to run on a 1% agarose gel. E) Test digestions of 16 potential pOZ-FH-N-OTUD6B clones. Test digestion was performed with restriction enzymes Xho1 and Not1 for 1.5 hours. A 1% agarose gel was used and run for 30 minutes at 100 volts. Digested pOZ-FH-N empty vector plasmid can be observed at ~8000 base pairs and OTUD6B insert can be observed at 1000bp base pairs. Samples 4, 5, 11, 14 were sequenced (indicated with red stars). Clone 4 was renamed as clone 1, clone 5 was renamed as clone 2, clone 11 was renamed as clone 3, and clone 14 was renamed at clone 4 for simplicity. F) Expression test of pOZ-FH-N-OTUD6B clones 1, 2, 4, and 3 transiently transfected into HEK293T cells. Flag-HA-OTUD6B plasmid, with a pDEST_LTR_N_FLAG_HA_IRES_puro backbone, was used as a positive control. pOZ-FH-N-BMI1 plasmid was used as a negative control. MCM7 was used as a loading control. G) Vector map of pOZ-FH-N-OTUD6B.

on ice [52]. Transformed cells were grown up at 37^{o}C for 1 hour in 180uL of Lysogeny broth (LB) and then plated on LB Agar ampicillin resistant plates. Colonies that developed were inoculated with ampicillin and grown-up in 10mL volumes with LB for plasmid preparation (mini-prep) of potential pOZ-FH-N-OTUD6B plasmids using Qiagen QIAprep spin miniprep kit. 1-2ug of DNA from four mini-prepped clones were sent to Eurofins Lancaster Laboratories for DNA sequence verification (Figure 9, E). DNA sequencing of potential pOZ-FH-N-OTUD6B plasmids show clone number 4 as a successfully created pOZ-FH-N-OTUD6B plasmids. Plasmids were also confirmed by western blot analysis plasmid expression test using DNA transient transfections (described in Chapter 3, Experimental Design, DNA transfections) (Figure 9, F). pOZ-FH-N-OTUD6B clone 4 showed greatest similarity to OTUD6B isoform 1 nucleotide sequence as well as had best expression via western blot analysis and therefore was used for future experimental procedures when necessary.

Mutagenesis of OTUD6B Catalytic Cysteine

Site-directed mutagenesis was performed following the Stratagene QuikChange Site-directed Mutagenesis Protocol. OTUD6B 188S catalytic mutant was created using our newly developed p3XFlag-CMV-9-OTUD6B clone number 9 plasmid as the starting template (Figure 10, A). Briefly, primers were designed to contain and amplify the desired C188S catalytically inactive point mutation on the OTUD6B isoform 1 nucleotide sequence:

Forward: **5'** CCA TCT GAT GGC CAC TCT ATG TAT AAA GCC ATT G **3'**

Reverse: **3'** GGT AGA CTA CCG GTG AGA TAC ATA TTT CGG TAA C **5'**

where the point mutation is highlighted in cyan. GC content was 44% and melting temperature was 81.69^{o}C.

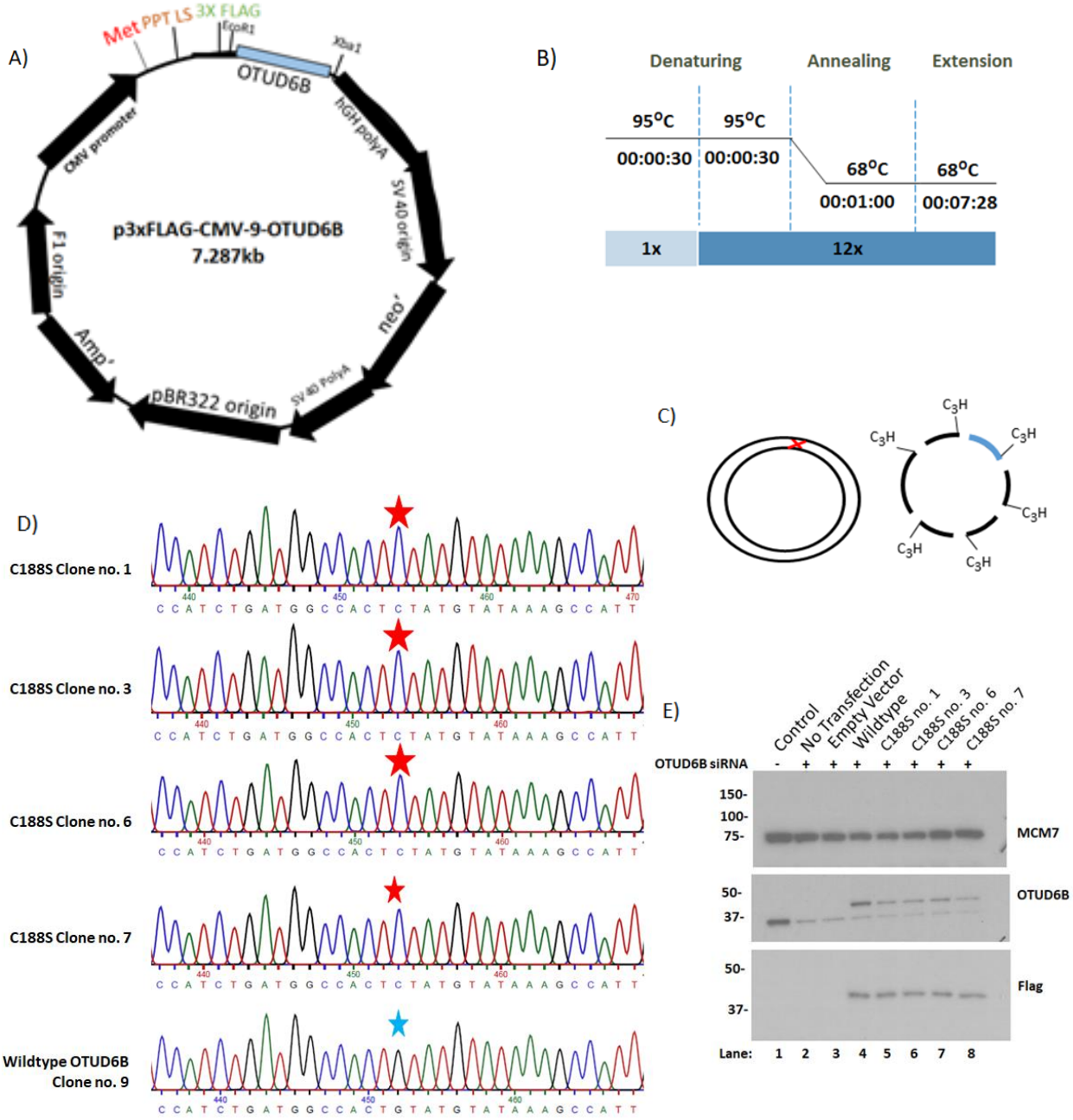

Figure 10. Creation of p3x-flag-CMV-9-OTUD6B-C188S plasmid. A) Plasmid map of p3XFlag-CMV-9-OTUD6B used as the starting template for mutagenesis. B) Conventional mutagenesis polymerase chain reaction (PCR). PCR had an annealing temperature of was 68°C and 12 cycles. C) Dpn1 digestion to destroy parental OTUD6B-3xFlag wildtype plasmid. Red X indicates mutant plasmid's mutation. D) Sequencing chromatogram results from Eurofins Lancaster Laboratories of four identified C188S mutant clones indicated by reported numbers. Sequencing chromatogram of OTUD6B wildtype clone number 9 is provided as a reference. Red stars indicate point mutations, blue star indicated no mutation. E). Plasmid expression test in MCF-7 cells with wildtype OTUD6B or C188S catalytic mutants. Plasmid backbone used was p3xFLAG-CMV-9-OTUD6B. C188S mutants listed are from individual clones. siRNA used was number #2 (described elsewhere). MCM7 was used as a loading control.

Conventional mutagenesis polymerase chain reaction (PCR) was used to amplify 100ng of p3xflag-CMV-9-OTUD6B plasmid with the desired point mutation. PCR reaction contained 1uL p3xflag-

CMV-9-OTUD6B plasmid, .5uL of Phusion High Fidelity DNA polymerase (Thermo Scientific), 5uL of 5x HF buffer, 4uL of DNTPs, 1uL of each the forward and reverse primer brought up to a total reaction mixture of 25uL with H_2O [53]. Annealing temperature was 68^oC with 12 cycles (Figure 10, B).

To destroy parental OTUD6B-3XFlag wildtype plasmid but keep C188S mutagenetic OTUD6B-3XFlag plasmid, Dpn1 digestion was performed on the 25uL PCR reaction with 1.25uL of Dpn1 (NEB) for 2 hours at 37^oC (Figure 10, C) [53].

Potential p3xflag-CMV-9-OTUD6B C188S plasmids were then transformed into Top10 competent E.coli cells via heat shocking method in which 50uL of E.coli are incubated with 5uL of the dnp1 digested reaction for 30 minutes on ice, followed by a 45 second incubation in a 42^oC water bath, and then a 2 minute incubation on ice [53]. Transformed cells were grown up at 37^oC for 1 hour in 250uL of LB and then plated on LB Agar ampicillin resistant plates. Colonies that developed were inoculated with ampicillin and grown-up in 10mL volumes with LB for mini-prep of potential p3xflag-CMV-9-OTUD6B-C188S plasmids using Qiagen QIAprep spin miniprep kit. 1-2ug of DNA from 11 mini-prepped clones were sent to Eurofins Lancaster Laboratories for DNA sequence verification. DNA sequencing and western blot plasmid expression test using transient transfections of p3xflag-CMV-9-OTUD6B wildtype and p3xflag-CMV-9-OTUD6B-C188S mutants (described in Chapter 3, Experimental Design, DNA transfections) showed clone numbers 1, 3, 6, and 7 were successful point mutations (Figure 10, D-E). p3xflag-CMV-9-OTUD6B-C188S clone 6 showed the strongest expression and therefore was used for future experimental procedures when necessary (Figure 10, E).

OTUD6B Knockout Cell Line

Clustered Regularly Interspaced Short Palindromic Repeats (CRISPR) technologies utilizes natural bacterial adaptive immune defenses to induce genetic modifications within cell genomes [54]. It involves a nuclease, such as CRISPR-associated protein (Cas9), to induce a single or double stranded break within

the DNA of interest, and an RNA structure, called a guide RNA (sgRNA), which recognizes complementary sequences within the genome [55]. Following the introduction of genomic breaks, DNA repair mechanisms will occur to fix the damage [55].

Non-homologous recombination (NHEJ) is an error prone DNA repair process often used by cells to repair double-stranded DNA breaks. It involves the removal of several nucleotide base pairs at the sites of damage, followed by direct ligation of separated genomic ends. CRISPR technologies takes advantage of this mechanism by relying on NHEJ to remove segments of the desired genetic sequence and in the process, introduce an early stop codon to inhibit targeted OTUD6B gene translation [56].

The OTUD6B Double Nickase Plasmid (h2): sc-407482-NIC from Santa Cruz technologies was used to create our OTUD6B Knockout cell line in HEK293T cells (Figure 11, A). This particular plasmid set utilizes the CRISPR-associated (Cas9) mutant D10A, which is only able to cut the single complimentary strand of the sequence guide RNA (sgRNA) (Figure 11, B) [56]. The sgRNA recognizes its complementary sequence upstream of OTUD6B coding region within the genome [55]. The OTUD6B Double Nickase Plasmid (h2): sc-407492-NIC from Santa Cruz technologies includes two plasmids with their own transient selection process, either a puromycin resistance gene or green fluorescent protein (GFP), and their own sgRNA: Plasmid 1: 5'-GCTGGGGTACCTGGTCGTCA 3', and Plasmid 2: 5'-AGAAACCTGCACCGGCTAGT 3' (Figure 11, B) [54]. These separate sgRNAs offset each other by approximately 20 base pairs and both are upstream of the OTUD6B targeted DNA (Figure 11, B) [54]. Thus, each plasmid is able to provide a single stranded cut in at a different region of the genome, imitating a double stranded break for NHEJ repair, while also allowing for gene knockout with greater specificity [54, 56].

To create the OTUD6B knockout cell line in HEK293T cells, HEK293T cells with a low passage number were seeded in a 6-welled plate and grown to a 60-70% confluency. Cells were then transfected

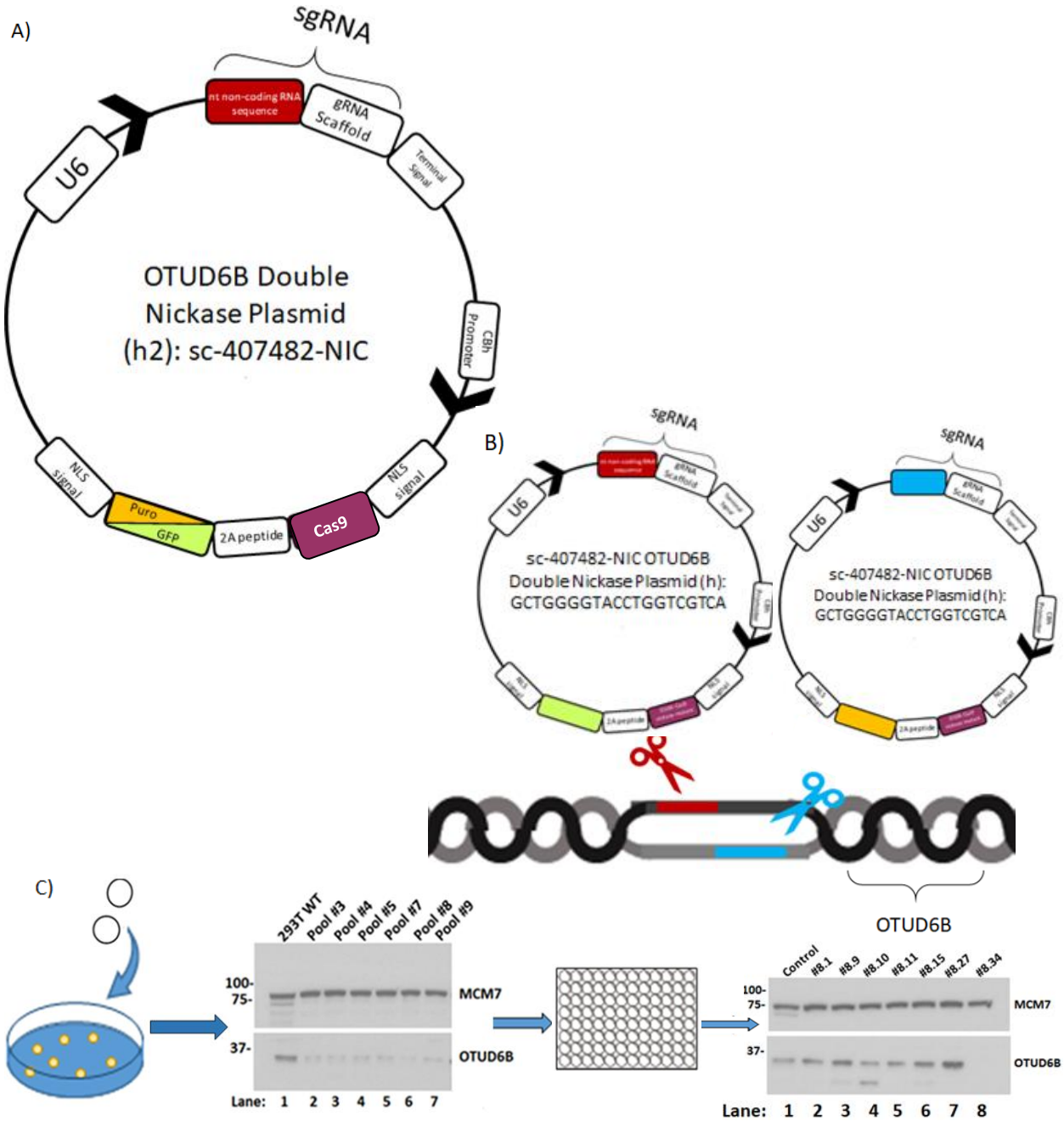

Figure 11. Creation of OTUD6B Knockout cell line in HEK293T cells. A) Vector map of OTUD6B Double Nickase Plasmid (h2): sc-407482-NIC adapted from Santa Cruz Biotechnologies, Inc. Plasmid includes a U6 promoter to promote sgRNA expression, a unique sgRNA sequence, a gRNA scaffold to encourage Cas9 D10A nickase mutant to DNA binding, a chicken β-actin hybrid (CBh) promoter to promote expression of the Cas9 D10A nickase mutant and the puromycin resistance gene, a 2A Peptide to allow production of both the Cas9 D10A nickase mutant and the puromycin resistance gene, either the puromycin resistance gene or GFP depending on the particular Plasmid of the set, and two nuclear localization signals (NLS). B) A schematic of the OTUD6B Double Nickase Plasmid (h2) plasmids targeting OTUD6B genomic DNA and inducing breaks, adapted from Santa Cruz Biotechnologies, Inc. [53]. Individual plasmid sgRNA sequences are displayed on each vector as well as either the puromycin resistance gene or the GFP for selection, indicated by orange and green respectively. Each plasmid provides a single stranded cut upstream of the target gene, indicated by colors red and blue. C) A schematic of the creation of the OTUD6B knockout cell line in HEK293T cells. OTUD6B Double Nickase Plasmid (h2) is transfected into HEK293T cells and treated with puromycin. Pool samples of remaining colonies after selection process are grown up and analyzed via western blot analysis. Pool #8 is chosen for 96 well plate single selection and individual cells from this plate were grown up and analyzed via western blot analysis. Numbers displayed for each sample indicate the HEK293T clone that was grown up from the Pool #8 sample. Control indicates our HEK293T wildtype cell line. MCM7 was used as a loading control.

with .5ug of the OTUD6B Double Nickase Plasmid. Transfection reagents included Opti-MEM (Invitrogen) and Turbofect (Thermofischer Scientific) used at a 1:100 DNA mass to volume ratio and a 1:2 DNA mass to volume ratio, respectively [53]. DNA transfected samples, once confluency was reached, were moved to a 6cm plate where they were subjected to 1ug/mL of puromycin for selection [53]. Puromycin selection occurred until no non-transfected cells in a separate control sample had survived, moving the cells to larger plate sizes once confluency had been reached [53].

Colonies remaining in the OTUD6B Double Nickase Plasmid transfected sample were individually moved to their own well within a 24 welled plate to see if reattachment occurred. Cells that reattached were grown up to 10cm plates and 1mL pellets were collected and subjected to western blot analysis (Figure 11, C). Six "pooled" samples were analyzed via western blot and pool number 8, as it showed the lowest OTUD6B expression, was subjected to 96 welled single cell selection (Figure 11, C). Single cells from this pooled group were grown up into 6cm plates and then subjected to western blot analysis to analyze OTUD6B expression. Single cell group number 8.34, later referred to as KO #34, showed a clean knockout of OTUD6B and therefore was used for future experiments (Figure 11, C). Two more OTUD6B knockouts were later discovered, KO #38 and KO #18, but upon further culturing, were determined to not be clean knockouts due to the return of OTUD6B expression levels.

DNA Transfections

Cells were cultured in Penicillin-Streptomycin free media. Once cell confluency reached 60-70% samples were transfected with 1ug/mL of media of designated DNA. Transfection reagents used included Opti-MEM (Invitrogen) and Turbofect (Thermofischer Scientific) used at a 1:100 DNA mass to volume ratio and a 1:2 DNA mass to volume ratio, respectively. DNA transfected samples were allowed to incubate for at least 24 hours post transfection to ensure desired protein was expressed.

RNA Interference

Cells were cultured in Penicillin-Streptomycin free media and seeded at 30% confluency. At the time of seeding, samples were transfected with 20nM of designated siRNA. Transfection reagents used included Opti-MEM (Invitrogen) and lipofectamine RNAimax (Invitrogen) used at a 1:100 mass to volume ratio and a 1:1 mass to volume ratio, respectively [51]. All siRNA transfected samples were allowed to incubate for 72 hours post transfection unless otherwise instructed [51]. The following siRNA sequences were used: OTUD6B siRNA #1: 5' -AGGGUCAUUGAUAGCAAGUAA 3' from Qiagen, OTUD6B siRNA #2: 5' -UAGUAUGGUGAUGGUCAAUUU 3' from Qiagen, OTUD6B siRNA #3: 5'-CAGUGUAAAAGGUCCAAG 3' from Bioneer, OTUD6B siRNA #4: 5'- CACCAAUAGAGAUAAUACA 3' from Ambion, UBR5 siRNA #3: 5' -AAGGUUCUUGUAUAGAGGGAA 3' from Qiagen, and SKP2 siRNA: 5'CCUUAGACCUCACAGGUAA 3' from Ambion. A scrambled siRNA was used as control: All-Star Negative from Qiagen or Negative control siRNA from Bioneer, as indicated.

Protein lysis and Western Blotting

Cell samples were washed with 1-2mLs of 1x phosphate buffered saline (PBS) depending on well size prior to harvest by scraping with commercially available cell scrapers [51]. Harvested samples were spun down at 4000rpm for 5 minutes followed by administration of RPPA lysis buffer containing 1% Triton X-100, 50nM HEPES, 150nM NaCl, 1mM $MgCl_2$, 1mM EGTA, 10% glycerol, 1xprotease cocktail inhibitor (Thermofischer Scientific), and 1x phosphatase cocktail inhibitor (Thermofischer Scientific) [57]. Samples were incubated in lysis buffer for 1 hour at 4^oC following a 10 minute centrifuge spin at 14000rpm [57]. Protein concentration assessment involved optical density measurements compared to a standard bovine serum albumin (BSA) curve using Protein Assay Dye (Bio-Rad). 2x laemmli sample buffer (Bio-Rad) was added to samples following a 5 minute ~95^oC heat block incubation [51].

Prepared protein samples were run on SDS-PAGE gels at 105 constant volts for ~120 minutes unless otherwise indicated. Separated proteins were transferred to a PVDF membrane using a semi-dry Trans-blot Turbo [51]. Membranes were probed with primary antibodies overnight at 4^{o}C followed by a 1 hour wash in 1x tris-buffered saline with Tween (TBST) at room temperature. Membranes were then incubated for 1 hour at room temperature with mouse or rabbit secondary antibody linked to horseradish peroxidase (Cell Signaling Technologies (CST)) followed by an additional 4 hours of room temperature washing in 1xTBST [51]. Results were observed using Pierce ECL Western Blotting Substrate (Thermofischer Scientific). When indicated, band intensities were quantified using imageJ to find the areas under the curve of each of the protein intensity levels and normalized to the loading control.

The following antibodies were used: anti-β-Tubulin [1:3000] (M) (CST), anti-OTUD6B [1:333] (R) (Abcam), anti-p21 [1:500] (R) (CST), anti-UBR5 [1:1000] (R) (CST), anti-MCM7 [1:1000] (R) (Bethyl), anti-SKP2 [1:500] (R) (CST), anti-p27 [1:333] (R) (CST), p53 [1:1000] (M) (CST), Cyclin D1 [1:500] (M), (CST), CHK1P [1:500] (R) (CST).

Immunofluorescent Microscopy

Cell samples grown on 12mM in width, .13-.17mM in thickness, sized coverslips were washed twice with 1mL of cold 1x PBS following a 10 minute fixation with 4% paraformaldehyde in the dark [51]. Cells were then washed again with 1mL of cold 1x PBS and permeabilized with .25% Triton x-100 diluted in H_2O for 5 minutes in the dark [51]. Coverslips were washed as described earlier and incubated with 30uL of primary antibody diluted in 1x PBS for 1 hour in the dark [51]. After, samples were washed again with PBS as described previously and incubated with 30uL of either Alexa Flour 488-anti-mouse or anti-rabbit secondary antibody diluted in 1x PBS for 1 hour in the dark [51]. After additional 1mL 1x PBS washing, coverslips were placed on slides using Vectashield mounting medium for fluorescence with DAPI (Vector Laboratories Inc) to stain nuclei [51]. Images were collected using Lecia DMi8 fluorescence

microscope under a 63x oil objective. The program used for image capturing was Leca Las X imaging and analysis software. Using imageJ, between 100 and 300 cells were counted for quantification as indicated in data. Primary antibodies used were anti-p21 [1:800] (R) (CST) and anti-NFKβ (1:200) (R) (Santa Cruz).

Results

OTUD6B Protein Depletion Results in an Induction of the Cyclin Dependent Kinase Inhibitor p21

Previous evidence has suggested that OTUD6B in mice lymphocytes participate in cell cycle progression after cytokine stimulation. To determine if OTUD6B was implicated in cell cycle progression of human cell lines, we performed siRNA knockdowns of OTUD6B using different sequences and observed if this had an impact on expression levels of various cell cycle regulators (Figure 5, A). p21 is a cyclin-dependent kinase inhibitor which mainly functions to halt cell cycle progression at the G1/S phase and the G2 phase of the cell cycle [11]. CHK1 is an important kinase of the ATR DNA damage checkpoint signaling cascade and facilitates the phosphorylation and stabilization of p53 as well as regulates additional proteins needed for cell cycle progression [11]. Cyclin D1 is an important cyclin needed for activation of cdk4 and cdk6 and helps to progress cells through G1 phase of the cell cycle [29]. Moreover, literature has suggested that cyclin D1 expression levels are impacted by OTUD6B in lung tissue cancers [20]. When OTUD6B protein expression was knocked down, a slight induction of p21 levels was observed in HEK293T cells (Figure 12, A).

To test whether OTUD6B depletion could consistently increase p21 protein expression in multiple cell lines we performed similar experiments in triple negative epithelial breast cancer, luminal A epithelial breast cancer, osteosarcoma tumor, and epithelial ovarian cancer cell lines (Figure 12, B). In all cell types, p21 induction was observed under OTUD6B protein depletion conditions (Figure 12 B).

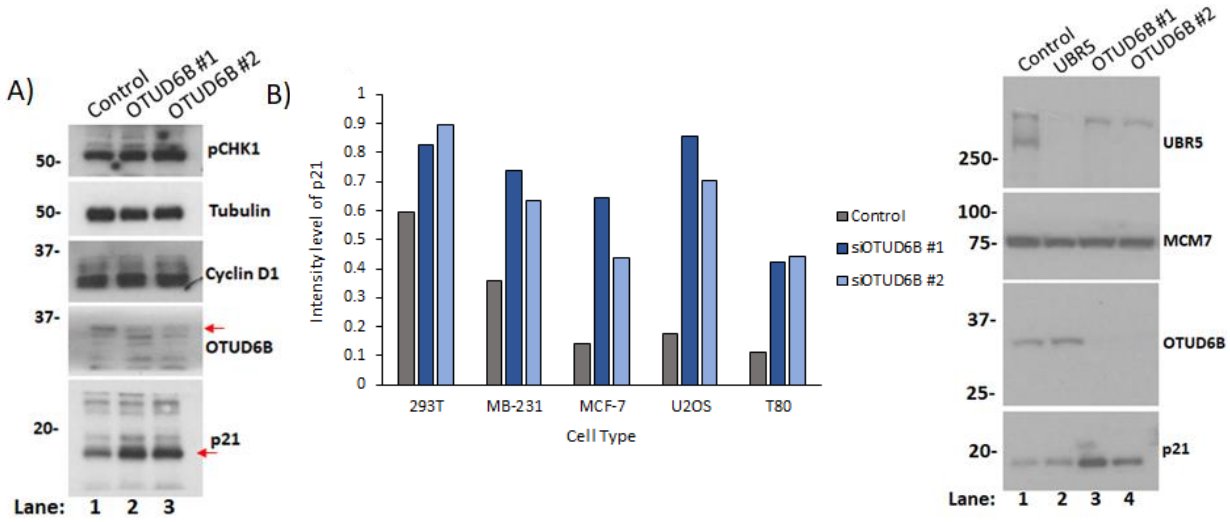

Figure 12. Depletion of OTUD6B protein levels results in p21 induction in multiple human cancer cell lines. A) OTUD6B knockdown was conducted with two siRNAs in HEK293T cells resulting in increased p21 levels. Control represents All-Star Negative control from Qiagen. Red arrows indicate protein labeled. Tubulin was used as a loading control. B) OTUD6B knockdown was conducted with two siRNAs in multiple cells lines as indicated. Intensity levels of p21 were quantified on ImageJ and normalized to MCM7 loading control. To the right, a western blot of OTUD6B knockdown using two siRNAs in MCF-7 cells resulting in increased p21 levels as a reference to the bar graph. Control represent All-Star Negative control from Qiagen. MCM7 was used as a loading control.

Moreover, to observed if overexpression of OTUD6B had an opposite impact on p21 protein levels, our pOZ-FH-OTUD6B-N clone number 4 was transfected into a T80 epithelial ovarian cancer cell line. Results showed decreased p21 levels compared to OTUD6B knockdown conditions as well as control (Figure 13).

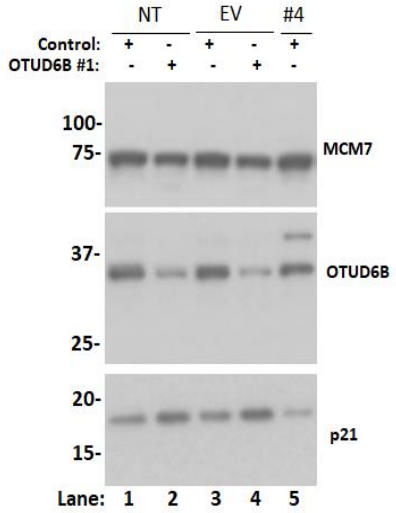

Figure 13. p21 levels decrease compared to control conditions when OTUD6B is overexpressed. T80 cells lines were administered with OTUD6B siRNA #1, represented by OTUD6B #1, or All-Star Negative control from Qiagen, represented by control, for 48 hours before being treated with empty vector pOZ-FH-N plasmid (EV) or pOZ-FH-N-OTUD6B clone number 4 plasmid (#4) for 24 hours. NT represents non-transfected samples. MCM7 was used as a loading control.

Because HeLa cervical cancer cells are notorious for holding unstable p53 protein levels and because p53 is a major transcription factor of p21 protein expression, we wanted to observe if HeLa cells could also show an increase in p21 levels under OTUD6B knockdown conditions [31, 58]. Results again supported that under OTUD6B depletion, p21 levels were increased (Figure 14, A). Furthermore,

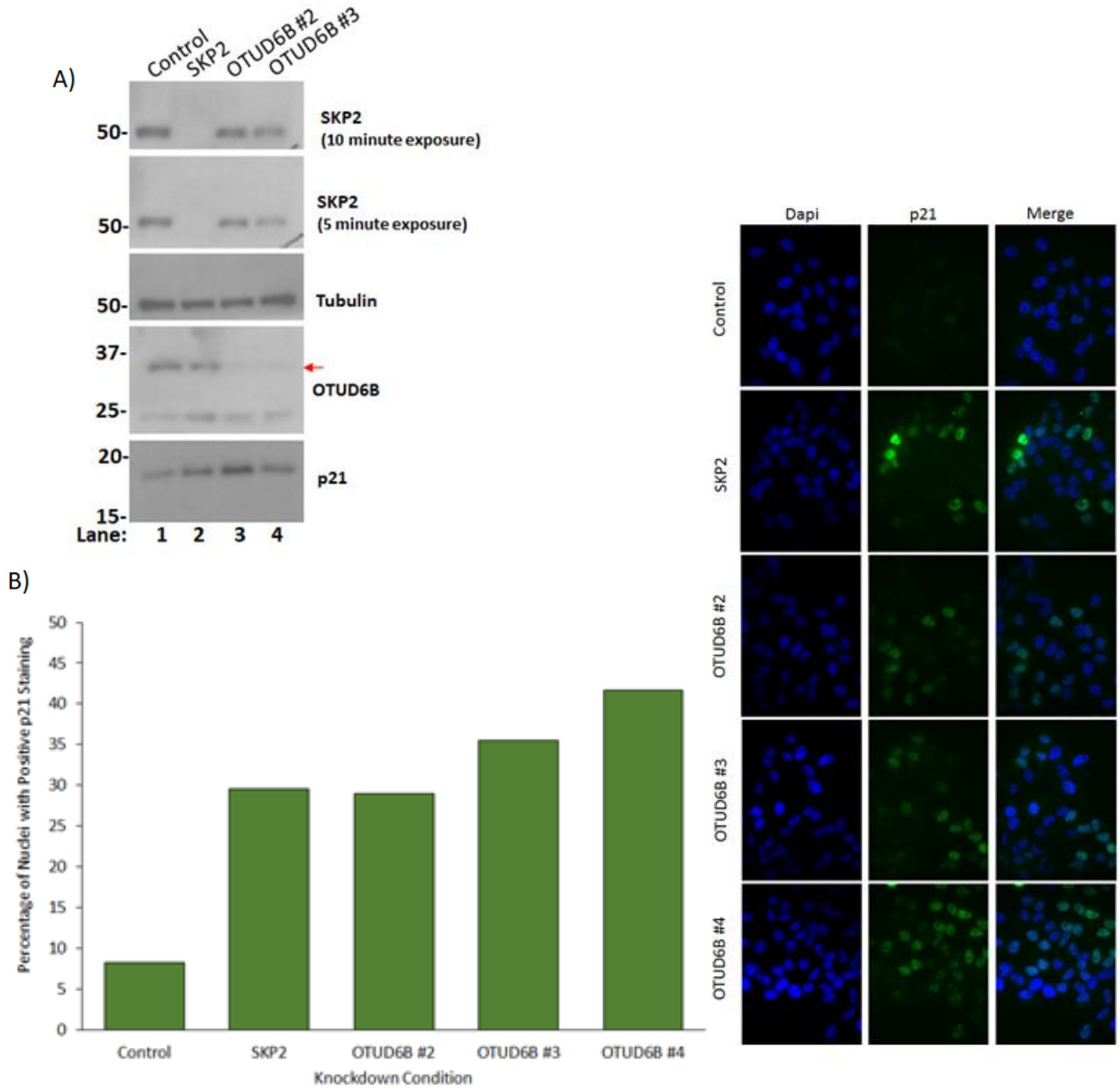

Figure 14. p21 levels are induced in HeLa cells under OTUD6B knockdown. A) OTUD6B knockdown was conducted with two siRNAs in HeLa cells resulting in increased p21 levels. Control represents control siRNA from Bioneer. SKP2, as it regulates p21 stability, was used as a positive control. Red arrows indicate protein labeled. Tubulin was used as a loading control. B) OTUD6B knockdown was conducted with three siRNAs in HeLa cells. Nuclei stained green indicate p21 protein levels. SKP2 was used as a positive control. Control represents control siRNA from Bioneer. Quantification of the number of nuclei positively stained for p21 for each knockdown condition is quantified in the bar graph to the left. Between 100 and 300 cells were counted for quantification.

an induction of p21 was also observed in HeLa cells via immunofluorescence microscopy (Figure 14, B). Of note, p21 staining is observed exclusively in the nucleus, suggesting these increased p21 levels hold tumor suppressor functions rather than oncogenic [30].

OTUD6B Depletion Does Not Stabilize p21 Protein Levels

DUBs have been shown to increase protein stability of their corresponding substrates by removal of ubiquitin and thus, the prevention of proteasome-mediate degradation [6]. To determine if p21 protein stability, rather than transcription level, was altered under OTUD6B expression level a cycloheximide (CHX) chase assay was performed under OTUD6B knockdown conditions. CHX is a translation elongation inhibitor discovered from *Streptomyces griseus* bacterium [59]. Results showed no difference in p21 depletion rates under OTUD6B knockdown conditions compared to controls, suggesting that OTUD6B does not affect p21 stability (Figure 15).

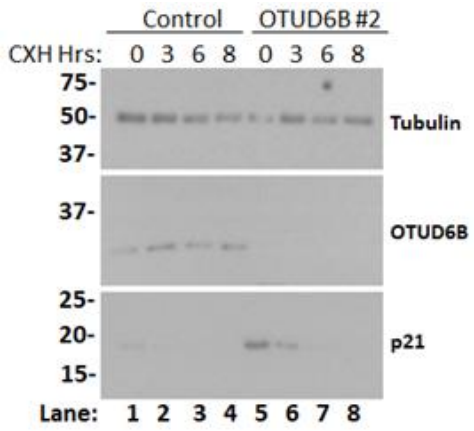

Figure 15. p21 protein levels are not stabilized by OTUD6B knockdown. A) A CHX chase assay was performed under OTUD6B knockdown conditions using siRNA #2 in HeLa cells. 10uM of CHX was administer to samples at indicated time points. Control represents control siRNA from Bioneer. Tubulin was used as a loading control.

p21 Levels are Increased in OTUD6B KO Cell Lines but Cannot be Fully Rescued

In addition, an OTUD6B KO cell line was created in HEK293T cells (described in Chapter 3, Experimental Methods, OTUD6B Knockout Cell Line) and in three separate KO clones, p21 induction was still observed (Figure 16, A). Of note, clone numbers 38 and 18 were later determined to not be true KO

clones as OTUD6B expression levels later returned in these cell lines. This suggests an explanation for the differences in p21 induction levels between the three cell lines. In an attempt to return p21 expression to basal levels, a rescue experiment was performed in the OTUD6B KO clone number 34 cell line by transfecting back in either our p3xflag-CMV-9-OTUD6B clone number 9 or clone number 11 expression plasmids. Results showed a slight reduction in p21 expression levels however the introduction of OTUD6B could not fully rescue control conditions (Figure 16, B).

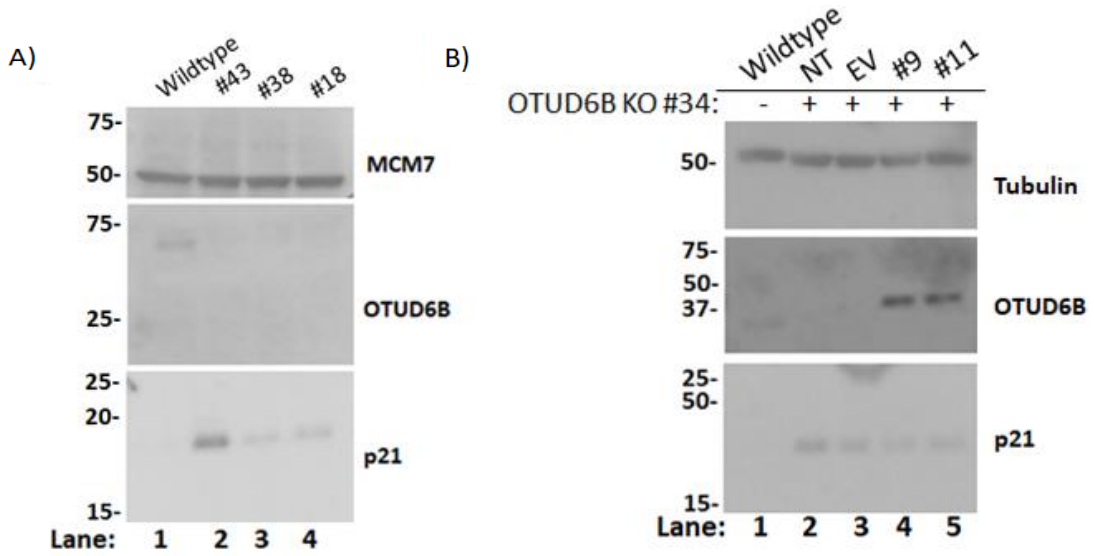

Figure 16. p21 levels are increased in OTUD6B KO cell lines but cannot be fully rescued. A) OTUD6B KO cells lines created in HEK293T cells result in increased p21 expression. Numbers listed refer to individual OTUD6B KO clones. Clones number 38 and 18 were later determined to not be true OTUD6B KO clones. Wildtype refers to HEK293T wildtype cell line. MCM7 was used as a loading control. B) Rescue experiment in HEK293T wildtype and OTUD6B KO #34 cell lines. NT refers to no transfection, EV refers to empty vector p3xFLAG-CMV-9 plasmid, #9 refers to our p3xFLAG-CMV-9-OTUD6B number 9 clone, #11 p3xFLAG-CMV-9-OTUD6B number 11 clone. Transfected samples were allowed to incubate for 36 hours before harvest. Tubulin was used as a loading control.

p21 Levels are Increased in a p53 Dependent Manner Under OTUD6B Knockdown Conditions

Because data supports that the p21 induction observed under an OTUD6B knockdown condition was due to an increased expression in p21 transcription, we sought to determine if this induction was p53 dependent. As mentioned previously, p21 transcription is regulated by a vase number of different mechanisms, both p53-dependent and p53-independent. Recently, it was shown that the NF-Kβ pathway was able to activate the expression of p21, independent of p53, in myeloid leukemia cells [60].

As other DUBs have been implicated in regulating NF-Kβ activation, and because p21 induction under an OTUD6B knockdown was observed in HeLa cells which do not express high levels of p53, we wanted to observe if OTUD6B levels negatively impact the nuclear localization of NF-Kβ [60]. Results showed that depletion of OTUD6B using siRNA had no change on NF-Kβ nuclear localization (Figure 17).

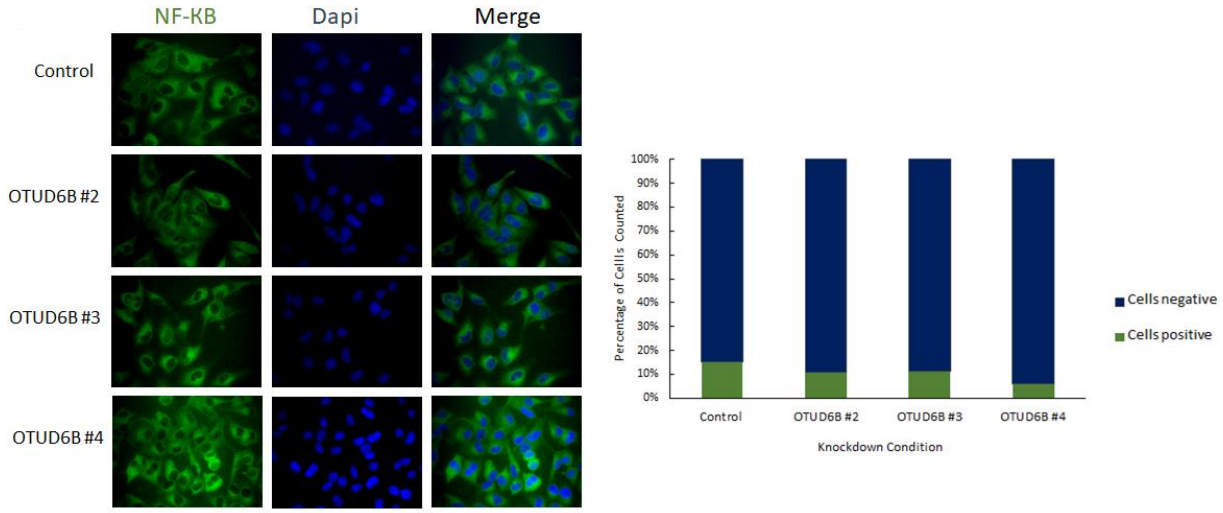

Figure 17. p21 induction under OTUD6B knockdown does not occur through NF-Kβ signaling. A) OTUD6B knockdown was conducted with three siRNAs in HeLa cells. Nuclei stained green indicates NF-Kβ nuclear entry and pathway activation. Control represents control siRNA from Bioneer. Quantification of the number of nuclei positively stained for NF-Kβ for each knockdown condition is quantified in the bar graph to the right where cells positive represent nuclei with positive NF-Kβ staining and thus positive NF-Kβ pathway activation and where cells negative represent nuclei with negative NF-Kβ staining and thus negative NF-Kβ pathway activation. Between 100 and 300 cells were counted for quantification.

It has also been shown, more recently, that p21 levels can still be induced in HeLa cells in a p53 dependent manner [61]. To test the possibility that our observed p21 induction is in fact occurring in a p53-dependent manner, a MIA-PaCa-2 pancreatic cancer cell line was used. This MIA-PaCa-2 cell line has been reported to contain a deleterious mutation at Arginine residue 248 which falls within the DNA binding domain of p53 (Figure 18, A). The resulting, R248W missense mutation is statistically and experimentally shown to be damaging mutation in which p53 tumor suppressor function is lost but a tumorigenesis-promoting function has been gained, most likely do to a disruption in wildtype p53 transcriptional activity (Figure 18, B) [25, 26, 62]. Thus, we attempted to observe if, under an OTUD6B knockdown condition, p21 would still be induced in this cell line. Results strikingly failed to show any

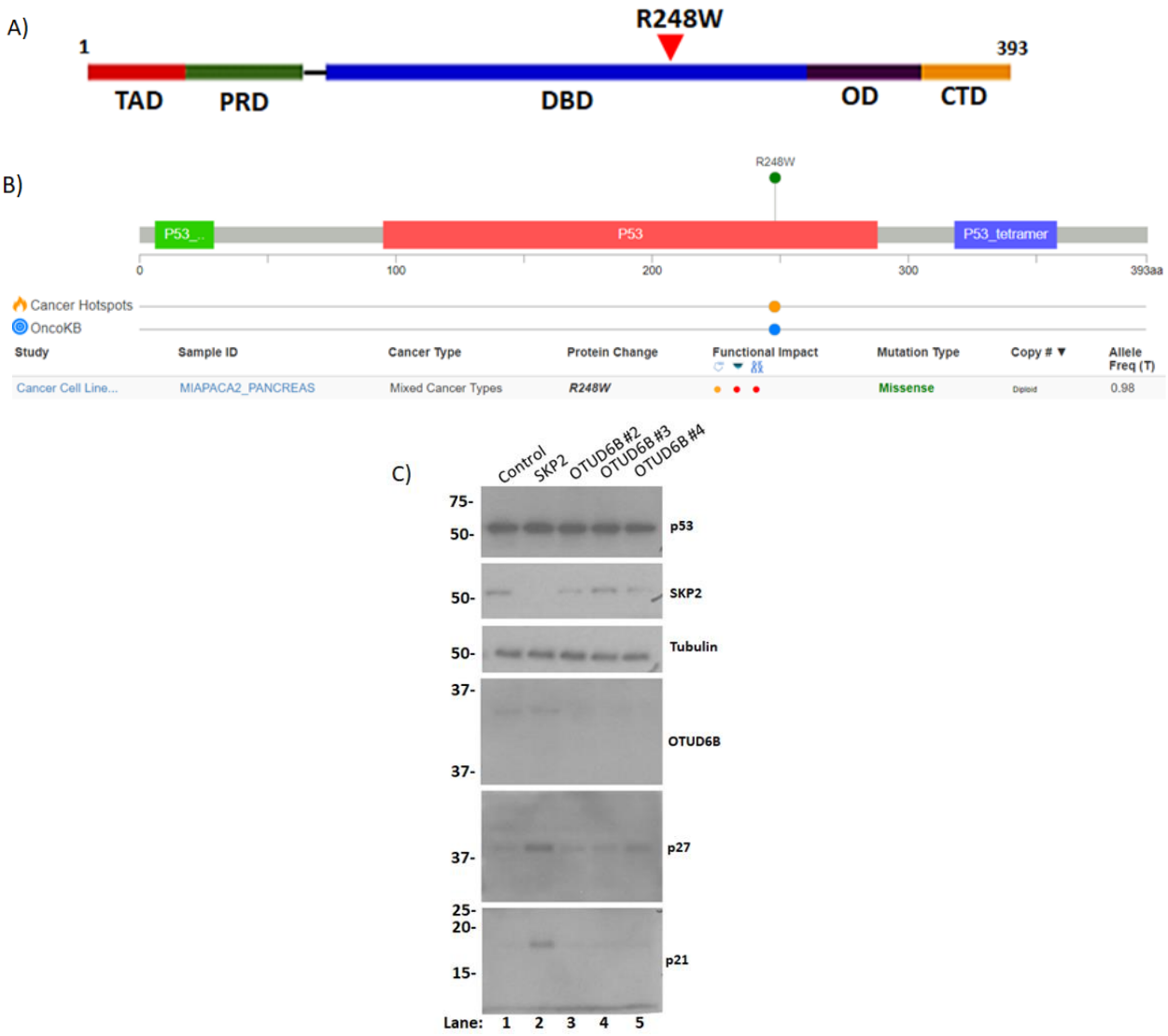

Figure 18. MIA-PaCa-2 cell line suggests p21 induction under OTUD6B protein depletion occurs in a p53-dependent manner. A) Schematic mapping of p53 with domain structures adapted from Freed-Pastor et al. (1997) where TAD refers to the transactivation domain, PRD refers to the proline-rich domain, DBD refers to the DNA-binding domain, OD refers to the oligomerization domain, as p53 functions as a homotetramer, and CTD refers to the C-terminal regulatory domain [63]. The R248W deleterious mutation present in the MIA-PaCa-2 cell line is indicated by the red arrow and found within the DNA-binding domain of p53[63]. B) CBioPortal mutation summary for MIA-PaCa-2 cell lines in a 1020 tumor samples study. Report shows a high variant allele frequency for R248W mutations with a poor survival rate [24, 25]. Shown under functional impacts, Cbioportal considers this mutation to be deleterious for affecting protein function and damaging for p53 structure and function [24, 25]. OncoKB database reports this mutation as likely oncogenic and cancer hotspots considers it as a reoccurring, statistically significant, hot spot [24, 25]**.** C) OTUD6B knockdown was conducted with three siRNAs in MIA-PaCa-2 cells. Control represents control siRNA from Bioneer. SKP2, as it regulates p21 and p27 protein stability, was used as a positive control. Tubulin was used as a loading control.

induction of p21 levels under an OTUD6B knockdown within the MIA-PaCa-2 pancreatic cancer cell line, even though our positive control of a SKP2 knockdown, which impacts p21 protein stability rather than

transcription levels, showed high protein expression compared to the control sample (Figure 18, C). This suggests that the p21 induction observed is occurring in a p53-dependent manner.

Conclusions and Future Directions

Our data has shown convincing evidence that OTUD6B protein levels impact p21 induction. Through western blot analysis, an increase in p21 protein has consistently been observed across multiple epithelial cell lines, with the exception of Mia-PaCa-2 cells, under decreased OTUD6B conditions (Figure 12, B). In contrast, no change in cyclin D1 levels were observed with an OTUD6B knockdown in 293T cells, despite previous findings in non-small cell lung cancer that show OTUD6B isoform 2 expression regulates cyclin D1 levels in a positive correlation manner [20]. As our siRNA sequences #1 and #2 target both isoforms, and because p21 has been show to correlate with cyclin D1 expression for stability regulation, at least in breast cancer cell lines, it is surprising that no effect on cyclin D1 levels were observed in our results [12]. Future experiments should include a more in-depth analysis at cyclin D1 levels, perhaps in MCF-7 or MB231 breast cancer cell lines as this positive correlation between p21 and cyclin D1 was observe in breast cancer tumors

Because p21 induction often occurs through check point kinase pathway activation, it is also unexpected that no changes in phosphorylated levels of CHK1 was observed under an OTUD6B knockdown condition, however, p21 induction can also occur under activation of CHK2 (Figure 12, A) [11]. Thus, more experimental examination of CHK1 and CHK2 protein levels should be conducted to fully exclude the possibility that OTUD6B does not impact either of these checkpoint kinase cascade proteins.

In this research, it was also shown that in instances of OTUD6B overexpression, p21 levels were able to decrease to levels below control conditions (Figure 13). In argument to this, it was reported in HeLa cells via qPCR examination, that overexpression of OTUD6B resulted in no significant change in p21 levels [23]. T80 epithelial ovarian cancer cells and HeLa do have differences in protein expression levels

between each other which may explain the contradicting results; OTUD6B overexpression may be unable to reduce p21 levels in HeLa but can reduce p21 levels in T80. An additional alternative is that an increase in p21 translation, rather than transcription, is occurring under our conditions and that overexpressing OTUD6B decreases translation efficiencies. Indeed, Sobol et al. (2016) has reported that OTUD6B isoform 2 had the potential to increase protein synthesis by measuring methionine surrogate azidohomoalanine (AHA) incorporation rates [20]. Such speculations require further analysis to understand the discrepancies between previous literature findings and our results, such as analysis of translation rates and observations of p21 levels under OTUD6B overexpressed conditions in different cell lines. Despite this however, our findings report a novel relationship between OTUD6B and p21 protein levels.

Of interest it should be noted that while OTUD6B overexpression can decrease p21 levels to below that of control, we were not able to show full recovery of p21 basal levels in our rescue experiments with the HEK293T knockout cell lines (Figure 16, B). It is possible that once OTUD6B depletion induces p21 levels, it is difficult to inhibit this induction pathway. An example of such occurrences is during G2 phase cell cycle arrest when increased levels of p53 and p21 facilitate the degradation of mitotic proteins necessary for cell cycle progression and promote a permanent pause in cell cycle [11]. Thus, it is possible that as p21 is an initiator of senescent phenotypes, it becomes difficult to inhibit once it has been activated. To fully clarify this observation, further rescue experiments should be performed both within our OTUD6B KO 293T cell line as well as other cancer cell lines.

In addition, we also performed recovery experiments with our catalytically inactive p3x-flag-CMV-9-OTUD6B-C188S plasmids to determine if our p21 induction phenotype was dependent on OTUD6B deubiquitinating activity (Figure 19). Similar to our rescue experimental results with our OTUD6B KO 293T cell line, reintroducion of OTUD6B C188S inactive mutants in MCF-7 breast cancer cell lines showed partial recovery of p21 basal levels. Previous liturature has confirmed that mutating the

catalytic cysteine of this DUB to a serine is able to disrupt the isopeptidase activity of the enzyme [20]. Partial recovery of p21 basal levels observed by reintroduction of the C188S mutant suggests that OTUD6B regulation of p21 protein levels may not depend on OTUD6B deubiquitinating abilities. Additional OTUs have previously been reported to hold functions that are distinct from their isopeptidase abilities; OTUD4 has been shown to stabilze a single stranded DNA and RNA targeting demethylase, ALKBH2, protecting this protein from degradation in a catalytic independent manner [14]. Thus, our results showing equal p21 levels when rescued with either our wildtype OTUD6B plasmid or our C188S mutants, may suggest that OTUD6B is similar to OTUD4 and does not depend on its catalytic cysteine for all regulatory functions. Ideally, future experiments should include a stably expressing OTUD6B C188S mutant cell line that is absent of wildtype OTUD6B. Creation of this cell line will further support whether or not OTUD6B C188S mutants can increase p21 protein levels.

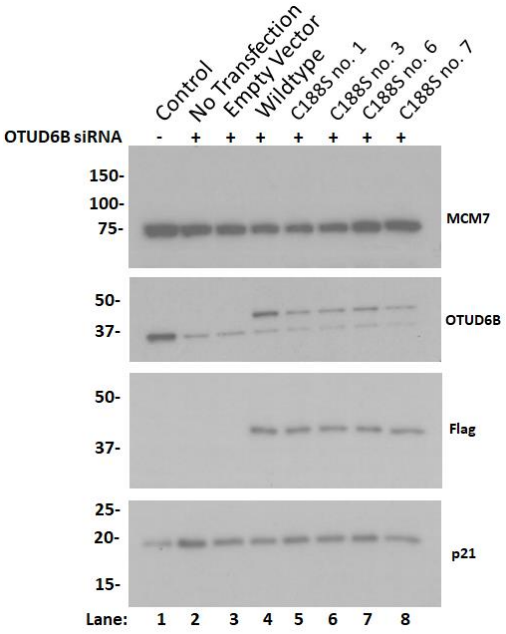

Figure 19. p21 basal levels are partially rescued by OTUD6B wildtype and catalytically inactive mutant introduction. Rescue experiment in MCF-7 breast cancer cell lines with p3xFLAG-CMV-9-OTUD6B or p3xFLAG-CMV-9-OTUD6B-C188S catalytically inactive mutants. Plasmid backbone used was p3xFLAG-CMV-9-OTUD6B. Wildtype refers to our p3xFLAG-CMV-9-OTUD6B clone number 9. C188S mutants listed are from individual clones. siRNA used was OTUD6B #2. Transfected samples were allowed to incubate for 36 hours before harvest. MCM7 was used as a loading control.

Through CHX analysis, we have shown evidence that suggests this OTUD6B dependent induction of p21 is not due to an increase in p21 protein stability (Figure 15). In its free form, p21 is an

unstructured protein and holds the ability to undergo proteasome-based degradation even without a ubiquitin tag [12]. When in complex with other proteins, p21 is a target for degradation by several different E3 ligases [30]. Thus, p21 is a relatively unstable protein with a short half-life [40]. On the other hand, p21 transcription is induced by a plethora of different proteins and pathways. Therefore, it is unsurprising, yet informative, that we observe a disappearance of p21 protein levels by the 6th hour of CHX administration and strengthens support for OTUD6B impacting p21 at the transcriptional level (Figure 15).

To investigate by which factor OTUD6B was inducing the transcription of p21, we analyzed a p53 independent pathway as well as tested p21 induction via p53 dependence. The NF-Kβ pathway is well-known as a mediator of inflammation however it is also a regulator of cell cycle progression through inducing the transcription of certain genes [63]. Once the pathway is activated, NF-Kβ inhibitors, which sequester the transcription factor within the cytosol, are degraded by DUBs A20 and OTUD7B allowing for NF-Kβ to translocate to the nucleus and initiate transcription of downstream genes [16]. Recently, it was shown that under conditions of damage, NF-Kβ induces p21 expression in myeloid leukemia cells, suggesting that p21 is another downstream target of NF-Kβ pathway activation [60]. In comparison, under our conditions of decreased OTUD6B protein expression, we were not able to see any NF-Kβ pathway activation, indicated by nuclear translocation of NF-Kβ, suggesting NF-Kβ pathway activation was an unlikely candidate for initiation of our observed phenotype (Figure 17).

Contrary to these results, we failed to observe p21 induction in cell lines with dysfunctional p53 mutations. MIA-PaCa-2 cells are a cancerous pancreatic cell line containing a missense mutation within the DNA binding domain of p53 in which a positively charged arginine is replaced with tryptophan [64]. While arginine is often found at DNA binding sites due to its positive charge, tryptophan is more commonly considered a hydrophobic or amphipathic amino acid and prevents efficient binding of protein to DNA [65]. Downstream implications of this mutation have shown to be oncogenic with a loss

of anti-tumorigenic function most likely due to p53 inability to bind to regions of the genome that induce the transcription of cell cycle inhibitors, such as p21 [25, 26]. In our analysis, under OTUD6B knockdown conditions, p21 levels were unable to be induced. Although this does not fully confirm that our observed p21 induction under an OTUD6B knockdown is solely through a p53 manner, it strongly suggests that p53 transcription is a promising candidate. Further analysis should be conducted to confirm these discoveries such as the use of p53 targeting siRNA and rescue experiments in which wildtype p53 is reintroduced into an OTUD6B overexpression cell line. As HeLa S3 cervical cancer cell lines have been reported to not express wildtype p53, this could be a potential cell line to investigation p21 induction in [62].

Furthermore, the suggestion of a p53 dependence infers other implications to our p21 phenotype. P21 induction by p53 is often considered to be initiated by the DNA damage check point kinase pathways which occur through ATR or ATM activation and result in a pause cell progression until errors can be fixed [11]. With this understanding, it is curious that our phosphorylated CHK1 levels were not altered between our control samples and our OTUD6B knockdowns. As such, to draw conclusions and fully validate our p53-dependent p21 induction under OTUD6B knockdown conditions, further experiments should be performed to observe if checkpoint pathways are regulated by OTUD6B levels. Additionally, the substrate of OTUD6B that results in our suspected p53 dependent p21 induction must be identified (Figure 20).

In conclusion, despite further needed experimental analysis into how p21 transcription is induced under an OTUD6B knockdown and whether or not this induction can be fully rescued by OTUD6B in a catalytically dependent manner, this work provides a novel and unique relationship between OTUD6B and p21.

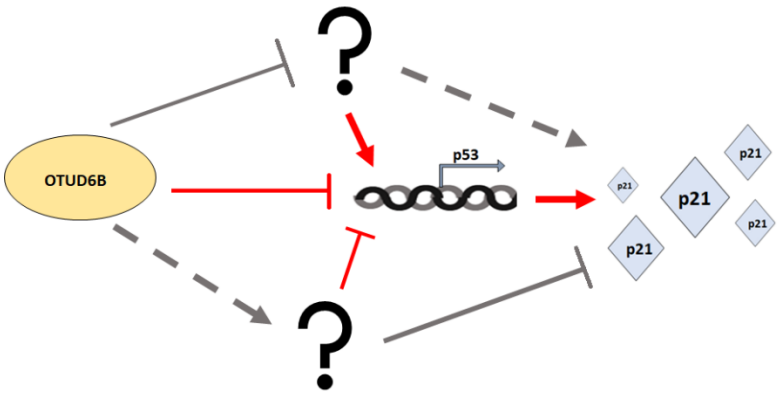

Figure 20. Schematic representing the novel relationship between OTUD6B and p21. Our data supports that OTUD6B inhibits increased expression of p21 most likely through inhibition of p53 transcription either directly or indirectly through the interaction of additional proteins. " ? "refers to currently unidentified proteins which regulate p53 transcription levels. Red arrows indicate pathways our data support. Grey arrows indicate additional pathways that could regulate p21 which our current data does not support.

Chapter Four: OTUD6B Expression Regulates Cell Proliferation Rates

Rational

Induction of p21 has traditionally been a marker for cell cycle arrest and cellular senescence as studies have shown cells absence of p21 acquire spontaneous tumors and uncontrolled growth [30, 38, 41]. Induction of p21 via DNA damage checkpoint kinases effectively pauses cellular progression and proliferation through inhibition of cell cycle phase specific cyclin-cdk complexes and mitotic or S phase proteins such as PCNA and PLK1 [30]. During instances of DNA damage, checkpoint kinase signaling cascades are initiated through the activation of ATM or ATR, depending on which phase of the cell cycle the damage had occurred [30]. While the activation of these kinases stimulate their own cascade of downstream proteins, both still result in increased transcriptional activity of p53 and subsequent expression of p21 [30]. Thus, p53 dependent p21 induction is often seen as an indicator of DNA damage checkpoint kinase activation.

In our previous work, we have shown evidence to suggest that OTUD6B depletion results in p53 dependent transcriptional induction of p21. As this phenotype is often a marker for DNA damage checkpoint kinase activation and downstream cell cycle arrest, we have subsequently explored the potential role OTUD6B may have within this pathway as well as analyzed OTUD6B potential to regulate cellular progression and proliferation rates.

Two published works have suggested OTUD6B may have a functional role within the nucleus or impact activation of checkpoint kinase signaling cascades. Sowa et al. (2009) has presented Gene Ontology (GO) analysis data that suggests OTUD6B may function within the nucleus [2]. Work by Nishi et

al. (2014) has shown that OTUD6B depletion results in checkpoint kinase cascade activation, increased DNA damage, and a decreased ability to repair damage [66]. Based on this data and our own work suggesting a p21 induction under OTUD6B protein depletion, we reasoned that OTUD6B may hold functional importance in the DNA damage response. To determine this, we analyzed OTUD6B impact on cell cycle progression and cellular growth, OTUD6B localization patterns, and how protein expression of this OTU impacts DNA damage response, senescence, and apoptotic markers.

Experimental Design

Cell Lines and Chemical Reagents Agents

HEK293T, WI-38, HeLa cells were purchased from the American Type Culture Collection (ATCC). MCF-7 and T80 cells were gifted from Dr. Meera Nanjundan at the University of South Florida's Cell and Molecular Biology Program. HEK293T OTUD6B KO #34 previously described in Chapter 3, Experimental Design, were also used. HEK293T, MCF-7, HeLa, and WI-38 cells were cultured in Dulbecco's Modified Eagle's Medium (DMEM) supplemented with 10% bovine serum and 10% Penicillin-Streptomycin with L-glutamine except for in cases of siRNA and DNA transfections. T80 ovarian cancer cells were cultured in RPMI supplemented with 10% bovine serum and Penicillin-Streptomycin with L-glutamine except for in cases of siRNA and DNA transfections. Cells were grown at 37^{o}C in 5% CO_2 atmosphere.

DNA damaging agents used were Etoposide (Selleckchem), Bleomycin (Selleckchem), UV irradiation. Unless otherwise indicated Etoposide was treated at 2uM for 15 hours, Bleomycin was treated at 5uM for 24 hours, and ultraviolet irradiation occurred at 70 J/m^2 UVC (UV stratalinker 2400) with a 1 hour recovery.

RNA Interference

Cells were cultured in Penicillin-Streptomycin free media and seeded at 30% confluency. At the time of seeding, samples were transfected with 20nM of designated siRNA. Transfection reagents used included Opti-MEM (Invitrogen) and lipofectamine RNAimax (Invitrogen) used at a 1:100 mass to volume ratio and a 1:1 mass to volume ratio, respectively [51]. All siRNA transfected samples were allowed to incubate for 72 hours post transfection unless otherwise instructed [51]. The following siRNA sequences were used: OTUD6B siRNA #1: 5' -AGGGUCAUUGAUAGCAAGUAA 3' from Qiagen, OTUD6B siRNA #2: 5' -UAGUAUGGUGAUGGUCAAUUU 3' from Qiagen, OTUD6B siRNA #3: 5'-CAGUGUAAAAGGUCCAAG 3' from Bioneer, OTUD6B siRNA #4: 5'- CACCAAUAGAGAUAAUACA 3' from Ambion, UAF1 siRNA #1: 5'-CUGGAAUAUUGGCCUAGAA 3' from Bioneer. RAD51 siRNA #1: 5' -CAGUAGUCACAAACUGAUC 3' from Bioneer, and OTUD5 siRNA #2: 5'-GGGUGCCGAAGAUAGACAAUU 3'.

A scrambled siRNA was used as control: All-Star Negative from Qiagen or Negative control siRNA from Bioneer, as indicated.

Cell Cycle Analysis

Cells, seeded in 6cm plates, were transfected with siRNA as previously described in Chapter 3 and in Chapter 4 (Experimental Design, RNA Interference).

If synchronous, after 48 hours of siRNA treatment, cells were treated with 2.5mM of thymidine for 18 hours [52]. Cell samples were then washed with warm DMEM, supplemented with 10% bovine serum and 10% Penicillin-Streptomycin with L-glutamine, twice and left in fresh DMEM supplemented media for 8 hours [52]. Samples were split into larger plates within the first 4 hours if confluency was reached at the end of the 8 hours. After 8 hours a second thymidine treatment occurred at 2.5mM per sample [52]. After another 18 hours, cells were released by washing twice with warm DMEM supplemented media [52].

Regardless if cells were synchronous or asynchronous, samples were collected at given timepoints via trypsinization with 500uL and subjected to a 5 minute spin at 4^{O}C and 3500rpm [53]. Samples were washed with 500uL of 1x PBS and subjected to an additional 5 minute spin at 4^{O}C and 3500rpm [53]. Samples were then fixed with 500uL of 70% ethanol, vortexed, and incubated at 4^{O}C for 1 hour in the dark [53]. Samples were then washed twice with 500uL of 1x PBS and stained with 432uL of 50ug/mL propidium iodide (Millipore Sigma), 5uL of 10% triton x-100, and 63uL of 200ug/uL Ribonuclease A (RNase) (Sigma) per sample and subjected to a quick vortex before a 1 hour incubation at 4^{O}C in the dark [53]. Samples were then taken to the USF COM Fred Wright Jr Flow Cytometry Core at USF Health in Tampa to be analyzed via flow cytometry. Approximately 25,000 cells were counted from each sample.

Cell Doubling Rate/Trypan Blue Staining

Wildtype HEK293T cells and OTUD6B KO #34 HEK293T cells were each seeded into their own four wells of a 24 well plate at 100 cells per 500uL of DMEM media using a hemocytometer. Cells in respective wells were then collected at time points indicated via a 150uL wash with 1xPBS followed by 25uL of trypsin-EDTA (ThermoFisher) for 1 minute, and an additional 25uL of DMEM media to inactivate the trypsin. Samples were collected in a microcentrifuge tube and treated with 50uL of .4% Trypan Blue (ThermoFisher) for 3 minutes at room temperature. Viable cells were then counted using a hemocytometer and values were graphed on Excel. Three experimental replicates were performed for error bars. Occasionally, photographic images of cells in wells were recorded at a 4x objective and using a EO USB 2.0 CCD Machine Vision Camera from EO Edmund Optics Worldwide.

Senescence β-galactosidase Cell Staining

Senescent cells express increased lysosomal content which results in increased activity of 6.0 pH-dependent β-galactosidase [41, 47, 67]. Thus, cells expressing high levels of β-galactosidase have

become a biomarker for cellular senescence [41]. β-galactosidase cell staining was performed according to the Cell Signaling Technologies Senescence β-galactosidase Cell Staining Kit instructions. Briefly, WI-38 cells were seeded in 6 welled plates and treated to indicated siRNA following previously indicated procedures (Chapter 4, Experimental Design, RNA Interference). 72 hours after siRNA treatment wells were washed with 2mLs of 1xPBS [41]. 1mL of 1x fixative solution (CST) was administered to each well for 15 minutes at room temperature [41]. Wells were washed twice with 1mL of 1xPBS followed by the addition of 1.5mLs of 1x β-Galactosidase staining solution (CST) [41]. Plates were then sealed using parafilm to prevent evaporation, and subsequent crystal formation, following incubation at 37^{O}C overnight in a dry incubator as CO_2 can induce a change in pH [41]. Following overnight incubation, 1x β-Galactosidase staining solution was removed and replaced with 1mL of 70% glycerol and stored at 4^{O}C, still sealed with parafilm, for long term storage [41].

Images were captured using the brightfield on a Keyence microscope provided by Dr. Margaret Park at the University of South Florida's Cell and Molecular Biology Program. Quantification of cells positive for β-Galactosidase staining was conducted using the "multi-point" tool on ImageJ. Data was displayed at as percentage of the total number of cells counted.

Immunofluorescent Microscopy

Cell samples grown on 12mM in width, .13-.17mM in thickness, sized coverslips were washed twice with 1mL of cold 1x PBS following a 10 minute fixation with 4% paraformaldehyde in the dark [51]. Cells were then washed again with 1mL of cold 1x PBS and permeabilized with .25% Triton x-100 diluted in H_2O for 5 minutes in the dark [51]. Coverslips were washed as described earlier and incubated with 30uL of primary antibody diluted in 1x PBS for 1 hour in the dark [51]. After, samples were washed again with PBS as described previously and incubated with 30uL of either Alexa Flour 488-anti-mouse and/or anti-rabbit secondary antibody diluted in 1x PBS for 1 hour in the dark [51]. After additional 1mL 1x PBS

washing, coverslips were placed on slides using Vectashield mounting medium for fluorescence with DAPI (Vector Laboratories Inc) to stain nuclei [51]. Images were collected using either the Lecia DMi8 fluorescence microscope under a 63x oil objective and the Leca Las X imaging and analysis software or collected with a Zeiss Axiovert 200 microscope equipped with a Perkin Elmer ERS spinning disk confocal imager and a 63x oil objective using the Velocity software (Perkin Elmer). Using ImageJ, between 300 and 500 cells were counted for ϒ-H2AX staining quantification and about 200 cells were counted for pATM staining quantification.

Primary antibodies used were anti-pATM [1:300] (R) (Abcam), anti-Flag M2 (1:200) (M) (Sigma), ϒ-H2AX [1:500] (R) (Novus), ϒ-H2AX [1:500] (M) (Millipore sigma), and 53BP1 [1:500] (R) (CST).

Chromatin Enriched Fractionation

Cell samples were washed with 1mL of 1x PBS prior to harvest by scraping with commercially available cell scrapers [51]. Harvested samples were spun down at 4000rpm for 5 minutes at 4^{o}C followed by a 5 minute resuspension of the pellet on ice in .5% NP40 Buffer containing 100mM of NaCl, 50mM Tris, and 5X the volume of protease inhibitor (Thermofischer Scientific) [51]. Samples were then spun down at 3000rpm for 5 minutes at 4^{o}C [51]. Resulting supernatant was moved to a new microcentrifuge tube and spun for 5 minutes at 3000rpm at 4^{o}C [51]. Remaining supernatant, containing the S100 fraction, was then move to a new microcentrifuge tube, without disrupting the pellet, and subjected to optical density measurements compared to a standard bovine serum albumin (BSA) curve using Protein Assay Dye (Bio-Rad). 2x laemmli sample buffer (Bio-Rad) was then added to S100 fraction depending on volume, followed by a 5 minute ~95^{o}C heat block incubation.

The remaining pellet from the second 5 minute centrifugation was washed with the same volume of .5% NP40 buffer and immediately spun down at 3000rpm for 5 minutes at 4^{o}C [51]. Supernatant was then removed and the remaining pellet was lysed on ice for 10 minutes with 1% NP40

buffer containing 300mM of NaCl and 50mM of Tris, and 5X the volume of protease inhibitor (Thermofischer Scientific) [51]. This solution, containing the P fraction, was then subjected to optical density measurements compared to a standard bovine serum albumin (BSA) curve using Protein Assay Dye (Bio-Rad). 2x laemmli sample buffer (Bio-Rad) was then added to S100 fraction depending on volume, followed by a 5 minute ~95^{o}C heat block incubation.

DNA Transfections

Cells were cultured in Penicillin-Streptomycin free media. Once cell confluency reached 60-70% samples were transfected with 1ug/mL of media of designated DNA. Transfection reagents used included Opti-MEM (Invitrogen) and Turbofect (Thermofischer Scientific) used at a 1:100 DNA mass to volume ratio and a 1:2 DNA mass to volume ratio, respectively [51]. DNA transfected samples were allowed to incubate for at least 24 hours post transfection, unless otherwise indicated, to ensure desired protein was expressed [51].

Plasmids

Plasmids used were an empty vector p3XFlag-CMV-9 nonretroviral overexpression vector purchased from Addgene, a previously developed p3XFlag-CMV-9-OTUD6B clone number 9 plasmid (Chapter 3, Experimental Design, Plasmids), and a previously Kee lab developed p3XFlag-CMV-9-RNF2 plasmid created by Dr. Kim using similar procedures as our p3XFlag-CMV-9-OTUD6B plasmid.

Mutagenesis of OTUD6B Predicted Nuclear localization Signal (NLS)

Site-directed mutagenesis was performed following the Stratagene QuikChange Site-directed Mutagenesis Protocol. OTUD6B42_46del mutant was created using our newly developed p3XFlag-CMV-9-OTUD6B clone number 9 plasmid as the starting template (Figure 21, A). The predicted NLS of OTUD6B

was determined using the cNLS Mapper which predicts importin α-dependent NLS [68] (Figure 21, B). Briefly, primers were designed to contain and amplify the desired 42_46del mutation on the OTUD6B isoform 1 nucleotide sequence:

Forward: **5'** GTT CCC AAG AAT GAC CAA CTC ACC GAA GAA G **3'**

Reverse: **3'** CAA GGG TTC TTA CTG GTT GAG TGG CTT CTT C **5'**

where the predicted NLS is highlighted in yellow. GC content was 48% and melting temperature was 79.4^{o}C. With these primers, the 5 amino acid sequence KKRRK, of the predicted NLS, are exempted from the protein (Figure 21, B).

Conventional mutagenesis polymerase chain reaction (PCR) was used to amplify 100ng of p3xflag-CMV-9-OTUD6B plasmid with the desired deletion mutation. PCR reaction contained .5uL p3xflag-CMV-9-OTUD6B plasmid, .5uL of Phusion High Fidelity DNA polymerase (Thermo Fcientific), 5uL of 5x HF buffer, 4uL of DNTPs, 1uL of each the forward and reverse primer brought up to a total reaction mixture of 25uL with H_2O [53]. Annealing temperature was 61^{o}C with 18 cycles (Figure 21, C).

To destroy parental OTUD6B-3XFlag wildtype plasmid but keep 42_46del mutant OTUD6B-3XFlag plasmid, Dpn1 digestion was performed on the 25uL PCR reaction with 1.25uL of Dpn1 (NEB) for 1 hour and 45 minutes at 37^{o}C (Figure 21, D) [53].

Potential p3xflag-CMV-9-OTUD6B C188S plasmids were then transformed into Top10 competent E.coli cells via heat shocking method in which 50uL of E.coli are incubated with 5uL of the dpn1 digested reaction for 30 minutes on ice, followed by a 45 second incubation in a 42^{o}C water bath, and then a 2 minute incubation on ice [53]. Transformed cells were grown up at 37^{o}C for 1 hour in 250uL of LB and then plated on LB Agar ampicillin resistant plates. Colonies that developed were

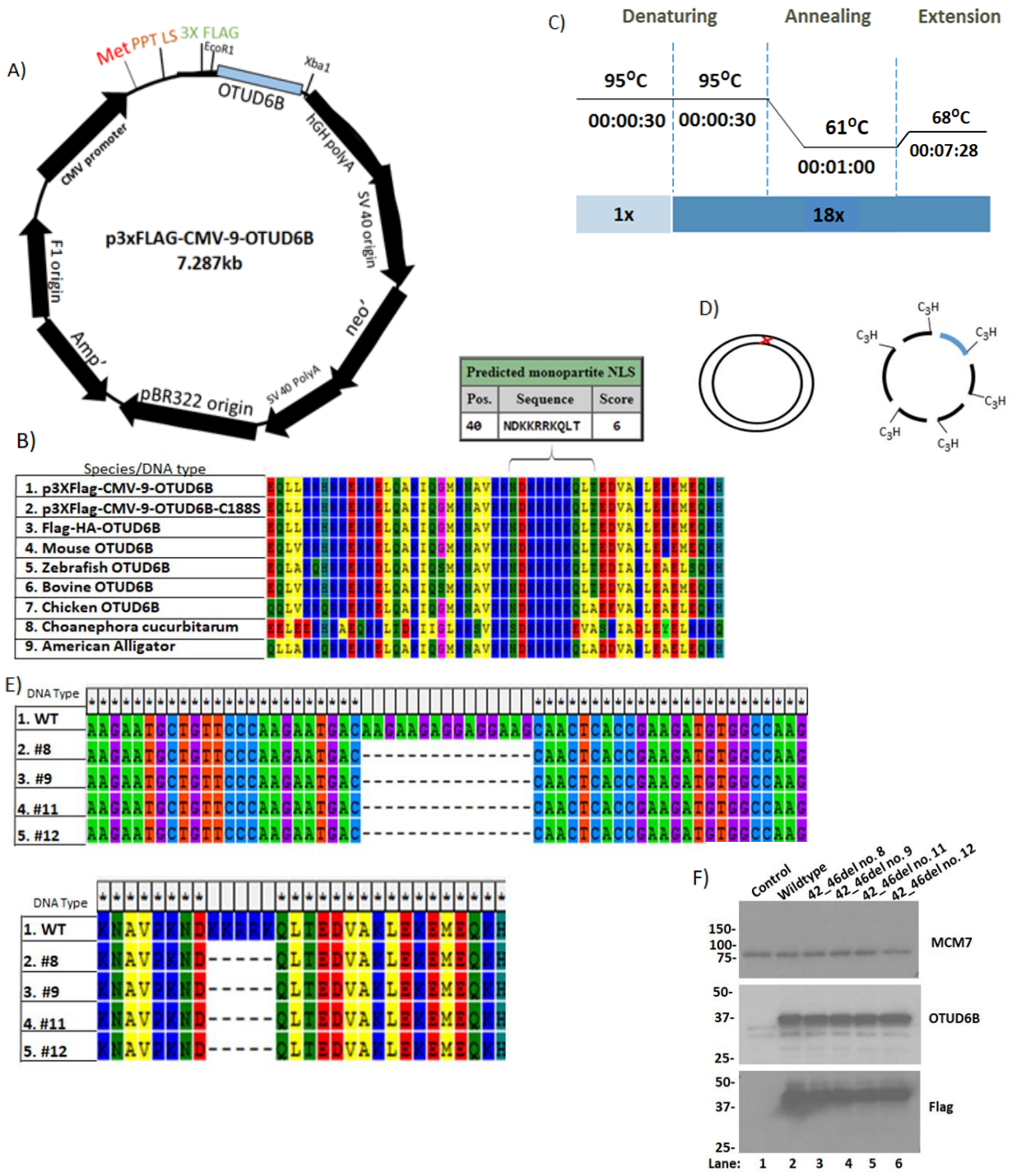

Figure 21. Creation of OTUD6B NLS mutant. A) Plasmid map of p3XFlag-CMV-9-OTUD6B used as the starting template for mutagenesis. B) Amino acid sequence alignment of OTUD6B in various species including our p3xFlag-CMV-9-OTUD6B wildtype and C188S mutant plasmids and our Flag-HA-OTUD6B plasmid (Addgene) created on MEGA. The predicted NLS sequence from cNLS Mapper is indicated and starts at residue 40 with a predicted cut-off score of 6. Higher score indicates stronger NLS activities with the highest score being 10 [67]. C) Conventional mutagenesis polymerase chain reaction (PCR). PCR had an annealing temperature of 61^{o}C and 18 cycles. D) Dpn1 digestion to destroy parental OTUD6B-3xFlag wildtype plasmid. Red X indicates mutant plasmid's mutation. E) Nucleotide (top) and amino acid (bottom) sequence alignments of resulting 42_46del predicted NLS mutants compared to wildtype OTUD6B created on MEGA. F) Plasmid expression test in MCF-7 cells with wildtype OTUD6B or 42_46del predicted NLS mutants. Plasmid backbone used was p3xFlag-CMV-9-OTUD6B. 42_46del predicted NLS mutants listed are from individual clones. Control represents empty vector p3xFlag-CMV-9 plasmid. MCM7 was used as a loading control.

inoculated with ampicillin and grown-up in 10mL volumes with LB for mini-prep of potential p3xflag-CMV-9-OTUD6B-42_46del predicted NLS mutant plasmids using Qiagen QIAprep spin miniprep kit. 1-2ug of DNA from 12 mini-prepped clones were sent to Eurofins Lancaster Laboratories for DNA sequence verification. DNA sequencing and western blot plasmid expression test using transient transfections of p3xflag-CMV-9-OTUD6B wildtype and p3xflag-CMV-9-OTUD6B-42_46del mutants (described in Chapter 4, Experimental Design, DNA transfections) showed clone numbers 8, 9, 11, and 12 were successful deletion mutations (Figure 21, E-F). p3xflag-CMV-9-OTUD6B-42_46del clone 9 was used for future experimental procedures when necessary (Figure 21, F).

Creation of p3xFlag-CMV-9 Stable cell lines

To analyze OTUD6B localization, three HeLa cells lines were created to stably express our p3xFlag-CMV-9 plasmid, either integrated with no insert (Empty Vector) or with our OTUD6B wildtype or 42_46del sequences. The p3xFlag-CMV-9 plasmid is a nonretroviral plasmid and therefore, integration of desired DNA must rely on transient transfection methods followed by drug selection processes.

Although unclear, research has shown that random integration of transfected DNA into cellular genomes does occur [69]. Theories of the mechanism behind these occurrences are mixed but it is agreed that integration of the sequence does not seem to rely on sequence similarity between the integration site within the genome and the exogenous DNA [69]. Data also suggests that the ligation events may be occurring between the plasmid and spontaneous breaks within cellular genomes and that these sites are not necessarily in repetitive sequences [69].

To create Empty vector p3xFlag-CMV-9, OTUD6B Wildtype p3xFlag-CMV-9, and OTUD6B 42_46del p3xFlag-CMV-9 stable cell lines, HeLa cells with a low passage number were seeded in a 6-welled plate and grown to a 60-70% confluency with Penicillin-Streptomycin free media. Cells were then transfected with 2ug of p3xFlag-CMV-9-empty vector, p3xFlag-CMV-9-OTUD6B wildtype, or p3xFlag-

CMV-9-OTUD6B-42_46del plasmid. An additional well was seed as a selection control and transfected with no DNA but was still administered transfection reagents. Transfection reagents included Opti-MEM (Invitrogen) and Turbofect (Thermofischer Scientific) used at a 1:100 DNA mass to volume ratio and a 1:2 DNA mass to volume ratio, respectively. Prior to transfection, 500uL of media was removed from each well in increase transfection efficiency. Samples, once confluency was reached, were moved to a 6cm plate where they were subjected to 10ug/mL of Geneticin-sulfate (G418) (Fisher Bioreagents) for selection for 12 hours. Following the 12 hour incubation, cells were washed with fresh DMEM media and replaced with new media containing G418 at 1ug/mL of media. Selection process occurred until no non-transfected cells in the control sample had survived, moving the cells to larger plate sizes once confluency had been reached.

After two weeks of selection, transfected cells were grown to 10mL plates and 1mL pellets were collected and subjected to western blot analysis (Chapter 4, Experimental design, Protein Lysis and Western blotting) (Figure 22, A-B). Once expression of Flag-tagged OTUD6B was observed, cells were examined through immunofluorescent microscopy to observe the extent of Flag-tagged OTUD6B wildtype and 42_46del expression (Chapter 4, Experimental design, Immunofluorescent Microscopy) (Figure 22, C).

Pooled HeLa stable cell lines Empty vector p3xFlag-CMV-9, OTUD6B Wildtype p3xFlag-CMV-9, and OTUD6B 42_46del p3xFlag-CMV-9 were then subjected to 96 welled single cell selection to improve expression efficiencies. Single cells from this pooled groups were grown up into 6cm plates and then subjected to immunofluorescent microscopy to analyze Flag-tagged OTUD6B or empty vector expression. Improved Flag-tagged OTUD6B or empty vector expression cell lines were stored as stocks for future use.

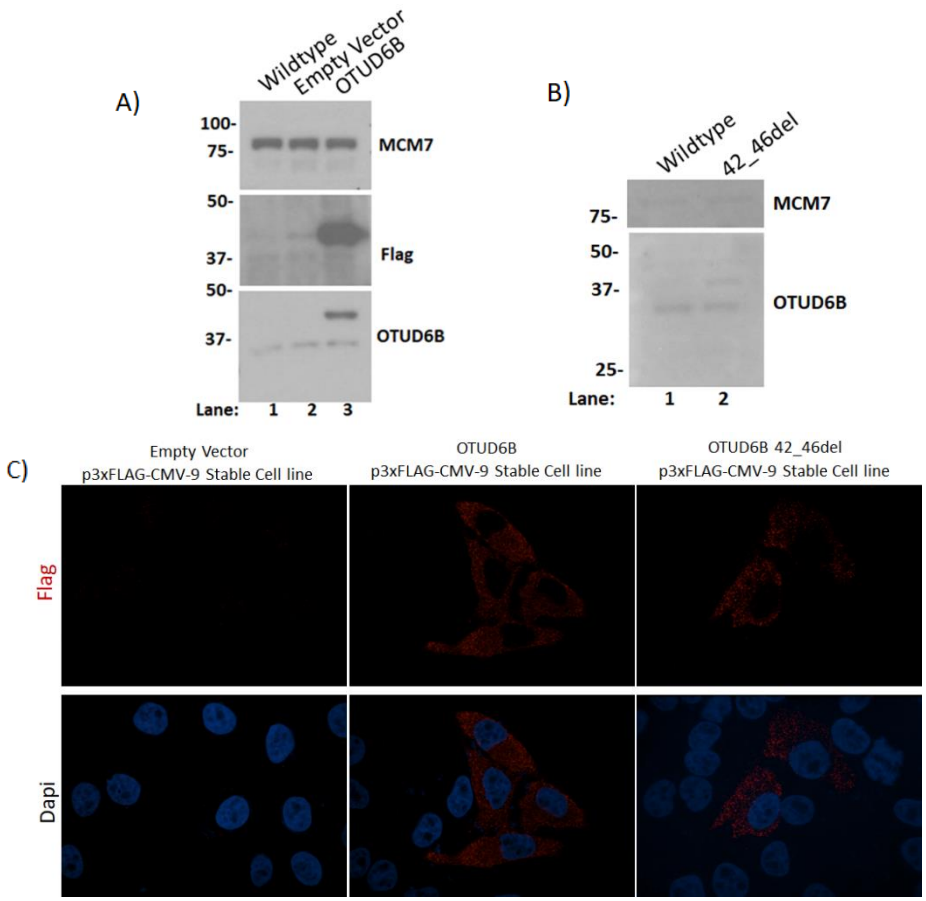

Figure 22. Verification of OTUD6B mutant and OTUD6B 42_46del p3XFlag-CMV-9 expressing stable cell lines. A) Expression test of pooled HeLa Empty Vector p3XFlag-CMV-9 and OTUD6B Wildtype p3Xflag-CMV-9 stable cell lines. Wildtype indicates a wildtype HeLa cell line for comparison. Empty vector refers to the Empty Vector p3XFlag-CMV-9 stable cell line and OTUD6B refers to the OTUD6B Wildtype p3Xflag-CMV-9 stable cell line. MCM7 is used as a loading control. B) Expression test of pooled OTUD6B 42_46del p3Xflag-CMV-9 stable cell line. Wildtype indicates a wildtype HeLa cell line for comparison. 42_46del refers to the OTUD6B 42_46del p3Xflag-CMV-9 stable cell line. MCM7 is used as a loading control. C) Immunofluorescent microscopy of pooled HeLa Empty Vector p3XFlag-CMV-9, OTUD6B Wildtype p3Xflag-CMV-9, and OTUD6B 42_46del p3Xflag-CMV-9 stable cell lines. Cells were stained with anti-Flag antibody (Sigma) and mounted with dapi to stain nuclei.

Protein lysis and Western Blotting

Cell samples were washed with 1-2mLs of 1x phosphate buffered saline (PBS) depending on pellet size**.** Harvested samples were spun down at 4000rpm for 5 minutes followed by administration of RPPA lysis buffer containing 1% Triton X-100, 50nM HEPES, 150nM NaCl, 1mM $MgCl_2$, 1mM EGTA, 10% glycerol, 1x protease cocktail inhibitor (Thermofischer Scientific), and 1x phosphatase cocktail inhibitor (Thermofischer Scientific) [57]. Samples were incubated in lysis buffer for 1 hour at 4^oC following a 10 minute centrifuge spin at 14000rpm [57]. Protein concentration assessment involved optical density

measurements compared to a standard bovine serum albumin (BSA) curve using Protein Assay Dye (Bio-Rad). 2x laemmli sample buffer (Bio-Rad) was added to samples following a 5 minute ~95^{o}C heat block incubation [51].

Prepared protein samples were run on SDS-PAGE gels at 105 constant volts for ~120 minutes unless otherwise indicated. Separated proteins were transferred to a PVDF membrane using a semi-dry Trans-blot Turbo [51]. Membranes were probed with primary antibodies overnight at 4^{o}C followed by a 1 hour wash in 1x tris-buffered saline with Tween (TBST) at room temperature. Membranes were then incubated for 1 hour at room temperature with mouse or rabbit secondary antibody linked to horseradish peroxidase (Cell Signaling Technologies (CST)) followed by an additional 4 hours of room temperature washing in 1xTBST [51]. Results were observed using Pierce ECL Western Blotting Substrate (Thermofischer Scientific).

The following antibodies were used: anti-p21 [1:500] (R) (CST), anti-OTUD6B [1:333] (R) (Abcam), anti-MCM7 [1:1000] (R) (Bethyl), anti-Flag [1:100] (M) (Sigma), anti-β-Tubulin [1:3000] (M) (CST), anti-Parp1 [1:500] (R) (CST), anti-OTUD5 [1:500] (R) (CST).

Results

OTUD6B Protein Depletion Suppresses Cell Cycle Progression and Cellular Proliferation

Increased levels of p21 occur at two phases of normal cell cycle progression, G1 and G2 [30]. Additionally, p53 activity during G2 has been shown to be sufficient to permanently arrest cells in G2, even in the absence of DNA damaging conditions [11]. As our previous data has shown a p21 induction, potentially through p53 activity under reduced OTUD6B protein conditions, we wanted to determine if cell cycle profiles of asynchronous cells depleted of OTUD6B resulted in a G1 or G2 phenotype. This would link our observed p21 induction to cellular arrest of a specific phase within the cell cycle. Thus, we used flow cytometry analysis methods with PI staining on asynchronous Hela cells treated with control

or OTUD6B siRNA. Results of three separate experimental trials reported a minor increase in asynchronous cells possessing a G1 profile when OTUD6B was depleted (Figure 23). These results suggest that our p21 induction phenotype may be resulting in a G1 cell cycle arrest.

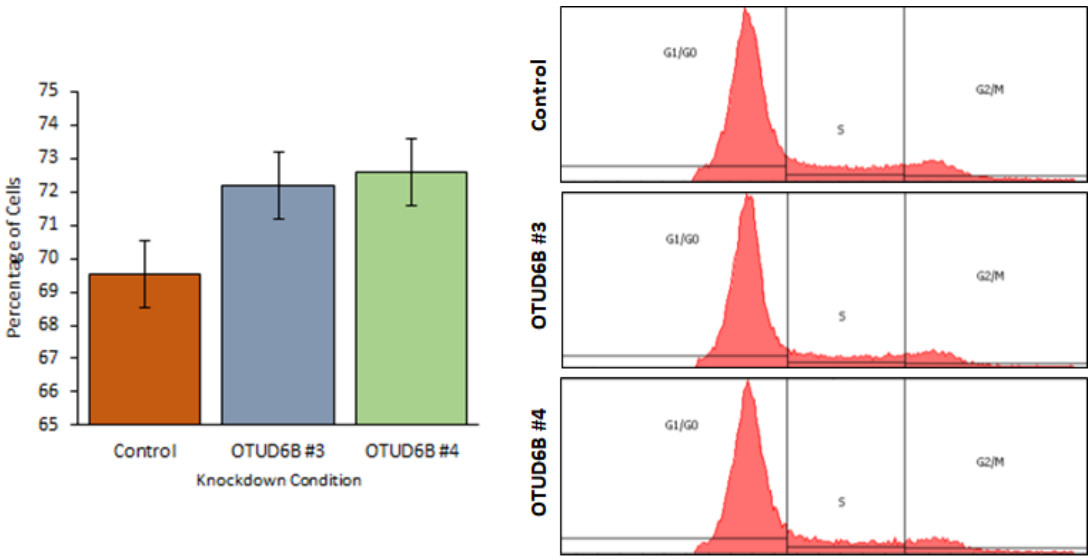

Figure 23. OTUD6B depletion in asynchronous cells results in minor G1 phase cell cycle arrest. Asynchronous HeLa cells treated with two different OTUD6B siRNAs and control siRNA from Bioneer were subjected to PI staining and flow cytometry analysis. To the left is a bar graph representing the percentage of cells in G1/G0 phase of the cell cycle 72 hours after siRNA treatment. To the right are representative cell cycle profile results.

As we observed only a minor effect of cells representing G1 profiles, we wished to further solidify our results that OTUD6B protein depletion results in a G1 cell cycle arrest. To do this, we used a double thymidine block method to observe HeLa progression from a G1/S phase cell cycle arrest to G2. Thymidine treatments induce competitive inhibition of deoxynucleotide synthesis resulting in inhibition of DNA replication processes, thus pausing cellular progression at the phase of cell cycle when p21 levels are expected to drop [30]. We hypothesized that if OTUD6B induces p21 and if this p21 induction results in a G1 phase cell cycle arrest, then cells depleted of OTUD6B should be unable or hold delayed progression abilities to move from G1/S to G2 because they contain increased levels of p21 compared to control conditions. Results presented a slight delay of cellular progression into G2 when OTUD6B siRNA was used; a higher percentage of cells were still present in G1 phase under an OTUD6B depletion compared to control samples 6 hours after they were released (Figure 24, A-B).

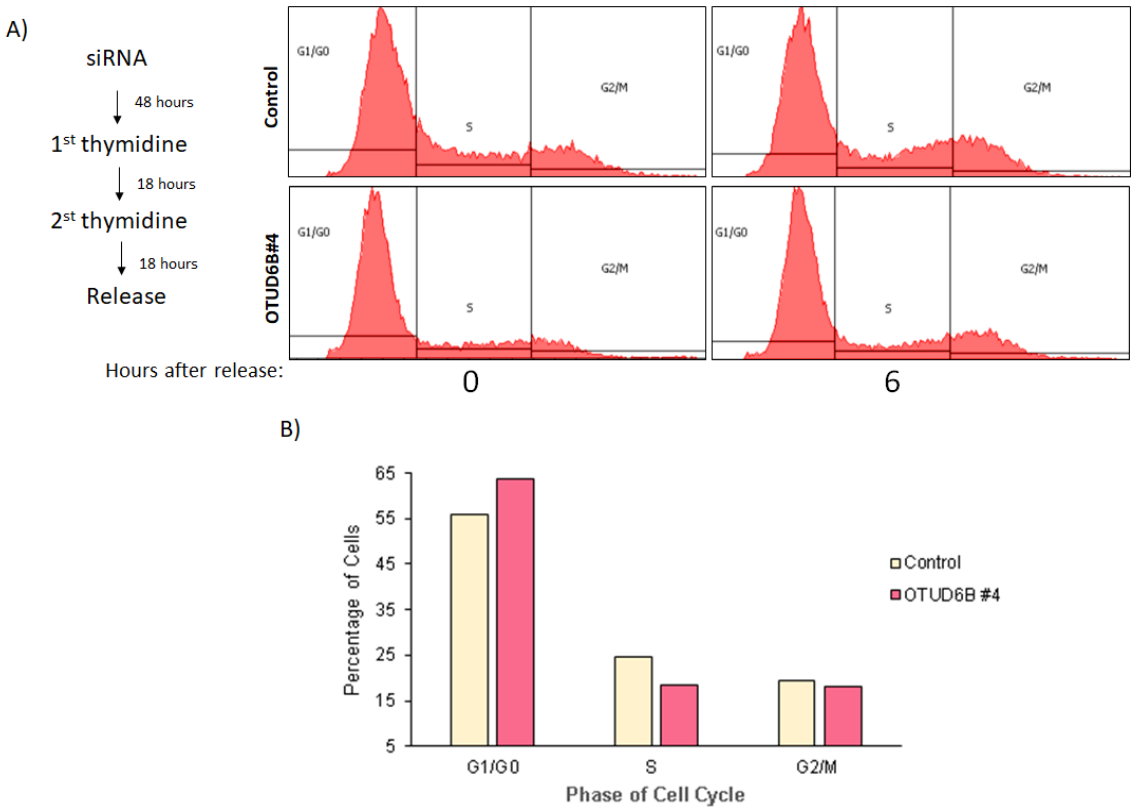

Figure 24. OTUD6B depletion results in slowed cell cycle progression into G2. A) A double thymidine block in HeLa cells treated with OTUD6B siRNA #4. Control represents siRNA control from Bioneer. To the left is a schematic of the experimental design. B) Bar graph representing the percentage of cells in each cell cycle phase 6 hours after double thymidine block release for control and OTUD6B #4 siRNA conditions.

As we have observed only a minor delay in cell cycle progression under an OTUD6B depletion, we wanted to determine if this delay was sufficient to slow cellular proliferation and doubling rate of cancer cells. To analyze this, we used our OTUD6B KO #34 HEK293T cell line and compared the cellular doubling rate to wildtype HEK293T kidney cancer cells using a .4% Trypan Blue staining methods [23]. Results showed that when HEK293T kidney cancer cells are absent of OTUD6B for an extended period of time, cellular dividing rate is significantly deterred (Figure 25). Representative images of each cell line after 72 hours of seeding showed smaller colonies and increased cellular granulation within the OTUD6B KO #34 HEK2293T cell line compared to wildtype (Figure 25, B). Thus, our results suggest decreased cell proliferation and cell cycle progression when OTUD6B protein levels are depleted.

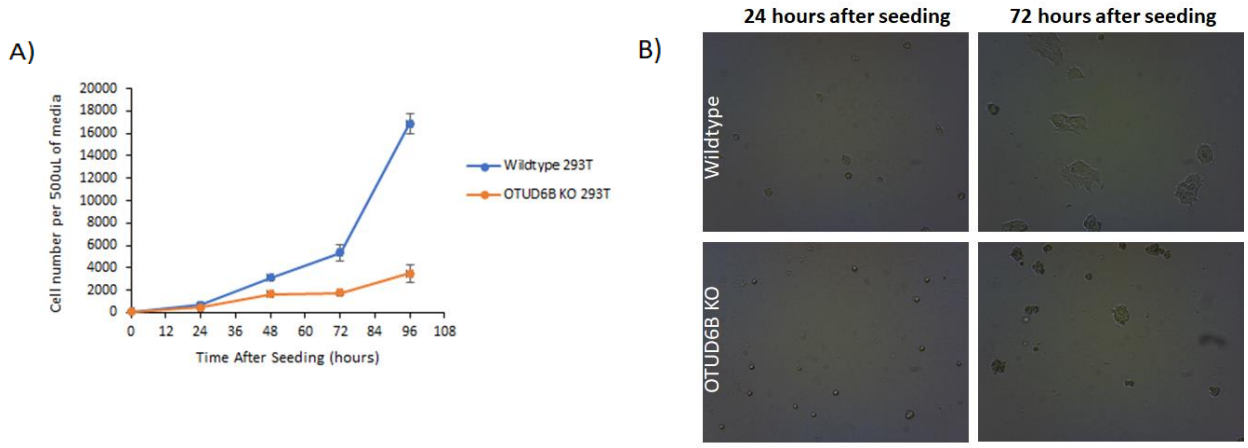

Figure 25. Decreased OTUD6B protein expression slows proliferation in HEK293T kidney cells. A) Wildtype HEK293T cells and our HEK293T OTUD6B KO #34 cells were each seeded at 100cells/500uL of media and analyzed in 24 hour intervals by cell counting with a hemocytometer with .4% trypan blue staining. B) Representative images of HEK293T cell growth under indicated conditions.

OTUD6B Depletion Promotes Cellular Senescence

As our data suggests slowed growth, minor G1 arrest, and an induction of p21 in cancer model cell lines under OTUD6B depletion we speculated if OTUD6B could promote permanent cell cycle arrest and cellular senescence. Cellular senescence is a term used to describe cells which are continuously paused in cell cycle arrest and do not experience proliferation of cell cycle progression [41, 50]. Cellular senescence is often the result of long-term activation of G1 checkpoint kinase cell cycle arrest or short-term activation of G2 checkpoint kinase cell cycle arrest [11]. It is thought that this cellular event had evolved as a mechanism to avoid transformation of DNA damaged cells; thus, entrance into senescence conventionally can only be investigated in non-transformed cell lines [50]. WI-38 fibroblasts are non-transformed cells derived from fetus lung tissue and were used to explore our studies of senescence onset

To test our hypothesis, we first wanted to observe if p21 induction could occur within WI-38 fibroblasts under our investigated conditions because long-term p21 induction is often considered a hallmark of senescence [41]. Upon depletion of OTUD6B protein levels with siRNA, we were able to

observe induction of p21 in WI-38 cell lines (Figure 26, A). We then depleted OTUD6B with siRNA and observed the degree of β-galactosidase staining that occurred in the WI-38 fibroblasts. β-galactosidase staining is a useful tool to examine cellular senescence because senescent cells express increased lysosomal content which results in increased activity of 6.0 pH-dependent β-galactosidase [41]. Increase of this pH-dependent β-galactosidase activity can then experimentally be observed by induction of cells stained blue. Results showed that upon depletion of OTUD6B, cellular senescence increased, indicated by an increase in the percentage of cells stained positive for β-galactosidase (Figure 26, A). UAF1 was used as a positive control because under the depletion of this protein and its binding partner, USP1, cellular senescence is induced through genomic instability, subsequent activation of checkpoint kinases signaling, and the induction of p21 [14, 50].

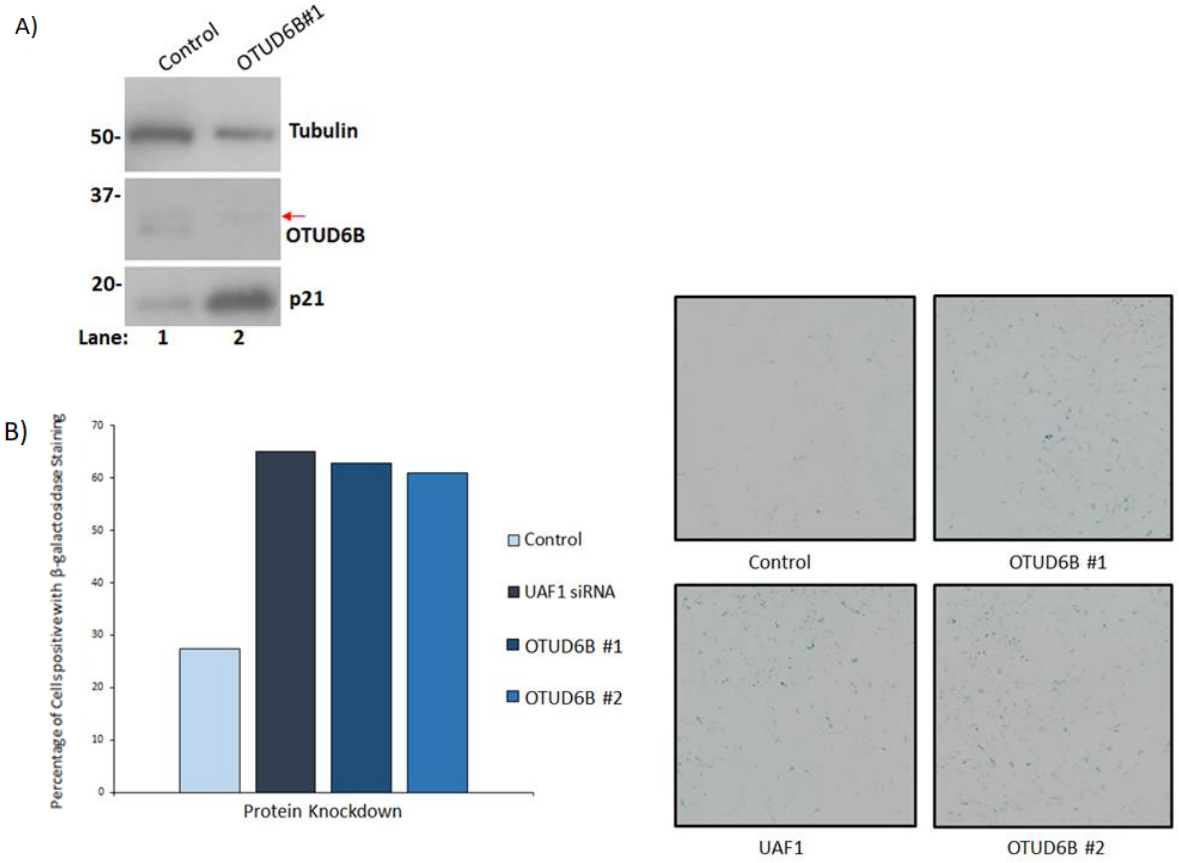

Figure 26. OTUD6B depletion induces p21 and β-galactosidase staining in WI-38 fibroblasts. A) OTUD6B knockdown was conducted with siRNA #3 in WI-38 cells resulting in increased p21 levels. Control represents control All-star negative siRNA from Qiagen. Red arrow indicates protein labeled. Tubulin was used as a loading control. B) β-galactosidase staining results of WI-38 fibroblasts under treatments of different siRNAs. Control represents All-star negative control siRNA from Qiagen. UAF1 siRNA was used as a positive control. To the left is a bar graph quantifying the percentage of cells for each knockdown condition positively stained for β-galactosidase. To the right is a representative image of WI-38 cells for each condition.

OTUD6B is a Primarily Cytosolic Protein Regardless of Cellular Exposure to DNA Damaging Agents

P53 dependent p21 induction often occurs through activation of the DNA damage checkpoint kinase cascades [11]. Because our previous work has shown that OTUD6B may regulate p21 induction in a p53 dependent manner and that our cell cycle profile analysis suggests a G1 arrest under depletion of OTUD6B, we wanted to determine if OTUD6B played a more direct role in DNA damage checkpoint activation.

First, we analyzed OTUD6B localization in response to DNA damage. DUB screenings have previously categorized OTUD6B as primarily a cytosolic protein, however, work has shown that other DUBs, such as OTUD5, can localize to the nucleus under instances of DNA damage or aberrant DNA [2, 53]. With this in mind, we sought to determine if OTUD6B could hold a similar phenotype.

Through exogenous DNA transfections of our p3XFlag-CMV-9-OTUD6B clone number 9 plasmid we exposed HeLa and MCF-7 cell lines to Bleomycin and Etoposide DNA damaging agents as well as UVC irradiation, to observed resulting flag-tagged OTUD6B localization. RNF2, part of the Polycomb Repressive Complex 1 (PRC1), was used as a positive control via exogenous transfection of the p3XFlag-CMV-9-RNF2 plasmid. PRC1 has been shown to localize to the nucleus under instances of damage [51]. ϒ-H2AX was used as an indicator of successfully damaged DNA [51].

Bleomycin, a chemotherapeutic agent, was used to induce double stranded breaks in DNA [46, 53]. Bleomycin was discovered from *Streptomyces verticillus* bacterium and is able to break DNA through two predicted processes, both requiring the use of O_2 and a metal ion such as Fe^{2+} or CU^{+}; Bleomycin can either separate an entire nucleotide from the DNA helix, inducing a break, or it can remove the nucleotide base from the phosphate sugar backbone of the helix, resulting in a “alkali-labile lesion” before forming an entire DNA break [70]. Either product is formed from the initiation of Bleomycin removing a hydrogen atom from the DNA substrate and creating an oxidative DNA structure

[70]. Interestingly, Bleomycin has shown to hold sequence specificity for 5'GC 3' and 5'GT 3' arrangements [70]. In our investigations, upon Bleomycin treatment, no flag-tagged OTUD6B was observed to localize to sites of DNA damage, indicated by ϒ-H2AX foci (Figure 27, A). These results suggest that OTUD6B does not exhibit any nuclear function under bleomycin treatment and experimental conditions used.

Etoposide, often used to treat testicular and other cancers, was also used to induce double stranded breaks in DNA [51]. Etoposide induces DNA damage through its interaction with topoisomerase II, an ATP dependent enzyme which relieves positive super-coiled DNA for successful DNA replication and transcriptional processes [46]. Specifically, Etoposide stabilizes the interaction between topoisomerase II and DNA, preventing double stranded breaks induced by topoisomerase II for DNA uncoiling from being re-ligated [46]. Thus, Etoposide induces double stranded breaks in DNA. Upon Etoposide treatment, our results showed no flag-tagged OTUD6B localization to the nucleus under DNA damage, indicated by ϒ-H2AX foci (Figure 27, B). These results suggest that OTUD6B does not exhibit any nuclear function under etoposide treatment and possibly, more broadly, double stranded DNA breaks in general, under our experimental conditions.

UV treatment was also used to observe OTUD6B localization under damage. While natural UVC is not an entirely clinically relevant DNA damaging agent, as it is almost completely absorbed by molecules in the ozone layer, at wavelengths greater than 280 nanometers it is considered the most damaging to DNA if this form of radiation reaches cells [71]. UV irradiation can result in pyrimidine dimers, such as cyclobutene-pyrimidine dimers and 6-4 photoproducts, which are covalent links between two pyrimidines, as well as double stranded breaks [71]. Double stranded breaks induced by UV irradiation are often created during replication by reactive oxygen species, which are increased under UV irradiation due to an increase in nitric oxide synthase synthesis (which can occur during melanin production) [71, 72]. It has been reported that pyrimidine dimers can also result in double

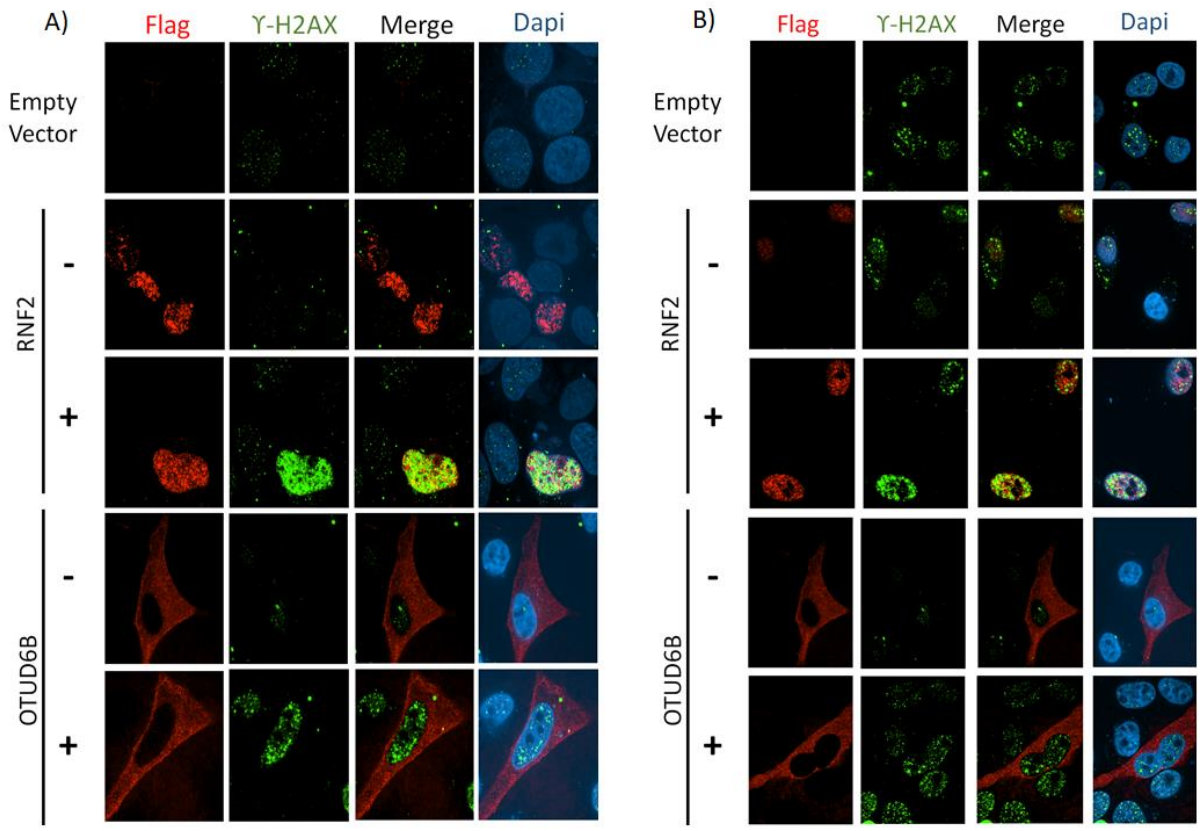

Figure 27. Bleomycin and Etoposide treatment do not exhibit nuclear localization of exogenous OTUD6B. A) HeLa cells treated with (+) or without (-) 5uM of Bleomycin for 24 hours. Flag represented in red indicates the localization of flag-tagged RNF2, flag-tagged OTUD6B, or empty vector. Y-H2AX represented in green indicates the degree of DNA damage within the cell. Plasmid backbone used was p3XFlag-CMV-9. Empty vector was used as a positive control. p3XFlag-CMV-9-OTUD6B clone number 9 was used to observe OTUD6B localization. B) HeLa cells treated with (+) or without (-) 2uM of Etoposide for 15 hours. Flag represented in red indicates the localization of flag-tagged RNF2, flag-tagged OTUD6B, or empty vector. Y-H2AX represented in green indicates the degree of DNA damage within the cell. Plasmid backbone used was p3XFlag-CMV-9. Empty vector was used as a positive control. p3XFlag-CMV-9-OTUD6B clone number 9 was used to observe OTUD6B localization.

stranded breaks during replication as well [71]. Thus, MCF-7 cells were irradiated with UVC to observe if flag-tagged OTUD6B would localize to chromatin under the creation of any UV induced lesions. Upon UVC treatment, no flag-tagged OTUD6B was observed to localize to sites of DNA damage, indicated by Y-H2AX foci (Figure 28, A). Furthermore, flag-tagged exogenous OTUD6B as well as endogenous OTUD6B was not observed in chromatin enriched fractions via western blot analysis (Figure 28, B). These results suggest that OTUD6B does not exhibit any nuclear entry under UVC treatment and our experimental conditions used.

Interestingly, degraded bands appeared at the relative size of endogenous OTUD6B within the chromatin enriched fractionation which was observed and suspected to be an altered form of OTUD6B (Figure 28, C). It has been reported that some posttranslational modifications, such as palmitoylation, can result in increased efficiency of proteins migrating through polyacrylamide gels and thus it was suspected that this might be occurring for OTUD6B [73]. Further examination however revealed that the degraded bands persisted under successful knockdown of OTUD6B with siRNA, therefore, it is unlikely that these bands are a modified form of OTUD6B (Figure 28, C).

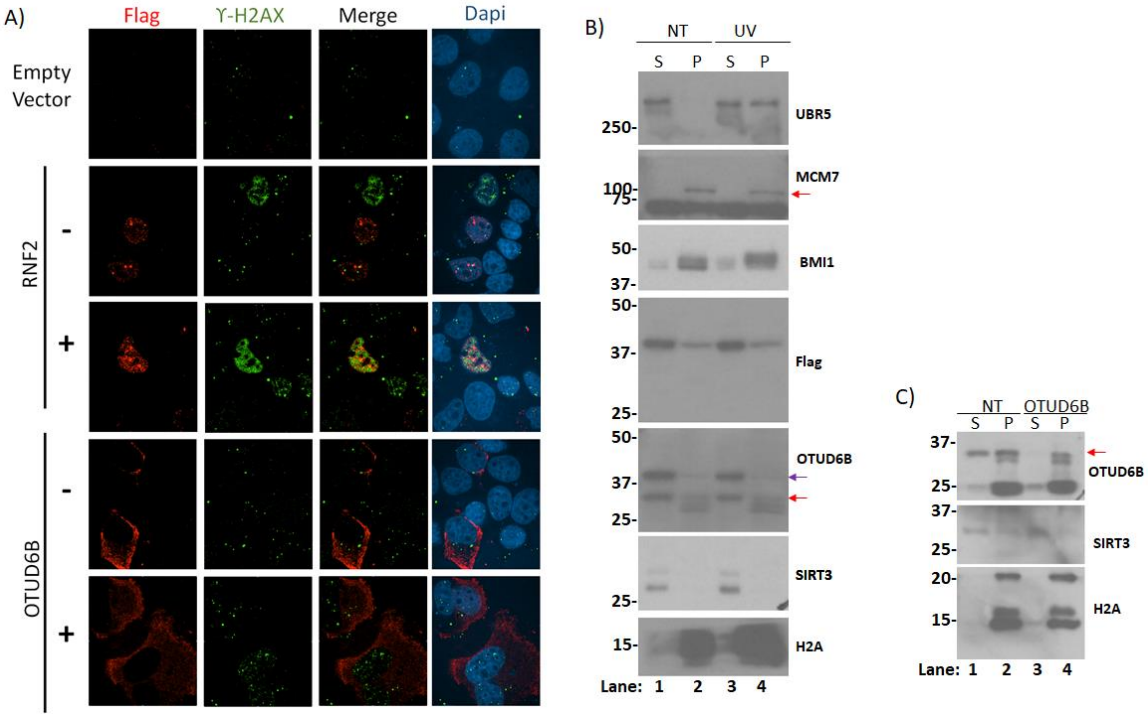

Figure 28. UV irradiation treatment does not exhibit nuclear localization of OTUD6B. A) MCF-7 cells treated with (+) or without (-) 70 J/m^2 UVC irradiation and a 1 hour recovery. Flag represented in red indicates the localization of flag-tagged RNF2, flag-tagged OTUD6B, or empty vector. Y-H2AX represented in green indicates the degree of DNA damage within the cell. Plasmid backbone used was p3XFlag-CMV-9. Empty vector was used as a positive control. p3XFlag-CMV-9-OTUD6B clone number 9 was used to observe OTUD6B localization. B) Chromatin enriched fractionation in MCM-7 cells transfected with p3XFlag-CMV-9-OTUD6B clone number 9 and treated with or without 70 J/m^2 UVC irradiation with a 1 hour recovery where S represents cytosolic and P represents chromatin enriched fractions. H2A, BMI1, and MCM7 were used as chromatin-enriched fraction controls. SIRT3 was used as a cytosolic fraction control. UBR5 was used as an indicator of successful UV damage. Red arrows indicate the protein labeled. Purple arrow indicated exogenous flag-tagged OTUD6B. C) Chromatin enriched fractionation in MCM-7 cells transfected with OTUD6B siRNA #4 or control siRNA from Bioneer where S represents cytosolic and P represents chromatin enriched fractions. H2A was used as a chromatin-enriched fraction control. SIRT3 was used as a cytosolic fraction control. Red arrow indicates the protein labeled.

OTUD6B depletion results in a mild induction of DNA damage markers

Cell cycle arrest through the G1 DNA damage checkpoint kinase signaling cascade occurs by the initial activation of phosphatidylinositol-3 kinase-like protein kinases (PIKKs), notably ATM [46]. In the presence of DNA damage, often in the form of double stranded breaks, ATM is activated via phosphorylation and subsequently initiates the phosphorylation of downstream proteins ϒ-H2AX at S130, CHK2 at T68, and p53 at S15, ultimately resulting in increased p21 transcription levels [46].

In a DUB screening performed by Nishi et al. (2014), various DUBs were knocked down in U2OS cells and subsequently analyzed for phosphorylated levels of S345 on CHK1, T68 on CHK2, and S139 on ϒ-H2AX [66]. Results showed OTUD6B had elevated levels of two of the three phosphorylated proteins tested, suggesting an activation of the DNA damage checkpoint pathways [66]. Because of this data and because our previous research has suggested depletion of OTUD6B results in an increased translation of p21 in a p53 dependent manner as well as our cell cycle profile analysis under OTUD6B depletion suggesting an inability of cells to progress efficiently to G2, we sought to determine if OTUD6B was implicated in ATM dependent DNA damage response pathways.

To test this, we depleted levels of OTUD6B with multiple siRNA sequences and analyzed levels of phosphorylated ATM (pATM) on serine 1981 via immunofluorescence microscopy in T80 ovarian cells. Results showed that under reduced OTUD6B levels, a slight increase in pATM foci was observed compared to control conditions, with more cells exhibiting at least one pATM foci per nuclei (Figure 29). However, an overall increase in foci per nuclei was not observed among all OTUD6B siRNA treatments (Figure 29). Of note, our most efficient siRNA sequence, OTUD6B #2 which often provides an 85%-95% reduction in OTUD6B protein levels assessed through western blot analysis, did show an increase in the number of pATM foci per nuclei (Figure 29).

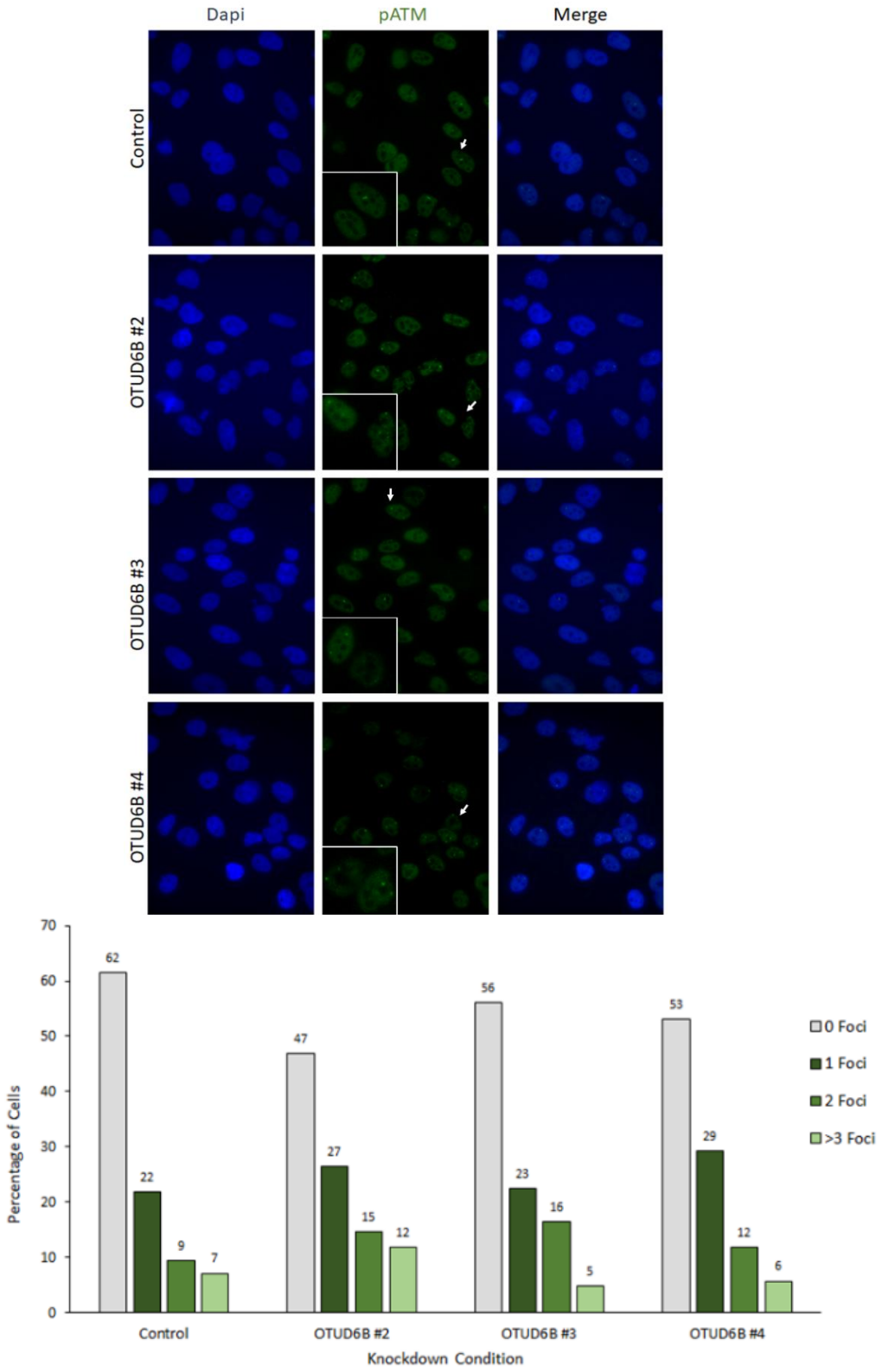

Figure 29. OTUD6B protein decrease results in a mild increase of pATM foci. OTUD6B knockdown was conducted with three siRNAs in T80 cells. Nuclei containing green foci indicate pATM induction. Control represents control siRNA from Bioneer. The percentage of nuclei positive for 0, 1, 2, or >3 foci per nucleus for each knockdown condition is quantified in the corresponding bar graph. ~200 cells were counted for quantification. Above are representative fields of view of pATM foci with arrows indicating example foci for each condition.

In the DUB screen by Nishi et al. (2014), U2OS cells depleted of OTUD6B protein were also analyzed for extent of DNA damage and for efficiency of repair after Phleomycin treatment via a comet assay [66]. Phleomycin is a compound similar in structure to Bleomycin and also induces double stranded breaks [70]. In this study, cells depleted of OTUD6B had increased levels of damaged DNA with knockdown alone and a decreased ability of DNA repair efficiency when damage was administered [66].

Based on this data and our own data showing a mild induction of pATM foci under OTUD6B protein level depletion, we postulated that decreased OTUD6B protein levels would also increase ϒ-H2AX protein expression. Thus, we depleted OTUD6B protein levels using siRNA treatment and assessed induction of cells positive for ϒ-H2AX staining. Results of three experimental trials did not show a statistically significant change in ϒ-H2AX staining for OTUD6B depletion compared to control conditions. As a positive control, RAD51 protein levels were depleted also through the use of siRNA (Figure 30). RAD51 is known to bind to single stranded DNA during initiation of homologous recombination (HR) as well as participate in homology search for a copy of the aberrant DNA [14]. Under conditions of its

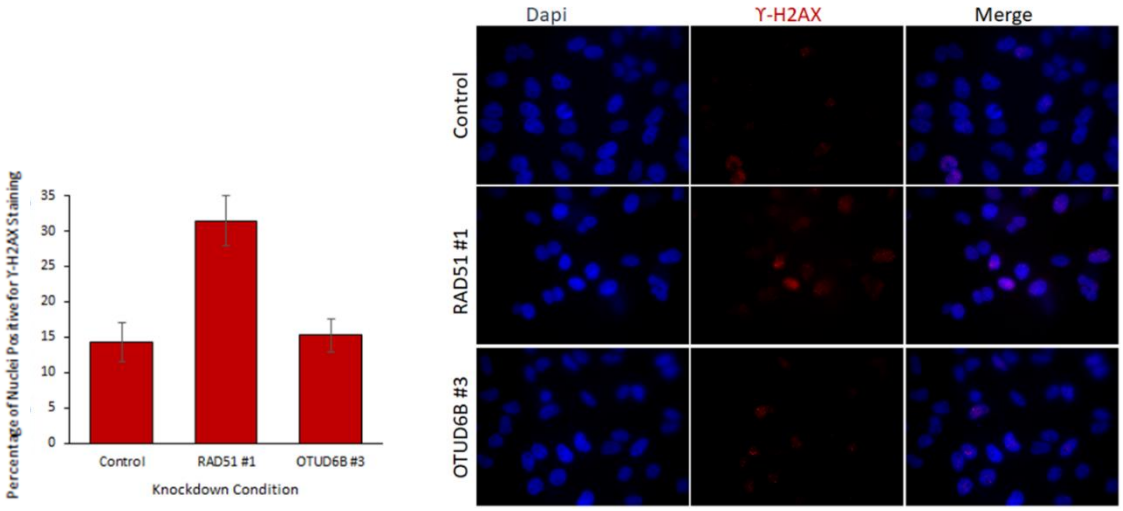

Figure 30. OTUD6B protein decrease does not induce ϒ-H2AX levels. OTUD6B knockdown was conducted with OTUD6B #3 siRNA in HeLa cells. Nuclei stained red indicate positive ϒ-H2AX staining. Control represents control siRNA from Bioneer. RAD51 siRNA #1 was used as a positive control. The percentage of nuclei positively stained for ϒ-H2AX for each knockdown condition is quantified in the bar graph to the left. 300 to 500 cells were counted for quantification. Error bars represent standard error of three experimental trials.

depletion, DNA damage will persist due to an inability to undergo HR repair of double stranded breaks [14].

Additionally, as Nishi et al. (2014) showed that an increase of repair defects occurred when U2OS cells depleted of OTUD6B were treated with phleomycin, we wanted to determine if depletion of OTUD6B resulted in any increased sensitivity to bleomycin treatment [66]. To asses Bleomycin sensitivity under OTUD6B depleted conditions we examined Poly (ADP-ribose) polymerase-1 (PARP-1) cleavage via western blot analysis under OTUD6B protein depleted conditions.

PARP-1 is a polymerase which functions by producing poly ADP-ribose on target proteins in the DNA damage response [46]. PARP-1 activation occurs during repair processes such as base excision repair, nucleotide excision repair, single strand base repair, and non-homologous end joining [74]. During intrinsic, also referred to as mitochondrial, programmed cell death, activation of a cascade of cysteinyl-aspartate proteases (caspases) initiate the cleavage of key proteins necessary for survival and cellular maintenance [74, 75]. One of such key proteins in PARP-1, which is cleaved by caspase-3 and caspase-7, and has become a hallmark for apoptosis [74]. Cleavage of PARP-1 in mitochondrial mediated apoptosis often results in two fragmented forms of ~24KDa and ~89KDa [74].

For analysis of Bleomycin sensitivity with OTUD6B expression decrease, the 89KDa sized fragment was analyzed. Using three different OTUD6B targeting siRNA, results showed no additive affect in PARP-1 cleavage under 5uM Bleomycin treatment with OTUD6B knockdown compared to control conditions (Figure 31). Additionally, OTUD6B knockdown alone did not consistently induce increased PARP-1 cleavage compared to control conditions (Figure 31). These results suggest that OTUD6B does not drastically induce intrinsic mediated apoptosis alone and only minorly increases sensitivity to Bleomycin treatment under represented conditions. OTUD5, another DUB which has been shown to increase Bleomycin sensitivity in HeLa and U2OS cell lines, was used as a positive control as it induces a

slight increase in expression of the 89KDa PARP-1 fragment (Figure 31) [53]. Of note, OTUD5 induced PARP-1 cleavage may have been more drastic with increased knockdown efficiency.

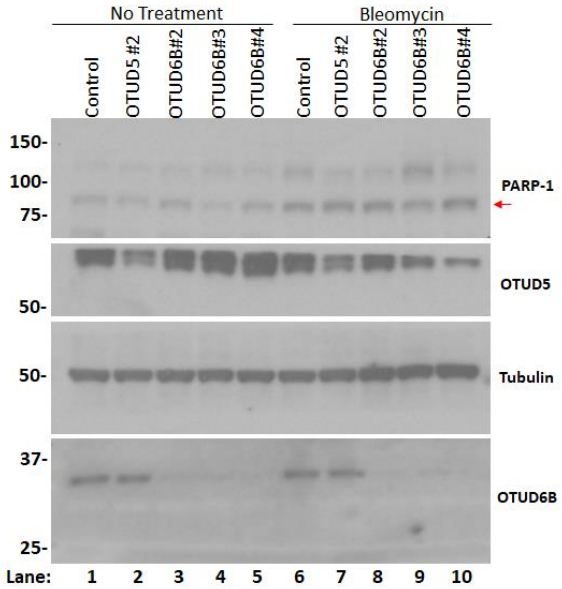

Figure 31. OTUD6B depletion suggests no increased levels of apoptosis under Bleomycin treatment. Western blot results were conducted with three siRNAs in HeLa cells. Control represents control siRNA from Bioneer. OTUD5, as it has been shown to increase cell sensitivity to bleomycin, was used as a positive control. Tubulin was used as a loading control.

Conclusions and Future Directions

Our data provides supporting evidence for our initial discovery of OTUD6B protein depletion inducing p21. We have shown evidence that OTUD6B depletion results in an accumulation of G1 phased cells in asynchronous HeLa cell lines (Figure 23). Furthermore, we have also shown that, when synchronized at the G1/S phase boundary, cells depleted of OTUD6B have a decreased ability to progress to G2 once released (Figure 24). P21 is known to accumulate at two phases of cell cycle progression, G1 and G2 [11]. In G1, p21 binds to and inhibits cyclin D-cdk4/6 and cyclin E-cdk2 complexes as well as PCNA, preventing PCNA from binding to DNA polymerase-delta and promoting DNA replication [31, 38, 39]. By these functions, p21 effectively arrests cells in G1 and prevents progression through S and into G2 phase. Our data supports that such events are occurring under our indicated phenotype.

However, while associating our G1 arrested cell cycle profiles with our p21 induction phenotype is appealing, further investigations should be performed to fully validate that p21 is implicated in these arrests. To analyze this, p21 negative cells should be used to observe if OTUD6B depletion still results in a G1 arrest. Additionally, it would be interesting to test if DNA damage produces a stronger G1 arrest phenotype. To observe if our G1 arrest is due to a depletion of OTUD6B catalytic activity, cell lines only expressing our C188S catalytically inactive OTUD6B mutant should be created and tests as well.

In further support that a G1 arrest under OTUD6B protein depletion is occurring through p21 function, long term OTUD6B protein depletion in cancer cell lines has shown a decreased cell proliferation rate compared to their wildtype counterparts (Figure 25). In untransformed, non-cancerous cell lines, OTUD6B depletion also resulted in an increase of pH-dependent β-galactosidase staining, representative of cellular senescence (Figure 26, B). Again, while further tests should be performed on these cell lines to validate this decrease in cell growth and proliferation is due to OTUD6B induction of p21, such data supports p21 functional implication because both our 293T KO cell line and our WI-38 cell line, when depleted of OTUD6B, showed induced levels of p21. Moreover, whether it is occurring in G1 or G2 phase of the cell cycle, senescence processes traditionally exhibit the requirement of p21 induction for permanent arrest [11]. Another important pathway to encourage senescent events is p16/pRB signaling, which should also be investigated in future directions for senescence induced under OTUD6B protein depletion [41]. However, p21 involvement is well established [41, 50].

Interestingly there are define differences between G2 induced senescence and G1 induced senescence. While G2 is more likely to occur under any induction of DNA damage checkpoint kinase signaling within hours of induction, G1 cellular arrest has been more likely to exhibit a quiescent state for up to several days before senescence is actually achieved [11]. Our data provides little evidence to whether quiescence has been induced or if full senescence is initiated under our OTUD6B knockdown phenotype since our cell cycle profile analysis suggests a G1 arrest is occurring. Additionally, as

quiescence in G1 has been reported to occur for up to 5 days and our knockdown conditions occur for only 72 hours before data collection, it is not entirely clear as to which condition is occurring under our phenotype [11]. Previously reported senescence studies using the same untransformed fibroblast cell line have shown that pH-dependent β-galactosidase could not be induced in quiescence cells [47]. However, other studies in macrophages have shown this quiescent ability can induce β-galactosidase staining [48]. It would be interesting to determine if long term OTUD6B protein depletion continues to result in permanent cell cycle arrest. It would also be interesting to see if a double knockdown of OTUD6B and p21 would restore a cellular growth and proliferative phenotype observed among control conditions.

Despite this decreased growth phenotype under OTUD6B knockdown conditions, we could not obtain strong evidence of OTUD6B implication in DNA damage checkpoint signaling or the DNA maintenance processes. Since our OTUD6B depletion resulted in phenotypes such as a p53-dependent p21 induction, G1 arrest, and depletion of cell growth progression, we had hypothesized that checkpoint kinase cellular arrest signaling may be occurring. Several literature publications have supported p21 transcriptional expression by p53 occurring downstream of DNA damage checkpoint kinase cell cycle arrest pathways [11, 45, 46]. Additionally, there have been reports of OTUD6B possessing nuclear entry abilities. Sowa et al. (2009) reported in a DUB screening, that under GO process analysis of Mass spectrometry data, OTUD6B was localized to the nucleus and the endoplasmic reticulum [2]. Additionally, examination of OTUD6B isoform 1 using the cNLS Mapper, which predicts importin α-dependent nuclear localization signals (NLS), reports a highly conserved predicted NLS sequence starting at the 40th residue with a cut-off score of 6 out of 10, supporting OTUD6B nuclear localization potential (Figure 20, B) [68].

However, despite these reports, we were not able to observe OTUD6B localization to damaged induced sites under our conditions of Bleomycin, Etoposide, or UVC treatments (Figure 27-28). Under

our conditions, OTUD6B remained cytosolically localized. Such results suggest that OTUD6B does not directly regulate or facilitate the DNA damage response or DNA maintenance processes in response to double stranded breaks, or the formation of pyrimidine dimers, that are created by Bleomycin, Etoposide, or UVC, respectively. While we did not observe OTUD6B nuclear translocation under these conditions, we cannot necessarily rule out a functional role of OTUD6B in in genomic maintenance by this data alone. It is possible, though unlikely, that OTUD6B holds a functional role in the cytosol in response to DNA stability regulation or repair; further experimental analysis should be performed to elucidate such a possibility.

Our chromatin enriched fractionation studies provided unpredicted results that warrant repeating. Under control conditions or UVC treatment and a 1 hour recovery, fragmented bands appear at the relative kDa size of OTUD6B (Figure 28 B). Upon successful knockdown of OTUD6B, these bands remained (Figure 28 B). Such bands however are not observed under our traditional lysing protocols for western blot analysis nor by our lysing protocol for immunoprecipitation techniques, which uses similar buffers as our fractionations. Thus, the appearance of these bands is unexpected. Nuclear fractionations which keep cellular compartments more intact should be conducted to obtain an accurate assessment of OTUD6B localization and a better understanding of these fragments.

In regards to UVC treatment, it is possible that a 1 hour recovery period is not sufficient for OTUD6B localization analysis. For example, reactive oxygen species (ROS) have been shown increase in production long after UVA damage has been induced and thus require repair processes several hours after initial damage [76]. Thus, it is possible that OTUD6B localization analysis requires a shorter or, more likely, longer UVC recovery time for accurate interpretation; repeat experiments focusing on these possibilities should be conducted. Treatment times for Bleomycin and Etoposide warrant further consideration as well.

Ultimately, these damaging agents were chosen because our cell cycle progression data suggested G1 arrest was occurring under our OTUD6B knockdown conditions. Because G1 arrest most often occurs through activated ATM-dependent DNA damage checkpoint signaling, and that ATM is traditionally the PIKK which is a first responder to double stranded breaks, we reasoned that OTUD6B was functioning under double stranded break repair and G1 cell cycle damage recovery [11, 46]. However, due to our lack of OTUD6B nuclear localization in response to these breaks, and as only minor pATM levels were detected under an OTUD6B knockdown, which will be further discussed below, it is possible that our G1 phenotype interpretation is incorrect. For example, reports have shown that under some cases of DNA damage occurring in G2 cell cycle phase, cells can successfully undergo mitosis and carry such damaged DNA into G1 phase of daughter cells, in which these daughter cells then undergo G1 phase cell cycle arrest in order to repair damage [11].

Thus, to fully analyze and explore OTUD6B localization in response to DNA damage and cell cycle checkpoint signaling pathways, we must also consider observed OTUD6B localization in response to additional DNA damaging agents such as Cisplatin, an inter- and intra-strand crosslinking agent, Camptothecin, a topoisomerase I inhibitor which functions similarly to Etoposide but promotes single stranded breaks, or Hydroxyurea, which can result in S phase arrest by depleting nucleotide production [46]. The administration of these additional agents, though all possessing the ability to induce double stranded breaks overtime, may illicit small yet significant repair activation pathway differences which OTUD6B may be functioning within. For example, ALKBH2 is an oxidative demethylase known to removed methyl groups from DNA [14]. A DUB which specifically facilitates this protein's stability for efficient repair is OTUD4, which has also been shown to promote innate immune signaling [14, 77]. Thus, future considerations should include additional forms of DNA damage such as oxidative stress, acetylation, interstrand or intrastrand crosslinks, and single stranded breaks.

Under the same understanding, it is possible that these investigations may also not produce nuclear OTUD6B localization and that OTUD6B may experience nuclear translocation in a cell cycle dependent manner such as functioning at G2/M boundaries. It is possible that OTUD6B depletion may alter the activation of the mitotic spindle checkpoint signaling cascade necessary for successful cellular division, resulting in unregulated cellular division and subsequent G1 arrest [11]. With the intention of observing OTUD6B localization under an entire cell cycle progression, we have developed and verified our OTUD6B wildtype and 42_46del mutant p3XFlag-CMV-9 expressing stable cell lines in HeLa cells. These OTUD6B cell lines will assist us in the identification of what particular circumstance OTUD6B experiences nuclear localization as well as, once such circumstance is identified, verify the identity of our predicted NLS sequence.

In our last analysis for this chapter, we investigated the effect of OTUD6B protein levels on G1 DNA damage checkpoint activation pathways and apoptotic markers. As mentioned previously, our G1 arrest and p21 induction phenotypes strongly mimic the downstream effects of ATM activation dependent checkpoint kinase signaling. Moreover, work by Nishi et al. (2014), provided evidence that OTUD6B depletion results in the activation and phosphorylation of two out of three major checkpoint activation events (the phosphorylation of CHK1, CHK2, or H2AX) [66]. The same work also showed that OTUD6B depletion resulted in an increase in damaged DNA and a decrease in DNA damage repair abilities [66]. Thus, we postulated that OTUD6B function may involve the regulation of ATM activation and subsequent downstream signaling. Under OTUD6B knockdown however, induction of pATM levels was minor and ϒ-H2AX staining was unchanged compared to control conditions suggesting that OTUD6B was not affiliated with the regulation of this pathway (Figure 29 and 30).

Of interest, a previous study however has shown that oxidative stress is able to induce ATM activation/phosphorylation via S1981 in the absence of DNA breakage but rather by ATM oxidation [78]. Under these conditions, activated ATM was able to activate/phosphorylate canonical downstream

proteins CHK2 and p53, however this activation was unable to phosphorylate H2AX [78]. In addition, this study showed that while ATM activation via S1981 still occurred, it was to a much lesser extent in comparison to Bleomycin treatment [78]. This study may offer a possible solution to our observed phenotypes as well as strengths the importance to analyze all possible forms of DNA damage and cellular stress for determination of OTUD6B affiliation with these pathways.

Future experiments for this analysis should include H_2O_2 treatment under OTUD6B knockdown to observe activation of ATM as well as the analysis of the activation of ATM downstream proteins CHK2 and p53 in the absence of any DNA damaging agents. Additionally, as it is possible OTUD6B may be affiliated with ATR activation dependent checkpoint kinase signaling pathways, the activation of ATR and CHK1 should also be examined. It is unlikely, however, that we will observe activation of these proteins because we have previously not observed changes in CHK1 activation under OTUD6B knockdown in 293T cells and because reports have suggested that ATR pathway requires activation of ATM to facilitate TOPBP1 activation and localization [46].

Our work was also unable to show an induction of apoptotic phenotypes under our conditions as shown by our inability to induce significant PARP-1 cleavage under OTUD6B knockdown alone, or synergistic PARP-1 cleavage under OTUD6B knockdown with Bleomycin treatment, compared to control conditions (Figure 31). In support of these results, there is strong evidence for p21 activity inhibiting events of apoptosis, but rather promoting cell cycle arrest and cellular senescence. Specifically, it has been shown that p21 protein depletion was necessary for cancer cell apoptosis initiation under various types of DNA damage treatment [38]. Our data supports this behavior by showing that OTUD6B depletion induces cellular senescence, rather than inducing apoptosis, in our non-transformed fibrotic cell lines. It would be interesting to test in future experiments if a double knockdown of OTUD6B and p21 increases Bleomycin sensitivity in cancerous cells.

In conclusion, while we could not find strong evidence to support OTUD6B in DNA stability or involvement in checkpoint kinase signaling, it would be unwise to fully conclude OTUD6B holds no involvement in the DNA damage response or cellular stress management until further experiments can be performed. However, our data has provided convincing evidence to suggest that depletion of OTUD6B results in decreased cellular growth and deterred cell cycle progression, potentially due to the induction of p21 protein levels.

Chapter Five: OTUD6B Potential Binding Partners and Role in Migration

Rational

We did not observe strong evidence that OTUD6B was implicated in DNA damage checkpoint kinase cascades or genomic maintenance, yet we have provided evidence that p21 expression is induced in a p53 dependent manner under OTUD6B protein depletion. Because several proteins are known to help encourage p53 transcriptional activity, such as oncogenic Ras GTPase or STAT1 pathway activation, we sought to identify OTUD6B interacting proteins that could provide an explanation for our phenotypes [38, 39].

Through mass spectrometry analysis of potential OTUD6B binding partners and proteomic expression changes under an OTUD6B protein depletion, we have identified lysine-rich CEAMCAM-1 (LYRIC) as a potential interacting protein for OTUD6B. While LYRIC is relatively newly identified and a functionally ambiguous protein, studies have associated it in a diverse variety of pathways mostly related to proliferation, cellular survival, invasion, angiogenesis, and metastasis [63]. This data, and reports of its overexpression in cancers such as prostate and breast cancer, has collectively led to LYRIC being considered as an oncogenic protein [63].

LYRIC has shown to be monoubiquitylated at two residues: K486 and K491 [79]. These monoubiquitination events sequester its localization to the cytoplasm, and in absence of these posttranslational modifications, it can relocate into the nucleus [79]. Apart from these sites, it is unknown if other ubiquitin events occur to regulate LYRIC stability or activity. In addition, no known DUB for this protein has been identified. To analyze the potential relationship between LYRIC and OTUD6B,

we have examined LYRIC protein stability and localization under OTUD6B depletion. In addition, as LYRIC is strongly considered to be a proliferation and metastasis promoting oncogene, we investigate OTUD6B protein levels on migration abilities in various cell lines to gain a better understanding of the connection between OTUD6B and cancer characteristics.

Experimental Design

Cell Lines and Chemical Reagents

HEK293T and HeLa cells were purchased from the American Type Culture Collection (ATCC). MDA-MB231 cells were gifted from Dr. Meera Nanjundan at the University of South Florida's Cell and Molecular Biology Program. HEK293T, HeLa, and MDA-MB231 cells were cultured in Dulbecco's Modified Eagle's Medium (DMEM) supplemented with 10% bovine serum and 10% Penicillin-Streptomycin with L-glutamine except for in cases of siRNA and DNA transfections. Cells were grown at 37^{O}C in 5% CO_2 atmosphere.

Cycloheximide (CHX) was purchased from Sigma-Aldrich and used at 10uM per sample at indicated timepoints 72 hours after siRNA transfection.

Plasmids

Plasmids used were an empty vector p3XFlag-CMV-9 nonretroviral overexpression vector purchased from Addgene and a previously developed p3XFlag-CMV-9-OTUD6B clone number 9 plasmid and p3xflag-CMV-9-OTUD6B-C188S clone number 6 plasmid (Chapter 3, Experimental Design, Plasmids and Mutagenesis of OTUD6B Catalytic Cysteine).

DNA Transfections using Turbofect

Cells were cultured in Penicillin-Streptomycin free media. Once cell confluency reached 60-70% samples were transfected with 1ug/mL of media of designated DNA. Transfection reagents used

included Opti-MEM (Invitrogen) and Turbofect (Thermofischer Scientific) used at a 1:100 DNA mass to volume ratio and a 1:2 DNA mass to volume ratio, respectively [51]. DNA transfected samples were allowed to incubate for at least 24 hours post transfection to ensure desired protein was expressed [51].

DNA Transfections using Polyethylenimine (PEI)

For PEI transfections, HEK293T cells were used and cultured in Penicillin-Streptomycin free media in 15cm dishes. Once cell confluency reached 60-70% samples were transfected with 25ug of designated DNA. Transfection reagents used included Opti-MEM (Invitrogen) and PEI (Polysciences) used at a 1:40 DNA mass to volume ratio and a 1:3 DNA mass to volume ratio, respectively [51]. DNA transfected samples were allowed to incubate for at least 24 hours post transfection to ensure desired protein was expressed before harvesting [51].

RNA Interference

Cells were cultured in Penicillin-Streptomycin free media and seeded at 30% confluency. At the time of seeding, samples were transfected with 20nM of designated siRNA. Transfection reagents used included Opti-MEM (Invitrogen) and lipofectamine RNAimax (Invitrogen) used at a 1:100 mass to volume ratio and a 1:1 mass to volume ratio, respectively [51]. All siRNA transfected samples were allowed to incubate for 72 hours post transfection unless otherwise instructed [51]. The following siRNA sequences were used: OTUD6B siRNA #3: 5'-CAGUGUAAAAGGUCCAAG 3' from Bioneer, OTUD6B siRNA #4: 5'-CACCAAUAGAGAUAAUACA 3' from Ambion, OTUD5 siRNA #1: 5' -GGGUGCCGAAGAIAGACAATT 3' from Quiagen, and SPT16 siRNA #3: 5'-ACCGGAGUAAUCCGAAACUGA 3' from Bioneer.

A scrambled siRNA was used as control: Negative control siRNA from Bioneer.

Isobaric tags for relative and absolute quantitation (iTRAQ)

iTRAQ is an isobaric quantitative labeling method used to determine changes in the entire proteome of cell samples compared to control groups and is thus useful for obtaining unbiased data of protein levels within the proteome under certain conditions [80].

Briefly, HeLa cells were seeded in 6cm plates and subjected to siRNA treatment following protocols previously described (Chapter 5, Experimental Design, RNA Interference). 72 hours after siRNA treatment, cells were washing with 1mL of 1x PBS depending on well size prior to harvest by scraping with commercially available cell scrapers. 200uL of harvested cells resuspended in 1x PBS were removed and subjected to western blotting to validate knockdown efficiency (Chapter 5, Experimental Design, Protein lysis and Western Blotting). The remaining samples were spun at 4000rpm, supernatant was removed, and pellets were snap frozen and brought to Moffitt Cancer Center's Proteomics and Metabolomics Core Facility. iTRAQ and mass spectrometry was performed by Moffitt Cancer Center's Proteomics and Metabolomics Core Facility. Three experimental replicates for each knockdown was performed.

Data analysis was performed using the program GraphPad Prism 8.0.1. Volcano plots produced were created through GraphPad Prism 8.0.1.

Large Scale Immunoprecipitation for Mass Spectrometry

Wildtype p3xflag-CMV-9-OTUD6B

Wildtype p3xflag-CMV-9-OTUD6B clone number 9 was transfected into six 15cm plates of HEK293T cells using the PEI transfection method (Chapter 5, Experimental Design, DNA Transfections using Polyethylenimine (PEI)). After 24 hours of transfection, cell samples were washed with 3 mLs of 1x PBS and harvested by scraping with commercially available cell scrapers. Samples were collected into

one 15mL conical tube and spun down for 10 minutes at 4000rpm. Following centrifugation, the remaining pellet was resuspended in 10mLs of 1% NP40 lysis buffer containing 300mM of NaCl and 50mM of Tris, and 5X the volume of protease inhibitor (Thermofischer Scientific) followed by sonication with 10 pulses at a 50% amplitude three times. Lysed protein sample was then rotated for 10 minutes at 4^{o}C and spun at 14000rpms for 30 minutes also at 4^{o}C. Remaining supernatant was then collected and 5% was taken for input. The remaining volume was incubated overnight with 16uL of anti-Flag m2 Affinity beads (Sigma) per every 400uL of supernatant. Sample was then washed with 500uL of 1% NP40 buffer 5 times and resuspended with 200uL of PBS with 3% SDS. Sample was then heated at 95^{o}C for 5 minutes followed by a 10 minute spin. 20uL of remaining supernatant was taken for western blot verification, remaining volume was given to Moffitt Cancer Center's Proteomics and Metabolomics Core Facility for Mass Spectrometry analysis.

p3xflag-CMV-9-OTUD6B-C188S

p3xflag-CMV-9-OTUD6B-C188S clone number 6 was transfected into six 15cm plates of HEK293T cells using the PEI transfection method (Chapter 5, Experimental Design, DNA Transfections using Polyethylenimine (PEI)). After 24 hours of transfection, cell samples were washed with 1 mLs of 1x PBS and harvested by scraping with commercially available cell scrapers. Samples were collected into one 15mL conical tube and spun down for 10 minutes at 4000rpm. Following centrifugation, the remaining pellet was resuspended in 10mLs of .5% NP40 lysis buffer containing 100mM of NaCl and 50mM of Tris, and 5X the volume of protease inhibitor (Thermofischer Scientific) followed by sonication with 10 pulses at a 50% amplitude once. Lysed protein sample was then rotated for 10 minutes at 4^{o}C and spun at 14000rpms for 30 minutes also at 4^{o}C. Remaining supernatant was then collected and 5% was taken for input. The remaining volume was incubated overnight with 20uL of anti-Flag m2 Affinity beads (Sigma) per every 400uL of supernatant. Sample was then washed with 1mL of .5% NP40 buffer four times and resuspended with 200uL of PBS with 3% SDS. Sample was then heated at 95^{o}C for 5 minutes followed by

a 10 minute spin. 20uL of remaining supernatant was taken for western blot verification, remaining volume was given to Moffitt Cancer Center's Proteomics and Metabolomics Core Facility for Mass Spectrometry analysis.

Small Scale Immunoprecipitation

Wildtype p3xflag-CMV-9-OTUD6B clone number 9 and empty vector p3xflag-CMV-9 were transfected into their own one 6cm plate of HEK293T cells using the Turbofect transfection method (Chapter 5, Experimental Design, DNA Transfections using Turbofect). After 24 hours of transfection, cell samples were washed with 1 mL of 1x PBS and harvested by scraping with commercially available cell scrapers. Samples were and spun down for 5 minutes at 3500rpm. Following centrifugation, the remaining pellets were resuspended in 70uL of .5% NP40 lysis buffer containing 100mM of NaCl and 50mM of Tris, and 5X the volume of protease inhibitor (Thermofischer Scientific) followed by a rotation for 10 minutes at 4^{o}C. Samples were then spun at 14000rpms for 10 minutes also at 4^{o}C and the remaining supernatants were then collected and 5% of the initial volume was taken for the inputs. The remaining volume was incubated overnight with 17uL of anti-Flag m2 Affinity beads (Sigma). Samples were then spun down for 1 minute at 3000rpm and at 4^{o}C and washed with 70uL of .5% NP40 buffer 3 times. Samples were next resuspended with an equal volume of 2x laemmli sample buffer (Bio-Rad), boiled at 95^{o}C for 5 minutes, followed by a 10 minute spin before subjected to SDS-PAGE.

Protein lysis and Western Blotting

Cell samples were washed with 1-2mLs of 1x PBS depending on well size prior to harvest by scraping with commercially available cell scrapers [51]. Harvested samples were spun down at 4000rpm for 5 minutes followed by administration of RPPA lysis buffer containing 1% Triton X-100, 50nM HEPES, 150nM NaCl, 1mM $MgCl_2$, 1mM EGTA, 10% glycerol, 1x protease cocktail inhibitor (Thermofischer Scientific), and 1x phosphatase cocktail inhibitor (Thermofischer Scientific) [57]. Samples were incubated

in lysis buffer for 1 hour at 4^{o}C following a 10 minute centrifuge spin at 14000rpm [57]. Protein concentration assessment involved optical density measurements compared to a standard bovine serum albumin (BSA) curve using Protein Assay Dye (Bio-Rad). 2x laemmli sample buffer (Bio-Rad) was added to samples following a 5 minute ~95^{o}C heat block incubation [51].

Prepared protein samples were run on SDS-PAGE gels at 105 constant volts for ~120 minutes unless otherwise indicated. Separated proteins were transferred to a PVDF membrane using a semi-dry Trans-blot Turbo [51]. Membranes were probed with primary antibodies overnight at 4^{o}C followed by a 1 hour wash in 1x tris-buffered saline with Tween (TBST) at room temperature. Membranes were then incubated for 1 hour at room temperature with mouse or rabbit secondary antibody linked to horseradish peroxidase (Cell Signaling Technologies (CST)) followed by an additional 4 hours of room temperature washing in 1xTBST [51]. Results were observed using Pierce ECL Western Blotting Substrate (Thermofischer Scientific). When indicated, band intensities were quantified using imageJ to find the areas under the curve of each of the protein intensity levels and normalized to the loading control.

The following antibodies were used: anti-β-Tubulin [1:3000] (M) (CST), anti-OTUD6B [1:333] (R) (Abcam), anti-OTUD5 [1:500] (R) (CST), anti-SPT16 [1:1000] (R) (CST), anti-MCM7 [1:1000] (R) (Bethyl), anti-LYRIC [1:100] (R) (CST), and Flag [1:1000] (M) (Sigma).

Immunofluorescent Microscopy

Cell samples grown on 12mM in width, .13-.17mM in thickness, sized coverslips were washed twice with 1mL of cold 1x PBS following a 10 minute fixation with 4% paraformaldehyde in the dark [51]. Cells were then washed again with 1mL of cold 1x PBS and permeabilized with .25% Triton x-100 diluted in H_2O for 5 minutes in the dark [51]. Coverslips were washed as described earlier and incubated with 30uL of primary antibody diluted in 1x PBS for 1 hour in the dark [51]. After, samples were washed again with PBS as described previously and incubated with 30uL of either Alexa Flour 488-anti-mouse or anti-

rabbit secondary antibody diluted in 1x PBS for 1 hour in the dark [51]. After additional 1mL 1x PBS washing, coverslips were placed on slides using Vectashield mounting medium for fluorescence with DAPI (Vector Laboratories Inc) to stain nuclei [51]. Images were collected using Lecia DMi8 fluorescence microscope under a 63x oil objective. The program used for image capturing was Leca Las X imaging and analysis software.

Primary antibodies used were anti-LYRIC [1:500] (R) (CST).

Cell Migration Assay

Cellular migration assays analyze the ability of cellular monolayers to move, or migrate, into a "cell-free area" and in this way, this assay is able to represent a cell's ability to partake in epithelial-mesenchymal transition (EMT) under various conditions [81, 82]. Cells used in the assay include HeLa and MDA-MB231. Briefly, the middle of the each well of a 12 welled plate were marked vertically every 1mM with a sharpie. Cells were then seeded in designated wells of the 12 welled plate and subjected to the indicated siRNA following a previously described procedure (Chapter 5, Experimental Design, RNA Interference). Once cells had reached 80% confluency, the tip of a 200uL pipet tip, perpendicular to the bottom of the well, was use to scrape the cellular monolayers in such a way as to make a parallel line to the vertical markings at the bottom of the wells (Figure 33, A). Each well was then washed with 500uL of DMEM media twice and replaced with 1mL of fresh DMEM media, absent of bovine serum, to prevent cell proliferation [81].

Data was then collected at each indicated timepoint by photographing three fields of view of the created wound in each well. The fields of view were kept consistent over the experimental time course by recording which 1mM markings the images were parallel to; each image was ~1mM in the vertical axis. The camera used to record images was an EO USB 2.0 CCD Machine Vision Camera from EO Edmund Optics Worldwide at a 4x objective.

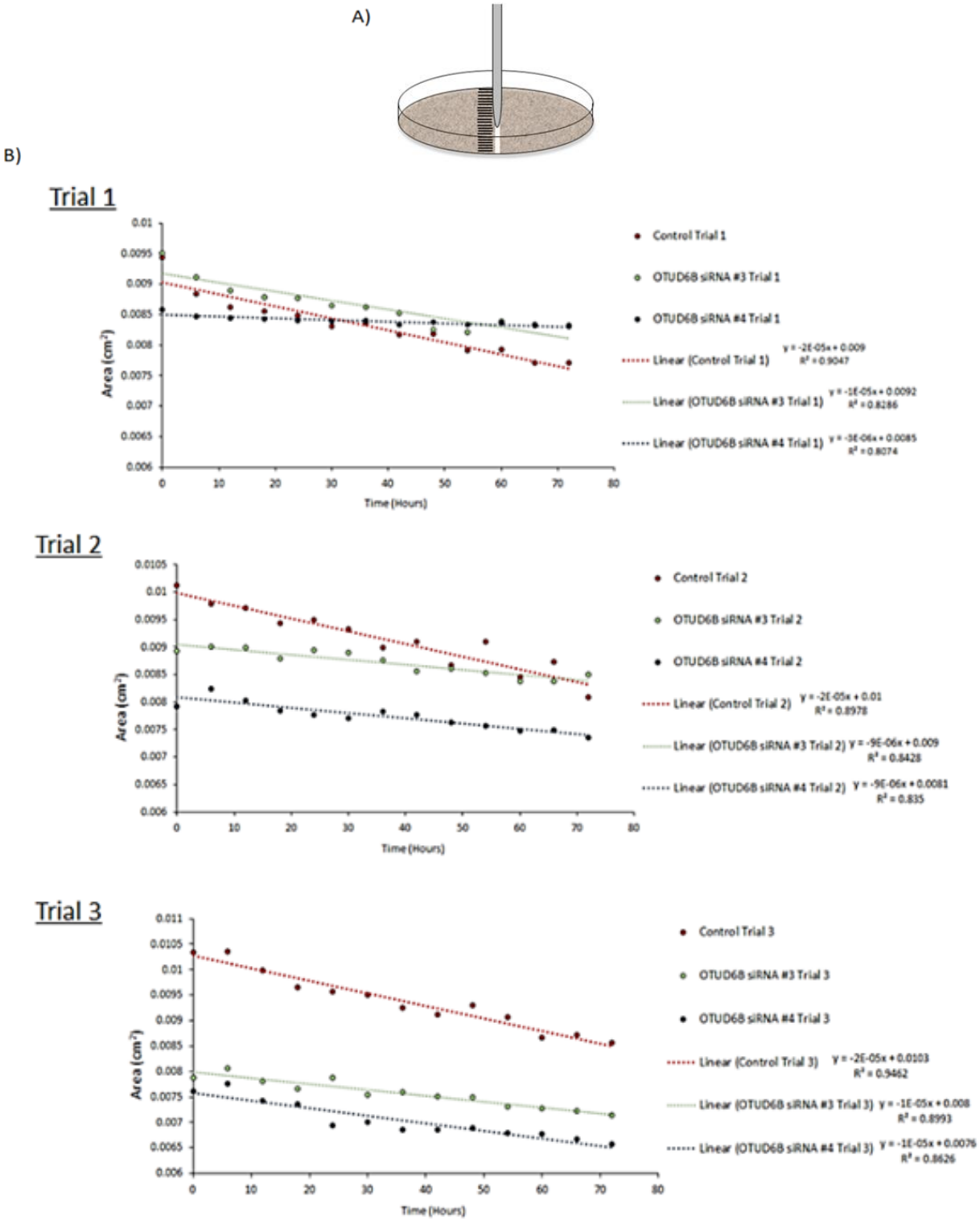

Figure 32. Methods of wound healing assay. A) A schematic of wound administration to the bottom of the wells using a 200uL pipet tip. Scratch was parallel to the 1mM markings made at the bottom of the plate. The length of the wells was 2.2cm as indicated by the markings. B). Scatter plots of the areas of the wounds as they relate to time for each sample in each experimental replicate. Experimental replicates are indicated by Trials 1, 2, or 3 in the upper left corners of each graph. The trendline, equation of the line, and R^2 values for each sample are displayed. The slopes of the equations of the line were used to calculate migration rate for each sample.

The area of the wound for each timepoint was measure using the freehand tool on imageJ and converting the area in pixels^2 to area in cm^2. The average area of each three fields of view for each time point was determined for each sample and used to represent the data collected for that particular experimental replicate. Data is presented by calculating the percentage of gap closure, in MDA-MB231 cell lines, or rate of cellular migration, in HeLa cell lines, due to the number of timepoints captured; the greater number of timepoints results in a more accurate analysis of the rate of cellular migration [81].

Three experimental replicates were performed for each experiment and the standard error was calculated for error bars displayed. For Hela cells, 13 time points were recorded in 6 hour intervals and plotted on a scatter plot showing the change in wound area in cm^2 as it relates to time (Figure 32, B). An equation of the line was then developed and the resulting slope was used to calculate the rate of migration using the equation:

$$V_{migration} = \frac{|slope|}{2 \times l}$$

where $V_{migration}$ represents the average velocity of cellular movement, *slope* is the slope of the equation of the best fit line of the developed scatter plot, and *l* represents the length of the wound, or the vertical length of the middle of the well [81] (Figure 32, B). $V_{migration}$ for each experimental replicate for each sample was averaged and displayed using excel.

Results

LYRIC is a potential binding partner of OTUD6B

As we did not observe strong evidence that OTUD6B was implicated in DNA damage or miotic spindle checkpoint kinase cascades, yet we did observed phenotypes of deterred cell cycle progression, slowed proliferation, and increased cellular senescence under OTUD6B depletion, we sought to determine the direct binding partner of OTUD6B that might explain our data. To identify potential

binding partners, we performed a large-scale flag-tagged immunoprecipitation (IP) assay followed by mass spectrometry (MS) analysis with our wildtype OTUD6B p3xFlag-CMV-9 plasmid and our OTUD6B C188S p3xFlag-CMV-9 plasmid (Figure 33, A-B).

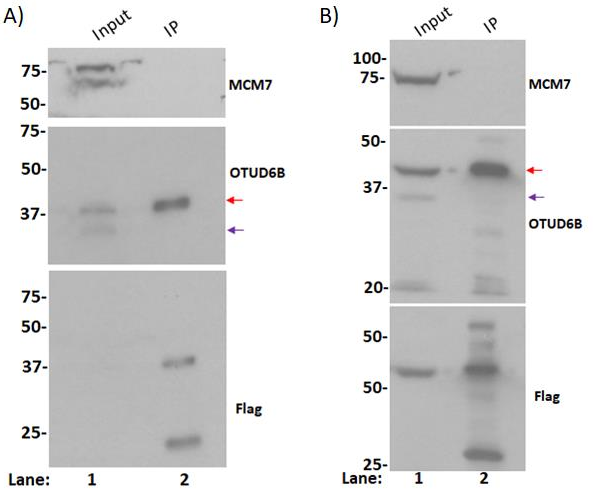

C)

	Mass spec		
Protein	Wildtype	C188S	CRAPome Percentage
OTU6B	11	7	N/A
★RPF2	1	4	6.6
★ASCC3	3	39	9.5
★LYRIC	3	19	12.2
P53	3	5	12.7
KIF11	51	35	39.7
U520	21	55	35.5
TOP2B	1	3	14.8

Figure 33. Verification of successful IPs for MS analysis and resulting potential binding partners of OTUD6B identified through MS analysis. A) Flag-tagged IP verification via western blot for wildtype p3XFlag-CMV-9-OTUD6B performed through a PEI transfection in 293T cells and using anti-flag m2 agarose beads. Six 15cm plates were pelleted and lysed. .5% of whole cell lysate was used for input. 5% of pulldown was run for western blotting. MCM7 was used as a negative control. Red arrow indicates flag-tagged OTUD6B. Purple arrow indicates endogenous OTUD6B. B) Flag-tagged IP verification via western blot for catalytically inactive OTUD6B mutant plasmid, p3XFlag-CMV-9-OTUD6B-C188S, performed through a PEI transfection in 293T cells and using anti-flag m2 agarose beads. Six 15cm plates were pelleted and lysed. .5% of whole cell lysate was used for input. 5% of pulldown was run for western blotting. MCM7 was used as a negative control. Red arrow indicates flag-tagged OTUD6B. Purple arrow indicates endogenous OTUD6B. C) Figure displaying proteins identified in IP-MS data for both the wildtype and mutant IPs and their respective unique peptide numbers. In the chart are proteins that were also identified by Sowa et al. (2009), indicated by red stars, as well as proteins that exhibited the highest unique peptide counts or are affiliated with DNA maintenance and gene expression [2]. Also displayed are each proteins' reported percentage in the Contaminant Repository for Affinity Purification (CRAPome), which is an online database of common contaminants in affinity purification-MS experiments [82].

Our catalytic inactive mutant was used in addition to wildtype because in previous reports, it has been shown that catalytically inactive DUB mutants bind more efficiently to their substrates due to an inability to cleave the isopeptide bond between the ubiquitin and target protein [2]. Previous work with C188S OTUD6B mutants has confirmed that mutating the catalytic cysteine of OTUD6B to a serine is able to disrupt isopeptidase activity of the enzyme, as serine contains a neutral charge and cannot facilitate the nucleophilic attack on the target substrate that is required for bond breakage [20]. MS results identified similar proteins reported in Sowa et al. (2009) paper as potential binding partners to OTUD6B as well as some additional candidates (Figure 33, C) [2]. Additionally, the contaminant

repository for affinity purification (CRAPome), which is an online database of common contaminants in affinity purification-MS experiments, was also used to assess IP-MS data accuracy (Figure 33, C) [83].

In addition to IP-MS analysis to identify binding partners, we also used isobaric tag for relative and absolute quantification (iTRAQ) followed by MS analysis to observe changes in the proteome of OTUD6B depleted HeLa cells with the objective of identifying pathways connecting OTUD6B and our observed phenotypes. OTUD6B was depleted in HeLa cells by siRNA transfection and knockdown efficiency was verified through western blot analysis (Figure 34, A). iTRAQ-MS results were able to identify ~7000 proteins within the Hela proteome with ~1000 proteins significantly downregulated and ~1100 proteins significantly upregulation, determined using a p value of 0.05 or lower, among our three experimental replicates (Figure 34, B-C).

To gain a better understanding of which potential binding partners should be investigated, we cross-referenced our IP-MS results with results from our iTRAQ-MS dataset, specifically looking for downregulated proteins that appeared in our IP-MS list. We reasoned that, if OTUD6B is functioning through its catalytic activity, it was possible that depletion of OTUD6B would decrease the expression of its binding partner to which it stabilizes. This relationship between DUBs and their substrates is often observed when analyzing DUB catalytic activity; an example of this relationship is between the E3 ligase UBR5 and the DUB OTUD5; when OTUD5 is depleted, UBR5 is destabilized [53]. Through cross-referencing, we found ~300 proteins which appeared in our significantly downregulated list of proteins and our IP-MS data. Among these proteins was the Lysine-rich CEAMCAM-1 associated protein (LYRIC), also termed metastasis adhesion protein (metadherin), which has been implicated in metastasis and is overexpressed in breast, brain, and prostate cancers (Figure 35, A) [21]. To validate the results of our IP-MS data suggesting that LYRIC is a potential binding partner of OTUD6B, we performed a small scale flag-tagged IP followed by western blot analysis of our OTUD6B wildtype p3XFlag-CMV-9 plasmid.

Results confirmed our IP-MS data in that flag-tagged OTUD6B was able to pull down LYRIC (Figure 35, B).

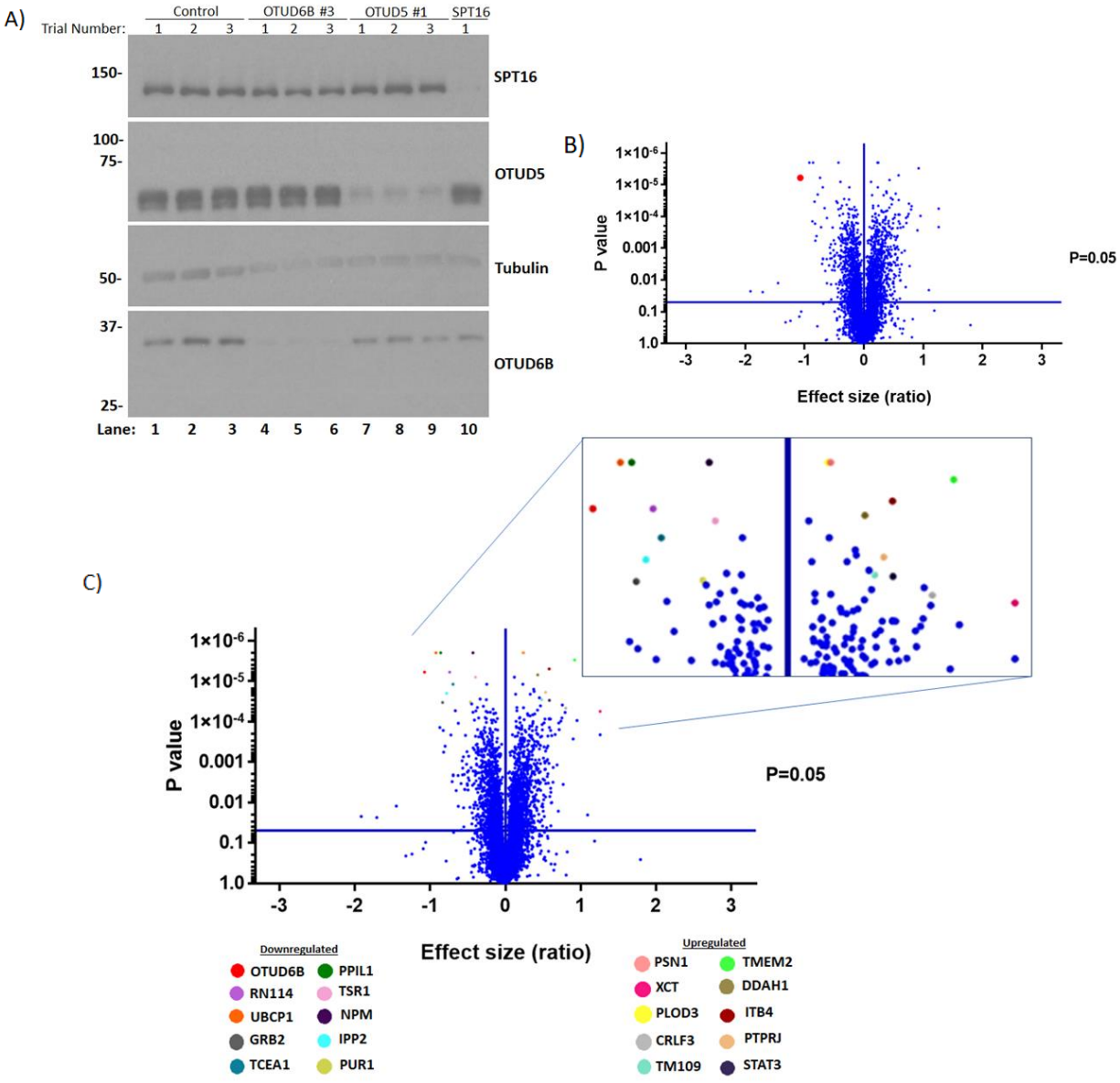

Figure 34. Verification and analysis of OTUD6B knockdown with iTRAQ-MS analysis. A) OTUD6B knockdown was conducted in HeLa cells in three replicates as shown. Control represents control siRNA from Bioneer. OTUD5 and SPT16 knockdown samples were also subjected to iTRAQ-MS analysis and used as controls for OTUD6B analysis. Tubulin was used as a loading control B) Volcano plot of resulting iTRAQ-MS proteome data under OTUD6B protein depletion. X-axis represents degree of fold change for each identified protein (blue dots). Y-axis represents statistical significance of fold change values. Blue horizontal line indicates the statistical cut off of p=0.05 and blue vertical line indicates no protein expression fold change. Red dot indicates OTUD6B. C) Volcano plot of resulting iTRAQ-MS proteome data under OTUD6B protein depletion highlighting 20 most significantly altered proteins detected. X-axis represents degree of fold change for each identified protein (blue dots). Y-axis represents statistical significance of fold change values. Blue horizontal line indicates the statistical cut off of p=0.05 and blue vertical line indicates no protein expression change. Proteins are highlight by different colored dots are labeled at the bottom of the figure.

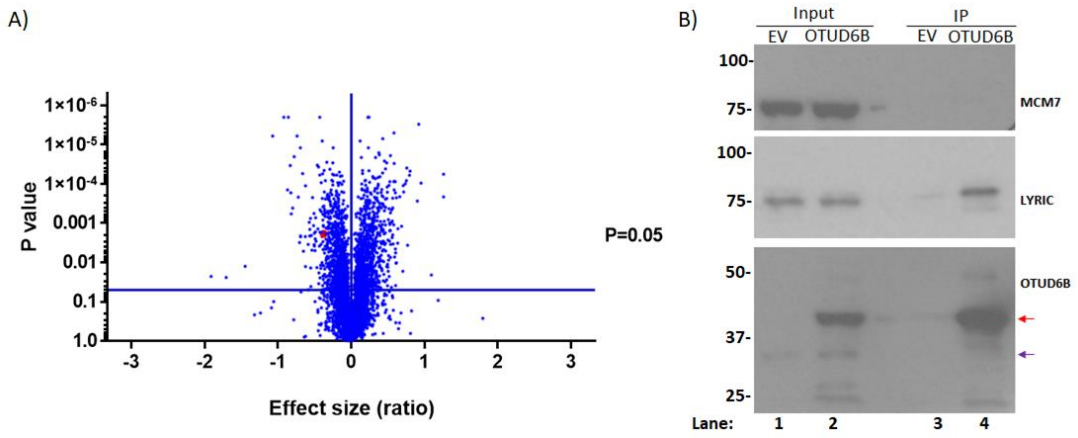

Figure 35. iTRAQ and IP results of LYRIC in relationship to OTUD6B. A) Volcano plot of resulting iTRAQ-MS proteome data under OTUD6B protein depletion. X-axis represents degree of fold change for each identified protein (blue dots). Y-axis represents statistical significance of fold change values. Blue horizontal line indicates the statistical cut off of p=0.05 and blue vertical line indicates no protein expression fold change. Red dot indicates LYRIC. B) Flag-tagged IP for wildtype p3XFlag-CMV-9-OTUD6B and empty vector p3XFlag-CMV-9 plasmid performed through transfection using turbofect in 293T cells and using anti-flag m2 agarose beads. One 6cm plate was used for each transfected plasmid. 5% of sample was used for inputs. 15uL of IPs was run. Red arrow indicates flag-tagged OTUD6B. Purple arrow indicates endogenous OTUD6B.

OTUD6B is a potential regulator of LYRIC stability

As we observed a significant decrease in LYRIC protein levels when OTUD6B was depleted in our iTRAQ-MS results, we performed a CHX chase assay under OTUD6B knockdown conditions to determine if LYRIC protein levels would be altered. Results showed that when OTUD6B protein levels were decreased, LYRIC expression minorly decreased (Figure 36, A). Specifically, by 8 hours of translation inhibition, LYRIC protein levels were noticeably reduced compared to control conditions (Figure 36, A).

Research has shown that LYRIC is monoubiquitylated to regulate its localization [21]. Specifically, the monoubiquitination at two different sites, each near one of three NLS sequences, promotes cytosolic sequestering of LYRIC and one report has identified TOPORS as the E3 ligase responsible for the ubiquitination [79]. TOPORS has also been shown to also ubiquitylate p53 and FOXO3a for localization regulation [79]. Unfortunately, TOPORS was not identified in our MS data sets.

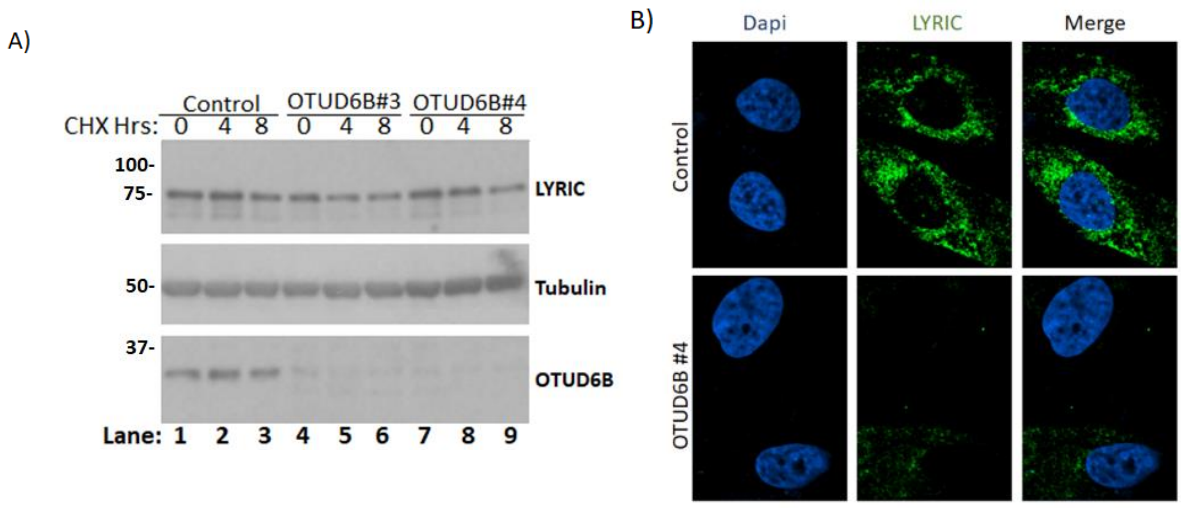

Figure 36. Decreased OTUD6B protein expression suggests decreased LYRIC protein expression. A) A CHX chase assay was performed under OTUD6B knockdown conditions using siRNA #3 and #4 in HeLa cells. 10uM of CHX was administered to samples at indicated time points. Control represents control siRNA from Bioneer. Tubulin was used as a loading control. B) OTUD6B knockdown was conducted with OTUD6B #4 siRNA in HeLa cells. Control represents control siRNA from Bioneer. 72 hours after knockdown administration samples were stained for LYRIC.

Due to this ubiquitination regulation of LYRIC, we wanted to observe if OTUD6B depletion impacted LYRIC localization. Immunofluorescence microscopy was performed to observe if depletion of OTUD6B could alter LYRIC localization. Interestingly, while we did not observe a change in localization, results showed a drastic change in LYRIC expression levels when OTUD6B was depleted in HeLa cells (Figure 36, B).

OTUD6B Depletion Alters Migration Abilities in Cancerous Cells

One of the first identified cases of LYRIC existence was in a LNCaP prostate cancer cell line as it was among a group of proteins significantly up-regulated [21]. Since then, multiple reports have affiliated LYRIC protein expression with cancerous phenotypes such as increased proliferation, increased migration, chemoresistance, angiogenesis, and metastasis [84]. Additionally, research has shown that inhibition of LYRIC also attenuates these major cancer characteristics, making targeting this protein for cancer treatments very appealing [84]. In fact, research is currently exploring LYRIC protein accumulation in serum as a potential early biomarker for aggressive cancers [84].

Because cBioPortal cancer gene expression summaries have also shown that *OTUD6B* is largely upregulated in prostate cancers, and because we have observed a decrease in cell proliferation and growth under OTUD6B depleted phenotypes, we postulated that our decreased growth phenotype could partially be due to OTUD6B-LYRIC interactions [25, 26]. As LYRIC has been largely associated with increased metastasis and migration, we wanted to observe if OTUD6B could exhibit a similar impact on such characteristics. To test this, we performed wound healing assays under OTUD6B knockdown in Hela cells and examined the subsequent change in the rate of migration compared to control conditions. Although migration rates were slow even under control conditions, we were able to detect a decrease in the rate of migration when HeLa cells were depleted of OTUD6B via two different siRNA sequences (Figure 37). Thus, OTUD6B depleted protein levels seemed to slow cellular ability to migrate into free space, similar in effect to decreased proliferation rates under OTUD6B protein depletion.

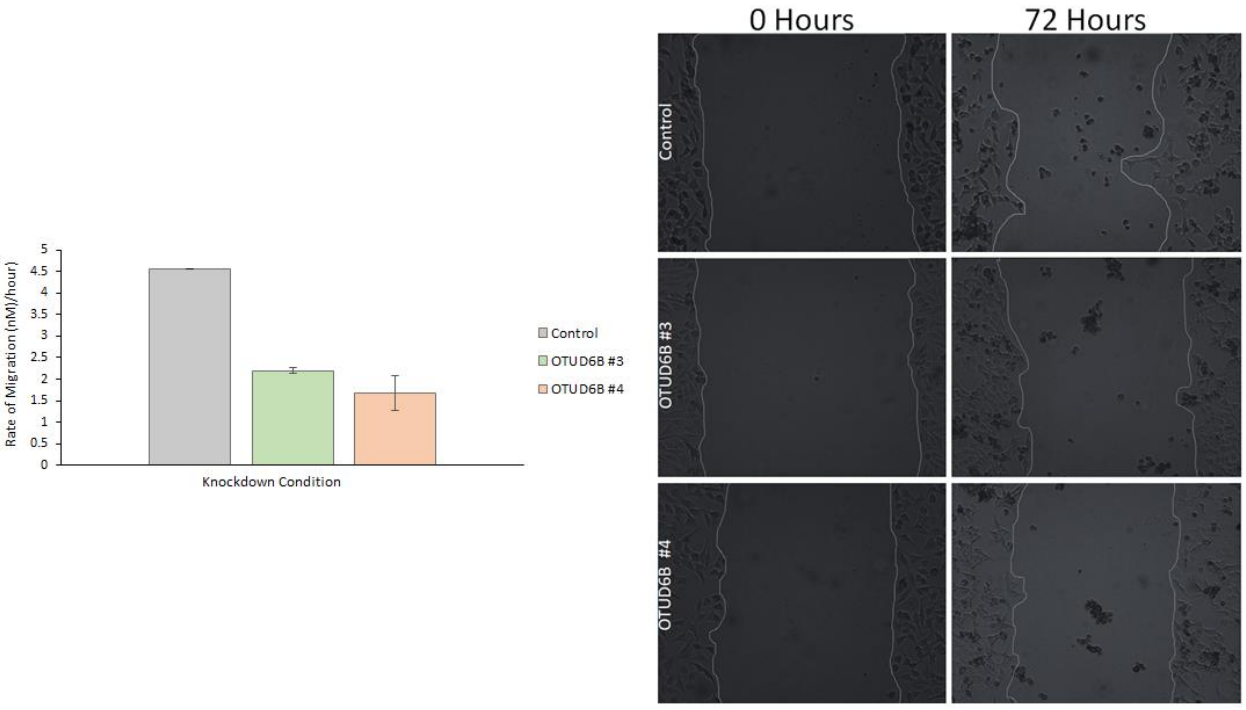

Figure 37. The rate of cellular migration in HeLa cell lines under OTUD6B protein depletion. To the left is a bar graph displaying the average rate of migration in nanometers per hour for indicated sample conditions. OTUD6B depletion was achieved through two different siRNA sequences as indicated. Control represents control siRNA from bioneer. Standard error reported is based off of three experimental replicates. Rates of migration were calculated as described in Chapter 5, Experimental Design, Cell Migration Assay. To the right are representative images of the first and last time points for each sample condition.

To observe a more drastic effect of depleted OTUD6B protein levels on cellular migration abilities, we decided to use a more aggressive cell line. Triple negative breast cancers, such as MDA-MB231, are an aggressive breast cancer cell line due to their lack of estrogen receptors (ER), progesterone receptors (PR), and human epidermal growth factor receptor 2 (HER2) expression; these cell lines have transformed to no longer depend on external growth factors for proliferation and thus are highly migratory and metastatic [85].

Additionally, OTUD6B and LYRIC have each been implicated in breast cancer survival rates. Overall survival estimates from cBioPortal breast cancer data summaries report a 50% survival among cancer cases exhibiting amplified *OTUD6B* compared to compared to a 73% survival for patients with no *OTUD6B* amplification (Figure 38) [25, 26]. Furthermore, median month survival comparisons for these breast cancer studies showed a 10.5 year survival rate for patients with amplified *OTUD6B* compared to patients without amplified *OTUD6B*, which was found to be 14 years [25, 26].

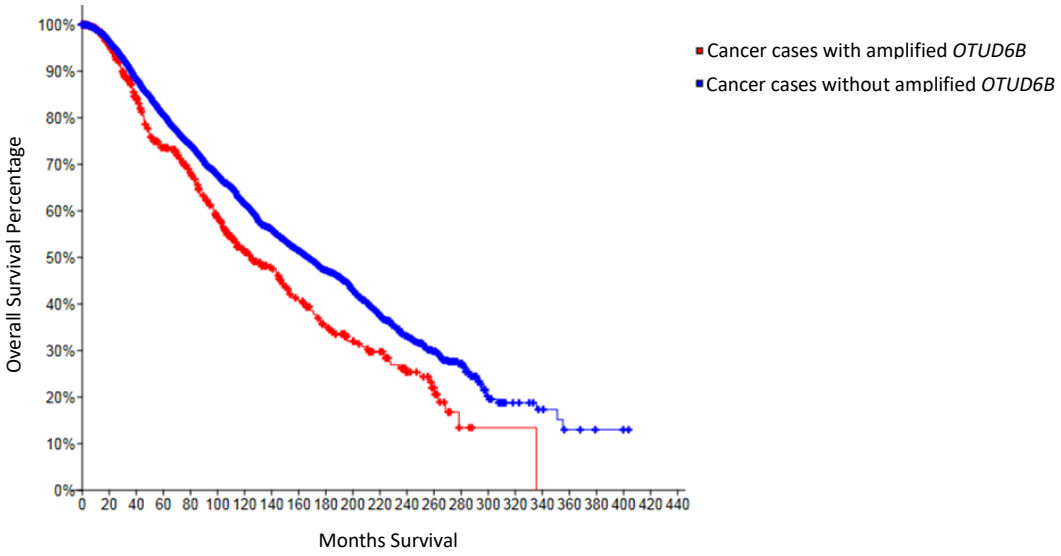

Figure 38. Overall Survival Kaplan-Meier Estimate of breast cancer patients with amplified *OTUD6B*. Analysis of breast cancer patient survival rates adapted from cBioPortal [24, 25]. Cases with amplified *OTUD6B* are represented in red. 554 cases were analyzed for the survival rates of patients with amplified *OTUD6B* [24, 25]. 5911 cases were analyzed for the survival rates of patients without amplified *OTUD6B* [24, 25].

Additionally, studies on LYRIC by Hu et al. (2009) has shown that LYRIC overexpression was associated with a higher risk of metastasis and shorter survival rate and since such studies have

emerged, LYRIC has been included in a risk assessment list of 70 signature genes for breast cancer metastasis [84]. It is suspected that LYRIC's association with metastasis is through its binding partner Staphylococcal nuclease domain-containing 1 (SND1), which it is believed to stabilize [86]. Interestingly, SND1 was also observed to be significantly downregulated in our iTRAQ-MS data set.

Thus, as LYRIC and OTUD6B overexpression have been associated with poor survival rates for breast cancer patients, we examined migration abilities of triple negative MDA-MB231 cell lines under depleted protein levels of OTUD6B. Results support our previous findings in HeLa cells, a decreased percentage of wound closure was observed 24 and 48 hours after scratch induction for cell samples depleted of OTUD6B compared to control conditions among three experimental replicates (Figure 39). This suggests that cells depleted of OTUD6B exhibit a decreased ability to migrate into free space, further suggesting a decrease in migration abilities. Additionally, because MDA-MB231 are triple negative breast cancer cell lines, this also suggests that OTUD6B functional role in regards to migration is independent of growth factor receptor dependent pathways. Interestingly, work by Hu et al. (2009) also did not find LYRIC overexpression and resulting increase in cancer migration abilities to correlate with a

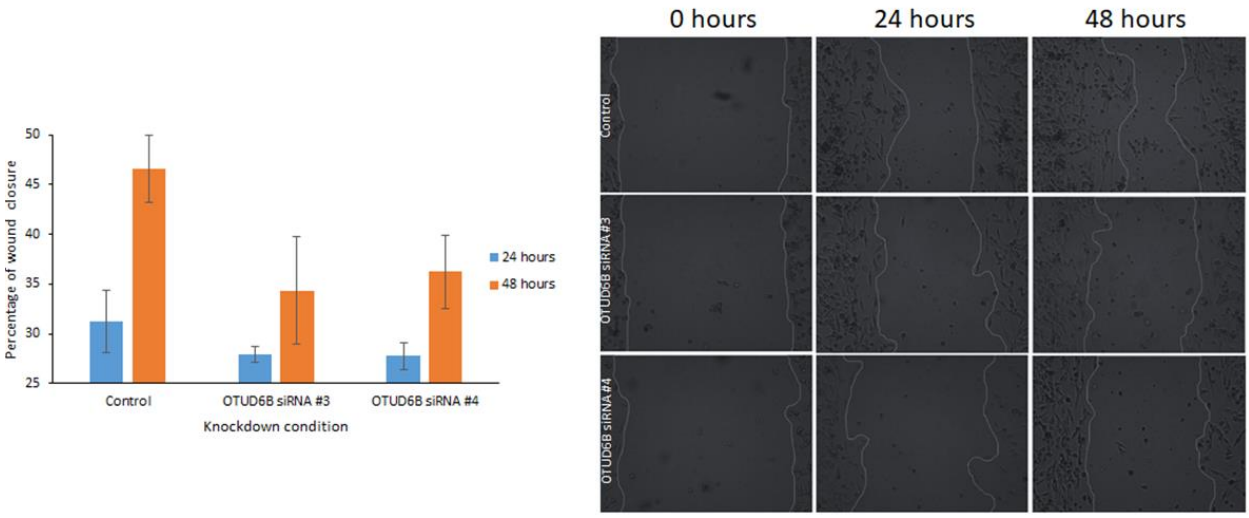

Figure 39. The percentage of wound closure in MDA-MB231 cell lines under OTUD6B protein depletion. To the left is a bar graph displaying the average percentage of wound closure for indicated sample conditions and indicated time points. OTUD6B depletion was achieved through two different siRNA sequences as indicated. Control represents control siRNA from bioneer. Standard error reported is based off of three experimental replicates. Percentage of wound closure for each sample was calculated as described in Chapter 5, Experimental Design, Cell Migration Assay. To the right are representative images of the first, second, and last time points for each sample condition.

particular breast cell line; ER, PR, and Her2 status did not impact LYRIC ability to promote metastasis [84]. It is potentially possible that OTUD6B and LYRIC may be functioning within the same pathway to promote cellular migration and growth.

Conclusions and Future Directions

Our work in this chapter involves MS techniques and proteome screenings to investigate the interacting pathways and binding partners of OTUD6B. Our previous experiments were not able to produce strong data connecting OTUD6B p21 regulation to the DNA maintenance or checkpoint kinase arrest pathways. As there are many additional enzymes and transcription factors that can facilitate p53-dependent p21 expression, we reasoned that proteomic screening via MS analysis would be an efficient method to uncover such pathways to explain our phenotypes.

In our IP-MS data, we identified several proteins that have previously been detected by similar methods, as potential OTUD6B binding partners: RPF2, ASCC3, and LYRIC. RPF2, or ribosome production factor 2 homologue (BXDC1), is reported to function in ribosomal subunit assembly [22]. Previous studies have associated OTUD6B isoform 1 as a negative regulator of translation as shown by methionine surrogate azidohomoalanine (AHA) incorporation rate analysis under different OTUD6B expression levels [20]. Thus, it is interesting that three separate cases, IP-MS analysis by Sowa et al. (2009), and our IP-MS work with our wildtype and C188S mutant p3xFlag-CMV-9 plasmids, have all reported RPF2 as a binding partner of OTUD6B [2]. Additionally, use of the contaminant repository for affinity purification (CRAPome), which is an online database of common contaminants in affinity purification-MS experiments, revealed RPF2 to have a low percentage of being identified in MS data sets at 6.6%, increasing the likelihood of RPF2 being a true binding partner of OTUD6B [83]. However, analysis of our iTRAQ-MS data set revealed RPF2 as an insignificantly altered protein under our OTUD6B knockdown conditions (Figure 40). For this reason, we did not pursue this protein for investigation of

OTUD6B interacting partners. This data, however, may be useful in future investigations of OTUD6B as several OTUs have been shown to hold more than one function which may be occurring for OTUD6B. Additionally, it is also possible that our iTRAQ-data results inaccurately identified RFP2 and thus, this protein should be further analyzed in future experiments.

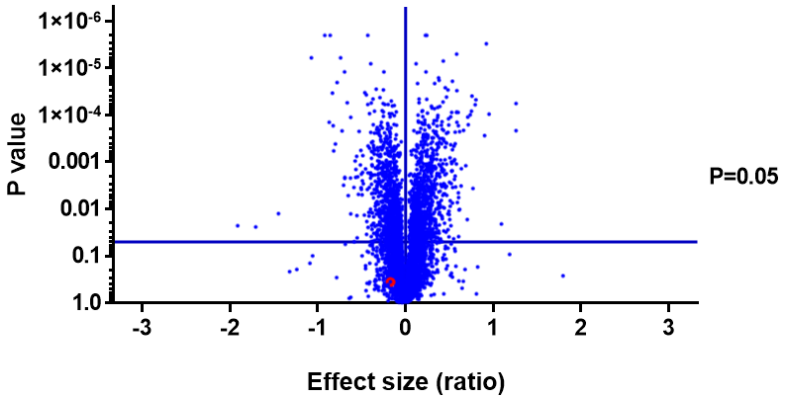

Figure 40. Volcano plot data of RPF2 protein fold change under OTUD6B depletion. Volcano plot of resulting iTRAQ-MS proteome data under OTUD6B protein depletion. X-axis represents degree of fold change for each identified protein (blue dots). Y-axis represents statistical significance of fold change values. Blue horizontal line indicates the statistical cut off of p=0.05 and blue vertical line indicates no protein expression fold change. Red dot indicates RPF2.

Another protein that was identified in both Sowa et al. (2009) work as well as our two IP-MS screenings was ASCC3, or activating signal co-integrator 1 complex subunit 3 [2]. This protein is a 3'-5' DNA helicase, which has been shown to be involved in repair of alkylated DNA [22]. Specifically, it promotes DNA unwinding for single stranded DNA generation, allowing the family member of the previously mentioned ALKBH2 demethylases, ALKBH3, to process alkylated N3-methylcytosine (3mC) within the DNA [22]. CRAPome analysis also revealed that this helicase to possesses a low percentage of appearing in IP-MS datasets at 9.5%, making this protein an appealing target for investigation [83]. However, ITRAQ-MS data analysis also revealed ASCC3 to be relatively unchanged under OTUD6B knockdown and thus, was not further perused in this study (Figure 41). However, it would be interesting to further investigate this helicase in future experiments as it could be a link to OTUD6B DNA integrity

maintenance pathways. This finding further strengthens the argument for a more in-depth analysis of OTUD6B and the DNA damage response.

The potential binding partner OTUDB1 reported in Sowa et al (2009) was not identified in our IP-

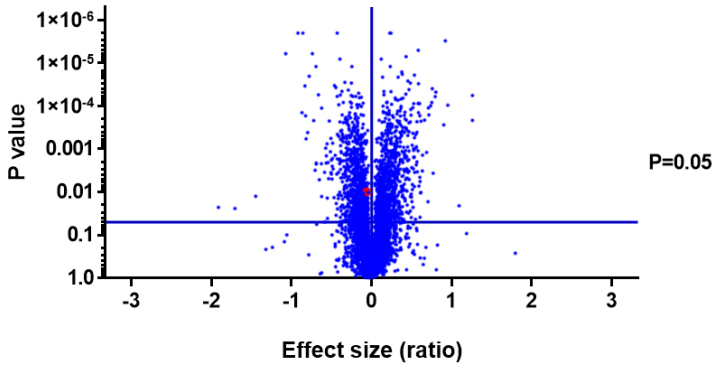

Figure 41. Volcano plot data of ASCC3 protein fold change under OTUD6B depletion. Volcano plot of resulting iTRAQ-MS proteome data under OTUD6B protein depletion. X-axis represents degree of fold change for each identified protein (blue dots). Y-axis represents statistical significance of fold change values. Blue horizontal line indicates the statistical cut off of p=0.05 and blue vertical line indicates no protein expression fold change. Red dot indicates ASCC3.

MS work in [2]. However, the last reported potential interacting partner, LYRIC, was identified in both our wildtype and catalytic inactivate C188S mutant IP-MS screenings [2]. Moreover, LYRIC was also shown to be significantly downregulated in our iTRAQ-MS screening (Figure 35). As mentioned previously, LYRIC also known as metaherin or astrocyte elevated gene-1 (AEG-1), is a functionally ambiguous protein known to regulate multiple pathways related to cell growth, proliferation, and metastasis as well as has been reported to be upregulated in various cancers [63, 84]. Specifically, LYRIC has been shown to facilitate NF-Kβ activation by promoting the degradation of IkB, increase phosphorylation of AKT and thus the activity of the P13K/AKT pathway while also inhabiting apoptosis, activate wnt/β-catenin signaling via ERK42/44 stimulation, promote the activation of SMAD pathways via its binding partner SND1, and inhibit p21 mediated cdk2 activity through the BRCA2-and CDKNIA interacting protein α (BCCIPα), as well as a great many other cellular growth pathways [63]. Thus, LYRIC is rightfully categorized as an oncogene if overexpressed [84]. Because of its pro-cellular growth and oncogenic promoting functions, and because it was found as a binding partner of OTUD6B in three

separate instances, as well as was identified to be downregulated in our iTRAQ-MS proteomic dataset, we perused this protein as a potential link between OTUD6B function and our observed phenotypes.

Aside from LYRIC, an additional ~2000 proteins were also detected to be significantly altered in our iTRAQ data; our volcano plot highlights twenty of some of the most significantly and drastically altered proteins identified in this work (Figure 34, C). Of note, three of the twenty listed proteins also appeared in our IP-MS dataset; PPIL1, also known as peptidyl-prolyl cis-trans isomerase-like 1, NPM, also known as nucleophosmin, and TSR1, also known as pre-rRNA-processing protein TSR1 homolog [22]. TSR1 has been reported to be required for 40S ribosomal subunit maturation within the nucleus and the CRAPome reports its detection in IP-MS datasets at 16% [22]. NPM is known to be involved in a diverse array of cell pathway and potentially regulates p53 and ARF functioning [22]. NPM reports a 61% detection in the CRAPome [83]. PPIL1 is involved in pre-mRNA splicing of the spliceosome and detected at 3% in the CRAPome [22, 83]. Interestingly all these proteins are also downregulated in our iTRAQ data and thus, warrant further investigation (Figure 34, C). As stated previously, it is possible that OTUD6B may be involved with a variety of cellular pathways and that OTUD6B diversity is stimulated by the OTU holding catalytic dependent and catalytically independent functionalities.

Our work shows that flagged-tagged OTUD6B bound to LYRIC via small scale IP, strengthening our MS findings. However, to truly confirm this interaction, additional experiments must be conducted including *in vitro* binding tests of purified OTUD6B and LYRIC to confirm a direct interaction. It would be also interesting to identify the site of LYRIC-OTUD6B binding within the OTUD6B amino acid sequence to observe if the predicted disordered region facilitates such interactions. However, such attempts may present difficulties such as altering OTUD6B structural and protein folding.

Because we observed a decrease in LYRIC fold change and because our C188S mutant reported more unique peptides matching LYRIC in our IP-MS work then did wildtype results, we reasoned that OTUD6B regulated LYRIC stability. Our CHX chase assay results support this rational as we observed

greater decrease in LYRIC protein levels overtime under our OTUD6B depleted conditions compared to control (Figure 36, A). Additional support is shown by a drastic decrease in our IF analysis under OTUD6B knockdown as well (Figure 36, B).

Ubiquitin modifications have been reported with LYRIC as a form of localization regulation, however it is unclear whether LYRIC also experiences ubiquitination for its degradation processes as well. Work has shown that monoubiquitination on two of three of LYRIC NLS sequences were required for cytosolic placement [79]. In the event of deubiquitination, LYRIC locates to the nuclease and nucleolus [79]. Interestingly, nuclear localized was predominantly only observed in benign tissue, while cytosolic localization primarily occurred in transformed cells, suggesting that further investigations on LYRIC localization and stability in non-transformed cell lines may need to be conducted [21]. It has also been suggested that the E3 ligase TOPORS is responsible for the monoubiquitination [79]. Unfortunately, TOPORS was not identified in either of our MS screenings, though further investigation into this protein's functional capacity in relation to OTUD6B may be of future interest.

In addition, we observed discrepancies in LYRIC kilodalton size compared to literature reports; the unmodified form of LYRIC according to previous reports is ~65kDa in size [22]. However, through modifications such as ubiquitination and sumoylation, which it also experiences, LYRIC has been shown to run at ~100kDa [21]. It is suspected that detected LYRIC at size 75kDa is the monoubiquitylated form of the protein, which promotes its cytoplasmic localization [21]. In our data, we have only detected LYRIC at 75kDa, however we do notice a lower band below the 75kDa that is decreased upon 6B knockdown with CHX analysis (Figure 36, A). Future experiments should include investigation of this lower band, as well as the unmodified and posttranslational modified forms of LYRIC, to determine if OTUD6B holds any impact on these alteration of LYRIC protein expression. It is important to note however, as previously mentioned, DUBs have been shown to hold additional functions outside their DUB abilities. It may be possible that OTUD6B also is of this DUB cohort in regards to its interaction with

LYRIC. This theory is unsupported, however due to our C188S IP-MS results which suggests more binding events between LYRIC and OTUD6B when OTUD6B isopeptidase activity is inhibited.

In support of our finding that OTUD6B is interacting with LYRIC, we have found several LYRIC interacting partners in our MS screenings. For example, ribosome synthesis 1 (Rrs1), which has been shown to localize in conjunction with LYRIC, was detected in our IP-MS data and was downregulated in our screenings (Figure 42, A and D) [22]. SND1, which may be the key protein behind LYRICs metastatic-inducing abilities, was also pulled down in our IP work, however, showed little change in our iTRAQ-MS data (Figure 42, B and D) [86]. Of note, SND1 is highly detected in MS work according to the CRAPome (Figure 42, D) [83]. Also, in support of our findings, the LYRIC binding partner BCCIPα, to which LYRIC has

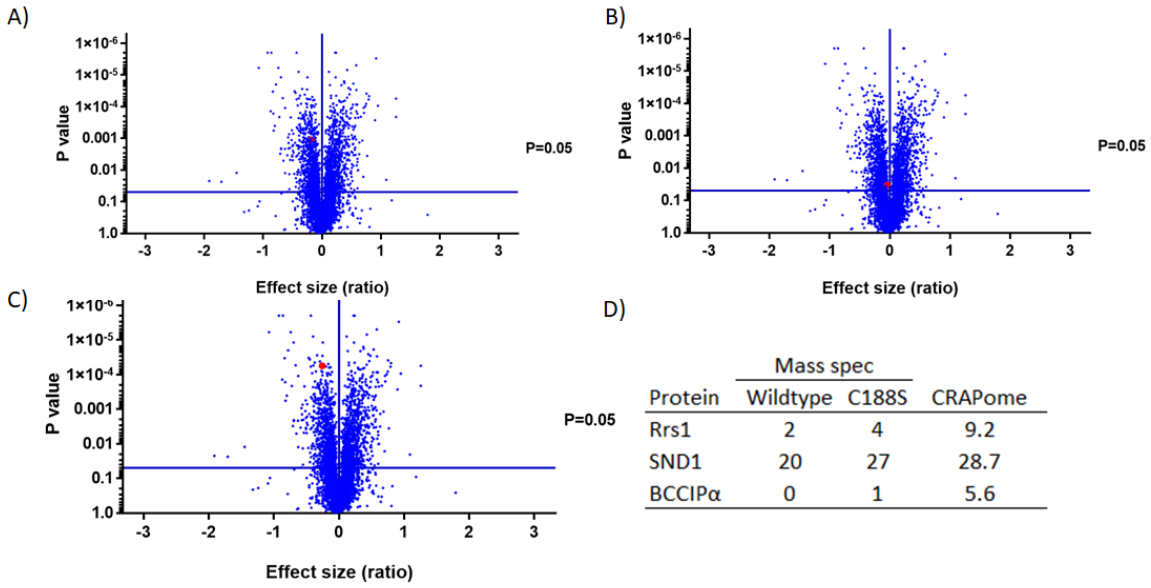

	Mass spec		
Protein	Wildtype	C188S	CRAPome
Rrs1	2	4	9.2
SND1	20	27	28.7
BCCIPα	0	1	5.6

Figure 42. iTRAQ-MS and IP-MS results of LYRIC interacting partners. A-C) Volcano plot of resulting iTRAQ-MS proteome data under OTUD6B protein depletion. X-axis represents degree of fold change for each identified protein (blue dots). Y-axis represents statistical significance of fold change values. Blue horizontal line indicates the statistical cut off of p=0.05 and blue vertical line indicates no protein expression fold change. Red dot indicates Rrs1 (A), SND1 (B), and BCCIPα (C). D) Figure displaying proteins identified in IP-MS data for both the wildtype and mutant IPs and their respective unique peptide numbers. Also displayed are each proteins' reported percentage in the Contaminant Repository for Affinity Purification (CRAPome).

been suggested to degrade, was also detected in our pulldown (Figure 42, D) [63]. BCCIPα is a tumor suppressor gene reported to promote p21 inhibition of cdk2 and thus could provide an explanation for our p21 induction phenotype [63]. However, iTRAQ-MS analysis reports this protein as being

downregulated as well (Figure 42, C). Because relationship between LYRIC and BCCIPα is not entirely understood, future investigations may want to include BCCIPα functional analysis to verify iTRAQ-MS results [63].

While our initial analysis of OTUD6B-LYRIC relationship appears promising, additional experiments should be conducted. It will be interesting to determine if OTUD6B rescue assays are able to restore LYRIC stability to mimic control. It will also be interesting to observe if LYRIC overexpression under an OTUD6B knockdown can restore our p21 induction and cellular growth phenotypes to control conditions. Verification of OTUD6B catalytic activity being responsible for LYRIC regulation should be also be conducted.

In an attempt to connect our OTUD6B phenotypes and LYRIC protein function, we analyzed OTUD6B impact on migration abilities in HeLa and MDA-MB231 cell lines. As mentioned previously, LYRIC is a promoter of metastasis. Cancer metastasis is achieved by several methods including an increase in cellular migration, angiogenesis promotion, and increased invasion abilities. Wound healing assays are a basic method to study cellular migration abilities and thus were performed to determine if OTUD6B depletion could inhibit cellular migration.

Our data supports OTUD6B protein levels as an impacting factor in cellular migration, HeLa cells shown decreased rates of migration and MDA-MB231 cancer cells exhibited decreased percentage of wound closure compared to controls at the same time points (Figures 37 and 49). Of interest, OTUD6B has previously been reported to regulate cellular migration. Specifically, the long non-coding RNA OTUD6B AS1, in kidney cancer cells, was shown to inhibit cell growth, proliferation, and migration by impacting wnt/β-catenin pathway signaling [27]. While long noncoding RNAs do not necessarily regulate their protein counter parts, our data suggests similar phenotypes and thus may require further future consideration.

To further confirm OTUD6B as a positive regulator of cellular migration, more extensive experiments should be conducted such as invasion analysis using transwell systems, which will provide more accurate results for migration interpretations, analysis of migratory promoting proteins expression levels, such as matrix metalloproteases and cadherins, and measurement of cell migration rates when OTUD6B is overexpressed [82, 85]. As HeLa cells reported a very slow rate of migration in our results, MDA-MB231 cells should be used for such further analysis. It would also be interesting to observe if increased LYRIC protein levels under OTUD6B protein depletion or if a double knockdown of OTU6B and p21 would be able to restore migration rates to control conditions. Such experiments could also provide insight into the role of p21 and LYRIC in OTUD6B regulated migration.

While it is promising that this migration phenotype may be related to LYRIC functionality, such speculations cannot be fully confirmed through presented work and require further analysis. It is possible that the decrease in migratory effect is due to our p21 discovered phenotype. P21 and LYRIC functionalities have fairly opposing outcomes; while LYRIC seems to promote pathways needed for cellular growth, p21 is traditionally required for increased senescence and cell proliferation inhibition [30, 84]. Whether these two proteins both regulate the same set of pathways remains to be investigated. It will be interesting to determine if OTU6B regulates LYRIC and p21 by the same pathway, resulting in manipulation of cell proliferation and growth, or if OTUD6B regulates expression levels of both proteins by completely different signaling cascades, which ultimately both result in similar phenotypes (Figure 43). Future experiments should be conducted to determine such a relationship.

Ultimately, our work has reported a potentially new relationship between LYRIC and the understudied DUB, OTUD6B. As LRYIC has been found as an oncogene, discovering a protein which helps to regulate its function creates a promising outlook for biomedical advancements in concerns to “cancer risk” biomarkers or anti-cancer therapies and thus, warrants further investigation of this potential protein interaction.

References

[1] D. Oudshoorn, G.A. Versteeg, M. Kikkert, Regulation of the innate immune system by ubiquitin and ubiquitin-like modifiers, Cytokine & Growth Factor Reviews 23(6) (2012) 273-282.
[2] M.E. Sowa, E.J. Bennett, S.P. Gygi, J.W. Harper, Defining the Human Deubiquitinating Enzyme Interaction Landscape, Cell 138(2) (2009) 389-403.
[3] C.M. Pickart, Mechanisms Underlying Ubiquitination, Annual Review of Biochemistry 70(1) (2001) 503-533.
[4] D.D. Sahtoe, T.K. Sixma, Layers of DUB regulation, Trends in Biochemical Sciences 40(8) (2015) 456-467.
[5] J.S. Thrower, L. Hoffman, M. Rechsteiner, C.M. Pickart, Recognition of the polyubiquitin proteolytic signal, The EMBO Journal 19(1) (2000) 94.
[6] L. Nguyen, M. Dobrzynski, D. Fey, B. Kholodenko, Polyubiquitin chain assembly and organization determine the dynamics of protein activation and degradation, Frontiers in Physiology 5(4) (2014).
[7] S.J.L. van Wijk, H.T.M. Timmers, The family of ubiquitin-conjugating enzymes (E2s): deciding between life and death of proteins, The FASEB Journal 24(4) (2009) 981-993.
[8] M.B. Metzger, V.A. Hristova, A.M. Weissman, HECT and RING finger families of E3 ubiquitin ligases at a glance, Journal of Cell Science 125(3) (2012) 531.
[9] D. Frescas, M. Pagano, Deregulated proteolysis by the F-box proteins SKP2 and β-TrCP: tipping the scales of cancer, Nature Reviews Cancer 8 (2008) 438.
[10] Tycho E.T. Mevissen, Manuela K. Hospenthal, Paul P. Geurink, Paul R. Elliott, M. Akutsu, N. Arnaudo, R. Ekkebus, Y. Kulathu, T. Wauer, F. El Oualid, Stefan M.V. Freund, H. Ovaa, D. Komander, OTU Deubiquitinases Reveal Mechanisms of Linkage Specificity and Enable Ubiquitin Chain Restriction Analysis, Cell 154(1) (2013) 169-184.
[11] I.A. Shaltiel, L. Krenning, W. Bruinsma, R.H. Medema, The same, only different – DNA damage checkpoints and their reversal throughout the cell cycle, Journal of Cell Science 128(4) (2015) 607.
[12] M.L. Coleman, C.J. Marshall, M.F. Olson, Ras promotes p21(Waf1/Cip1) protein stability via a cyclin D1-imposed block in proteasome-mediated degradation, The EMBO journal 22(9) (2003) 2036-2046.
[13] W. Joo, G. Xu, N.S. Persky, A. Smogorzewska, D.G. Rudge, O. Buzovetsky, S.J. Elledge, N.P. Pavletich, Structure of the FANCI-FANCD2 Complex: Insights into the Fanconi Anemia DNA Repair Pathway, Science 333(6040) (2011) 312.
[14] Y. Kee, T.T. Huang, Role of Deubiquitinating Enzymes in DNA Repair, Molecular and Cellular Biology 36(4) (2016) 524.
[15] D.D. Sahtoe, T.K. Sixma, Layers of DUB regulation, Trends in Biochemical Sciences 40(8) 456-467.
[16] S.-C. Sun, Deubiquitylation and regulation of the immune response, Nature Reviews Immunology 8 (2008) 501.
[17] T. Santiago-Sim, L.C. Burrage, F. Ebstein, M.J. Tokita, M. Miller, W. Bi, A.A. Braxton, J.A. Rosenfeld, M. Shahrour, A. Lehmann, B. Cogné, S. Küry, T. Besnard, B. Isidor, S. Bézieau, I. Hazart, H. Nagakura, L.L. Immken, R.O. Littlejohn, E. Roeder, Z. Afawi, R. Balling, N. Barisic, S. Baulac, D. Craiu, P. De Jonghe, R. Guerrero-Lopez, R. Guerrini, I. Helbig, H. Hjalgrim, J. Jähn, K.M. Klein, E. Leguern, H. Lerche, C. Marini, H. Muhle, F. Rosenow, J. Serratosa, K. Sterbová, A. Suls, R.S. Moller, P. Striano, Y. Weber, F. Zara, B. Kara, K. Hardies, S. Weckhuysen, P. May, J.R. Lemke, O. Elpeleg, B. Abu-Libdeh, K.N. James, J.L. Silhavy, M.Y. Issa, M.S. Zaki, J.G. Gleeson, J.R. Seavitt, M.E. Dickinson, M.C. Ljungberg, S. Wells, S.J. Johnson, L. Teboul,

C.M. Eng, Y. Yang, P.-M. Kloetzel, J.D. Heaney, M.A. Walkiewicz, Biallelic Variants in OTUD6B Cause an Intellectual Disability Syndrome Associated with Seizures and Dysmorphic Features, The American Journal of Human Genetics 100(4) (2017) 676-688.
[18] B. Mészáros, I. Simon, Z. Dosztányi, Prediction of Protein Binding Regions in Disordered Proteins, PLOS Computational Biology 5(5) (2009) e1000376.
[19] L. Straniero, V. Rimoldi, G. Soldà, M. Bellini, G. Biasucci, R. Asselta, S. Duga, First Replication of the Involvement of OTUD6B in Intellectual Disability Syndrome With Seizures and Dysmorphic Features, Frontiers in genetics 9 (2018) 464-464.
[20] A. Sobol, C. Askonas, S. Alani, M.J. Weber, V. Ananthanarayanan, C. Osipo, M. Bocchetta, Deubiquitinase OTUD6B Isoforms Are Important Regulators of Growth and Proliferation, Molecular Cancer Research 15(2) (2017) 117.
[21] H.J. Thirkettle, J. Girling, A.Y. Warren, I.G. Mills, K. Sahadevan, H. Leung, F. Hamdy, H.C. Whitaker, D.E. Neal, LYRIC/AEG-1 Is Targeted to Different Subcellular Compartments by Ubiquitinylation and Intrinsic Nuclear Localization Signals, Clinical Cancer Research 15(9) (2009) 3003.
[22] T.U. Consortium, UniProt: a worldwide hub of protein knowledge, Nucleic Acids Research 47(D1) (2018) D506-D515.
[23] Z. Xu, Y. Zheng, Y. Zhu, X. Kong, L. Hu, Evidence for OTUD-6B Participation in B Lymphocytes Cell Cycle after Cytokine Stimulation, PLOS ONE 6(1) (2011) e14514.
[24] A. Catic, E. Fiebiger, G.A. Korbel, D. Blom, P.J. Galardy, H.L. Ploegh, Screen for ISG15-crossreactive Deubiquitinases, PLOS ONE 2(7) (2007) e679.
[25] E. Cerami, J. Gao, U. Dogrusoz, B.E. Gross, S.O. Sumer, B.A. Aksoy, A. Jacobsen, C.J. Byrne, M.L. Heuer, E. Larsson, Y. Antipin, B. Reva, A.P. Goldberg, C. Sander, N. Schultz, The cBio Cancer Genomics Portal: An Open Platform for Exploring Multidimensional Cancer Genomics Data, Cancer Discovery 2(5) (2012) 401.
[26] J. Gao, B.A. Aksoy, U. Dogrusoz, G. Dresdner, B. Gross, S.O. Sumer, Y. Sun, A. Jacobsen, R. Sinha, E. Larsson, E. Cerami, C. Sander, N. Schultz, Integrative Analysis of Complex Cancer Genomics and Clinical Profiles Using the cBioPortal, Science Signaling 6(269) (2013) pl1.
[27] G. Wang, Z.-j. Zhang, W.-g. Jian, P.-h. Liu, W. Xue, T.-d. Wang, Y.-y. Meng, C. Yuan, H.-m. Li, Y.-p. Yu, Z.-x. Liu, Q. Wu, D.-m. Zhang, C. Zhang, Novel long noncoding RNA OTUD6B-AS1 indicates poor prognosis and inhibits clear cell renal cell carcinoma proliferation via the Wnt/β-catenin signaling pathway, Molecular Cancer 18(1) (2019) 15.
[28] C.P.C. De Souza, S.A. Osmani, Mitosis, Not Just Open or Closed, Eukaryotic Cell 6(9) (2007) 1521.
[29] P. Hydbring, M. Malumbres, P. Sicinski, Non-canonical functions of cell cycle cyclins and cyclin-dependent kinases, Nature Reviews Molecular Cell Biology 17 (2016) 280.
[30] N.N. Kreis, F. Louwen, J. Yuan, Less understood issues: p21Cip1 in mitosis and its therapeutic potential, Oncogene 34 (2014) 1758.
[31] A. Karimian, Y. Ahmadi, B. Yousefi, Multiple functions of p21 in cell cycle, apoptosis and transcriptional regulation after DNA damage, DNA Repair 42 (2016) 63-71.
[32] M. Malumbres, Cyclin-dependent kinases, Genome biology 15(6) (2014) 122-122.
[33] C.H. Yam, T.K. Fung, R.Y.C. Poon, Cyclin A in cell cycle control and cancer, Cellular and Molecular Life Sciences CMLS 59(8) (2002) 1317-1326.
[34] N. Bendris, B. Lemmers, J.-M. Blanchard, N. Arsic, Cyclin A2 mutagenesis analysis: a new insight into CDK activation and cellular localization requirements, PloS one 6(7) (2011) e22879-e22879.
[35] D.S. O'Connor, N.R. Wall, A.C.G. Porter, D.C. Altieri, A p34cdc2 survival checkpoint in cancer, Cancer Cell 2(1) (2002) 43-54.
[36] K. Kimura, M. Hirano, R. Kobayashi, T. Hirano, Phosphorylation and Activation of 13S Condensin by Cdc2 in Vitro, Science 282(5388) (1998) 487.

[37] M. Kapanidou, N.L. Curtis, V.M. Bolanos-Garcia, Cdc20: At the Crossroads between Chromosome Segregation and Mitotic Exit, Trends in Biochemical Sciences 42(3) (2017) 193-205.
[38] A.L. Gartel, A.L. Tyner, The Role of the Cyclin-dependent Kinase Inhibitor p21 in Apoptosis 1 Supported in part by NIH Grant R01 DK56283 (to A. L. T.) for the p21 research and Campus Research Board and Illinois Department of Public Health Penny Severns Breast and Cervical Cancer grants (to A. L. G.).1, Molecular Cancer Therapeutics 1(8) (2002) 639-649.
[39] T. Abbas, A. Dutta, p21 in cancer: intricate networks and multiple activities, Nature Reviews Cancer 9 (2009) 400.
[40] V. Amador, S. Ge, P.G. Santamaría, D. Guardavaccaro, M. Pagano, APC/C^{Cdc20} Controls the Ubiquitin-Mediated Degradation of p21 in Prometaphase, Molecular Cell 27(3) (2007) 462-473.
[41] C.S. Technologies, Senescence, 2019. https://www.cellsignal.com/contents/_/cellular-senescence/overview-of-cellular-senescence.
[42] A.L. Gartel, A.L. Tyner, Transcriptional Regulation of the p21(WAF1/CIP1)Gene, Experimental Cell Research 246(2) (1999) 280-289.
[43] Y. Kim, N.G. Starostina, E.T. Kipreos, The CRL4Cdt2 ubiquitin ligase targets the degradation of p21Cip1 to control replication licensing, Genes & Development 22(18) (2008) 2507-2519.
[44] L. Song, M. Rape, Reverse the curse--the role of deubiquitination in cell cycle control, Current opinion in cell biology 20(2) (2008) 156-163.
[45] M. Patil, N. Pabla, Z. Dong, Checkpoint kinase 1 in DNA damage response and cell cycle regulation, Cellular and Molecular Life Sciences 70(21) (2013) 4009-4021.
[46] D. Woods, J.J. Turchi, Chemotherapy induced DNA damage response: convergence of drugs and pathways, Cancer biology & therapy 14(5) (2013) 379-389.
[47] G.P. Dimri, X. Lee, G. Basile, M. Acosta, G. Scott, C. Roskelley, E.E. Medrano, M. Linskens, I. Rubelj, O. Pereira-Smith, A biomarker that identifies senescent human cells in culture and in aging skin in vivo, Proceedings of the National Academy of Sciences of the United States of America 92(20) (1995) 9363-9367.
[48] D.J. Holt, D.W. Grainger, Senescence and quiescence induced compromised function in cultured macrophages, Biomaterials 33(30) (2012) 7497-7507.
[49] H. Hu, S.-C. Sun, Ubiquitin signaling in immune responses, Cell Research 26 (2016) 457.
[50] M. Ogrunc, R.I. Martinez-Zamudio, P.B. Sadoun, G. Dore, H. Schwerer, P. Pasero, J.-M. Lemaitre, A. Dejean, O. Bischof, USP1 Regulates Cellular Senescence by Controlling Genomic Integrity, Cell Reports 15(7) (2016) 1401-1411.
[51] A. Sanchez, A. De Vivo, N. Uprety, J. Kim, S.M. Stevens, Y. Kee, BMI1–UBR5 axis regulates transcriptional repression at damaged chromatin, Proceedings of the National Academy of Sciences 113(40) (2016) 11243.
[52] S. Cukras, N. Morffy, T. Ohn, Y. Kee, Inactivating UBE2M impacts the DNA damage response and genome integrity involving multiple cullin ligases, PloS one 9(7) (2014) e101844-e101844.
[53] A. de Vivo, A. Sanchez, J. Yegres, J. Kim, S. Emly, Y. Kee, The OTUD5–UBR5 complex regulates FACT-mediated transcription at damaged chromatin, Nucleic Acids Research 47(2) (2018) 729-746.
[54] I. Santa Cruz BioTechnology, OTUD6B Double Nickase Plasmid (h): sc-407492-NIC, Europe, 2019.
[55] Patrick D. Hsu, Eric S. Lander, F. Zhang, Development and Applications of CRISPR-Cas9 for Genome Engineering, Cell 157(6) (2014) 1262-1278.
[56] F.A. Ran, P.D. Hsu, C.-Y. Lin, J.S. Gootenberg, S. Konermann, A.E. Trevino, D.A. Scott, A. Inoue, S. Matoba, Y. Zhang, F. Zhang, Double nicking by RNA-guided CRISPR Cas9 for enhanced genome editing specificity, Cell 154(6) (2013) 1380-1389.

[57] K.M. Kodigepalli, M. Nanjundan, Induction of PLSCR1 in a STING/IRF3-Dependent Manner upon Vector Transfection in Ovarian Epithelial Cells, PLOS ONE 10(2) (2015) e0117464.
[58] S. Hietanen, S. Lain, E. Krausz, C. Blattner, D.P. Lane, Activation of p53 in cervical carcinoma cells by small molecules, Proceedings of the National Academy of Sciences 97(15) (2000) 8501.
[59] F. Müller, P. Ackermann, P. Margot, Fungicides, Agricultural, 2. Individual Fungicides, Ullmann's Encyclopedia of Industrial Chemistry (2011).
[60] C.M. Nicolae, M.J. O'Connor, D. Constantin, G.-L. Moldovan, NFκB regulates p21 expression and controls DNA damage-induced leukemic differentiation, Oncogene 37(27) (2018) 3647-3656.
[61] T. Nojima, M. Tellier, J. Foxwell, C. Ribeiro de Almeida, S.M. Tan-Wong, S. Dhir, G. Dujardin, A. Dhir, S. Murphy, N.J. Proudfoot, Deregulated Expression of Mammalian lncRNA through Loss of SPT6 Induces R-Loop Formation, Replication Stress, and Cellular Senescence, Molecular Cell 72(6) (2018) 970-984.e7.
[62] L.-Q. Jia, M. Osada, C. Ishioka, M. Gamo, S. Ikawa, T. Suzuki, H. Shimodaira, T. Niitani, T. Kudo, M. Akiyama, N. Kimura, M. Matsuo, H. Mizusawa, N. Tanaka, H. Koyama, M. Namba, R. Kanamaru, T. Kuroki, Screening the p53 status of human cell lines using a yeast functional assay, Molecular Carcinogenesis 19(4) (1997) 243-253.
[63] L. Emdad, S.K. Das, S. Dasgupta, B. Hu, D. Sarkar, P.B. Fisher, Chapter Three - AEG-1/MTDH/LYRIC: Signaling Pathways, Downstream Genes, Interacting Proteins, and Regulation of Tumor Angiogenesis, in: D. Sarkar, P.B. Fisher (Eds.), Advances in Cancer Research, Academic Press2013, pp. 75-111.
[64] W.A. Freed-Pastor, C. Prives, Mutant p53: one name, many proteins, Genes & Development 26(12) (2012) 1268-1286.
[65] S. Al-Karadaghi, The 20 Amino Acids and Their Role in Protein Structures, 2019. https://proteinstructures.com/Structure/Structure/amino-acids.html. 2019).
[66] R. Nishi, P. Wijnhoven, C. le Sage, J. Tjeertes, Y. Galanty, J.V. Forment, M.J. Clague, S. Urbé, S.P. Jackson, Systematic characterization of deubiquitylating enzymes for roles in maintaining genome integrity, Nature cell biology 16(10) (2014) 1016-8.
[67] B.Y. Lee, J.A. Han, J.S. Im, A. Morrone, K. Johung, E.C. Goodwin, W.J. Kleijer, D. DiMaio, E.S. Hwang, Senescence-associated β-galactosidase is lysosomal β-galactosidase, Aging Cell 5(2) (2006) 187-195.
[68] S. Kosugi, M. Hasebe, M. Tomita, H. Yanagawa, Systematic identification of cell cycle-dependent yeast nucleocytoplasmic shuttling proteins by prediction of composite motifs, Proceedings of the National Academy of Sciences 106(25) (2009) 10171.
[69] J.P. Murnane, M.J. Yezzi, B.R. Young, Recombination events during integration of transfected DNA into normal human cells, Nucleic Acids Research 18(9) (1990) 2733-2738.
[70] S.M. Hecht, Bleomycin: New Perspectives on the Mechanism of Action, Journal of Natural Products 63(1) (2000) 158-168.
[71] R.P. Rastogi, Richa, A. Kumar, M.B. Tyagi, R.P. Sinha, Molecular Mechanisms of Ultraviolet Radiation-Induced DNA Damage and Repair, Journal of Nucleic Acids 2010 (2010).
[72] T.L. de Jager, A.E. Cockrell, S.S. Du Plessis, Ultraviolet Light Induced Generation of Reactive Oxygen Species, in: S.I. Ahmad (Ed.), Ultraviolet Light in Human Health, Diseases and Environment, Springer International Publishing, Cham, 2017, pp. 15-23.
[73] T. Wiedmer, J. Zhao, M. Nanjundan, P.J. Sims, Palmitoylation of Phospholipid Scramblase 1 Controls Its Distribution between Nucleus and Plasma Membrane, Biochemistry 42(5) (2003) 1227-1233.
[74] G.V. Chaitanya, A.J. Steven, P.P. Babu, PARP-1 cleavage fragments: signatures of cell-death proteases in neurodegeneration, Cell communication and signaling : CCS 8 (2010) 31-31.
[75] K. McArthur, B.T. Kile, Apoptotic Caspases: Multiple or Mistaken Identities?, Trends in Cell Biology 28(6) (2018) 475-493.
[76] S. Premi, S. Wallisch, C.M. Mano, A.B. Weiner, A. Bacchiocchi, K. Wakamatsu, E.J.H. Bechara, R. Halaban, T. Douki, D.E. Brash, Chemiexcitation of melanin derivatives induces DNA photoproducts long after UV exposure, Science 347(6224) (2015) 842.

[77] Y. Zhao, M.C. Mudge, J.M. Soll, R.B. Rodrigues, A.K. Byrum, E.A. Schwarzkopf, T.R. Bradstreet, S.P. Gygi, B.T. Edelson, N. Mosammaparast, OTUD4 Is a Phospho-Activated K63 Deubiquitinase that Regulates MyD88-Dependent Signaling, Molecular Cell 69(3) (2018) 505-516.e5.
[78] Z. Guo, S. Kozlov, M.F. Lavin, M.D. Person, T.T. Paull, ATM Activation by Oxidative Stress, Science 330(6003) (2010) 517.
[79] H.J. Luxton, K. Barnouin, G. Kelly, S. Hanrahan, N. Totty, D.E. Neal, H.C. Whitaker, Regulation of the localisation and function of the oncogene LYRIC/AEG-1 by ubiquitination at K486 and K491, Molecular oncology 8(3) (2014) 633-641.
[80] P.L. Ross, Y.N. Huang, J.N. Marchese, B. Williamson, K. Parker, S. Hattan, N. Khainovski, S. Pillai, S. Dey, S. Daniels, S. Purkayastha, P. Juhasz, S. Martin, M. Bartlet-Jones, F. He, A. Jacobson, D.J. Pappin, Multiplexed Protein Quantitation in Saccharomyces cerevisiae Using Amine-reactive Isobaric Tagging Reagents, Molecular & Cellular Proteomics 3(12) (2004) 1154.
[81] J.E.N. Jonkman, J.A. Cathcart, F. Xu, M.E. Bartolini, J.E. Amon, K.M. Stevens, P. Colarusso, An introduction to the wound healing assay using live-cell microscopy, Cell Adhesion & Migration 8(5) (2014) 440-451.
[82] G. Moreno-Bueno, H. Peinado, P. Molina, D. Olmeda, E. Cubillo, V. Santos, J. Palacios, F. Portillo, A. Cano, The morphological and molecular features of the epithelial-to-mesenchymal transition, Nature Protocols 4 (2009) 1591.
[83] D. Mellacheruvu, Z. Wright, A.L. Couzens, J.-P. Lambert, N.A. St-Denis, T. Li, Y.V. Miteva, S. Hauri, M.E. Sardiu, T.Y. Low, V.A. Halim, R.D. Bagshaw, N.C. Hubner, A. al-Hakim, A. Bouchard, D. Faubert, D. Fermin, W.H. Dunham, M. Goudreault, Z.-Y. Lin, B.G. Badillo, T. Pawson, D. Durocher, B. Coulombe, R. Aebersold, G. Superti-Furga, J. Colinge, A.J.R. Heck, H. Choi, M. Gstaiger, S. Mohammed, I.M. Cristea, K.L. Bennett, M.P. Washburn, B. Raught, R.M. Ewing, A.-C. Gingras, A.I. Nesvizhskii, The CRAPome: a contaminant repository for affinity purification–mass spectrometry data, Nature Methods 10 (2013) 730.
[84] D. Sarkar, P.B. Fisher, Chapter Two - AEG-1/MTDH/LYRIC: Clinical Significance, in: D. Sarkar, P.B. Fisher (Eds.), Advances in Cancer Research, Academic Press2013, pp. 39-74.
[85] X. Dai, H. Cheng, Z. Bai, J. Li, Breast Cancer Cell Line Classification and Its Relevance with Breast Tumor Subtyping, Journal of Cancer 8(16) (2017) 3131-3141.
[86] L. Yu, X. Liu, K. Cui, Y. Di, L. Xin, X. Sun, W. Zhang, X. Yang, M. Wei, Z. Yao, J. Yang, SND1 Acts Downstream of TGFβ1 and Upstream of Smurf1 to Promote Breast Cancer Metastasis, Cancer Research 75(7) (2015) 1275-1286.